JOHANNES GUTENBERG-UNIVERSITÄT MAINZ

Unraveling the Molecular Mechanisms of the BmrA Function: From Intramolecular Interactions to Membrane-Dependent Regulation

Dissertation
zur Erlangung des Grades
„Doktor der Naturwissenschaften“/
„Doktorin der Naturwissenschaften“
im Promotionsfach Chemie

am Fachbereich Chemie, Pharmazie, Geographie und Geowissenschaften
der Johannes Gutenberg-Universität Mainz

VERONIKA OSTEN

geb. in Isjum (Ukraine)

Mainz, 2025

1. Gutachter:in: [redacted]

2. Gutachter:in: [redacted]

Tag der mündlichen Prüfung: 12.12.2025

Eigenständigkeitserklärung

Hiermit erkläre ich Osten, Veronika

dass ich die vorliegende Arbeit mit dem Titel:

“Unraveling the Molecular Mechanisms of the BmrA Function: From Intramolecular Interactions to Membrane-Dependent Regulation”

selbstständig verfasst und keine anderen als die angegebenen Quellen und Hilfsmittel (dazu zählen auch KI-basierte Anwendungen oder Werkzeuge*) benutzt habe. Sämtliche wörtlichen oder sinngemäßen Übernahmen und Zitate sind kenntlich gemacht und nachgewiesen (dies gilt auch für Texte, die durch generative KI, wie Chat GPT erzeugt wurden). Ich versichere, dass ich keine Hilfsmittel verwendet habe, deren Nutzung die Prüferin oder der Prüfer explizit ausgeschlossen hat.

Im Anhang „Use of AI-tools“ habe ich die verwendeten KI-Tools dokumentiert.

Mit Abgabe der vorliegenden Leistung übernehme ich die Verantwortung für das eingereichte Gesamtprodukt. Ich verantworte damit auch jegliche KI-generierten Inhalte, die ich in meine Arbeit übernommen habe. Die Richtigkeit übernommener (KI-generierter) Aussagen und Inhalte habe ich nach bestem Wissen und Gewissen geprüft.

Mir ist bekannt, dass ein Verstoß gegen die genannten Punkte prüfungsrechtliche Konsequenzen hat und insbesondere dazu führen kann, dass die Promotionsleistung als mit „nicht bestanden“ bewertet wird. Die Einschreibung kann für bis zu zwei Jahre widerrufen werden, wenn Studierende zweimal oder häufiger bei Prüfungsleistungen täuschen (§ 69 Abs. 4 und 5 HochSchG).

_____

Ort, Datum und Unterschrift

* Weiterführende Informationen zu KI-basierte Anwendungen oder Werkzeuge unter: https://digitale-lehre.uni-mainz.de/ki-in-der-hochschulbildung/

Table of content

I. Summary 1

II. Zusammenfassung 3

III. Publications 5

1 Introduction 7

1.1 Biological membranes 7

1.1.1 Lipids in membranes 7

1.1.2 Membrane proteins 10

1.1.3 Transport across membranes 11

1.2 ABC transporter 12

1.2.1 Structure 12

1.2.2 Transport cycle 18

1.2.3 Human ABC transporters 20

1.2.4 Bacillus multidrug resistance ATP (BmrA) 21

2 Objectives of this thesis 25

3 Materials and Methods 29

3.1 Materials 29

3.1.1 Chemicals 29

3.1.2 Phospholipids 29

3.1.3 Buffers, solutions, and media 29

3.1.4 Bacterial strains 33

3.1.5 Plasmids 33

3.1.6 Oligonucleotides 35

3.1.7 Protein and DNA standards 36

3.1.8 Enzymes and kits 37

3.1.9 Consumables 38

3.1.10 Instruments 38

3.1.11 Softwares 39

3.2 Methods 41

3.2.1 Molecular biological methods 41
3.2.2 Microbiological methods 43
3.2.3 Biochemical methods 44
3.2.4 Biophysical methods 51
3.2.5 Bioinformatic analyses 54
4 Results and Discussion 57
4.1 Membrane properties control the ATPase activity of the ABC transporter BmrA 57
4.1.1 Publication 57
4.1.2 Abstract 58
4.1.3 Introduction 58
4.1.4 Results 60
4.1.5 Discussion 68
4.2 The C-terminal α-helix is crucial for the activity of the bacterial ABC transporter BmrA 73
4.2.1 Publication 73
4.2.2 Abstract 74
4.2.3 Introduction 74
4.2.4 Results 76
4.2.5 Discussion 83
4.3 A salt bridge pre-arranges the BmrA structure for proper NBD dimerization 89
4.3.1 Manuscript 89
4.3.2 Abstract 90
4.3.3 Introduction 90
4.3.4 Results 93
4.3.5 Discussion 102
5 Literature 107
6 Appendix 123
6.1 Plasmid maps 123
6.2 Sequences 125

6.3 Supplement 127
6.4 Methods performed by Collaborators 133
6.4.1 Cryo-EM Sample Preparation and Data Collection 133
6.4.2 Cryo-EM Data Processing 133
6.4.3 Model Building 134
Abbreviations 135
List of Figures 139
List of Tables 141
Use of AI-tools 142
Acknowledgments/ Danksagung 143
Curriculum vitae 144

I. Summary

Members of the membrane protein superfamily of ATP-binding cassette (ABC) transporters are crucial for the active transport of various exogenous and endogenous substances across biological membranes in all living organisms. Although different ABC transporters function similarly in principle, they differ in certain aspects of their mode of action. An ABC transporter's core consists of four entities: two nucleotide-binding domains (NBDs) and two transmembrane domains (TMDs). ATP binding and hydrolysis take place at the highly conserved NBDs, while the structurally diverse TMDs promote substrate binding and translocation. This requires perfectly synchronized NBD-TMD communication during the different steps in a transport cycle. Since ABC transporters play key roles in nutrient uptake and multidrug resistance (MDR) and are associated with several human diseases, understanding the molecular mechanisms of ABC transporter function is of great interest.

In my PhD project I focused on a bacterial member of the ABC transporter superfamily from *Bacillus subtilis* called BmrA (Bacillus multidrug resistance ATP). For over two decades, BmrA has served as a model protein for studying the structure and function of ABC transporters, as well as their role in multidrug resistance (MDR). In this thesis, the impact of the membrane environment as well as inter- and intramolecular interactions on the BmrA function are investigated.

The first part of this work aimed at unraveling the influence of specific lipids and membrane properties on the BmrA function, since the impact of the native lipid environment on membrane proteins is often neglected. Therefore, the *in vitro* ATPase activity of BmrA in different lipid compositions was systematically studied, and three lipid-dependent membrane parameters were found to modulate its basal ATPase activity: (i) the membrane hydrophobic thickness, (ii) a negative surface charge, and (iii) the lipid packing density. This study underlines the importance of carefully selecting the lipid composition in *in vitro* studies of membrane proteins and provides valuable insights into how a specific lipid composition can influence the basal ATPase activity of BmrA.

In the second part, the function of the C-terminal α-helix of BmrA was analyzed. The distal tip of the helix is dispensable and highly flexible, as demonstrated by systematic mutagenesis, which includes alanine- and cysteine-scanning approaches. In contrast, the first segment of the C-terminal α-helix is crucial for the BmrA activity, likely by establishing contacts with structural elements involved in ATP recognition, binding, and/or hydrolysis.

The last part of this thesis describes the identification of a yet unidentified potential intramolecular salt bridge between the coupling helix and the linker region of BmrA via mutational analysis of the relevant regions and functional and structural characterization of the respective alanine variants. This salt bridge appears to correctly position the NBDs relative to the TMDs, thereby stabilizing the cross-talk between the NBD and TMD. Additionally, the conservation of this structural element in bacterial and human ABC transporters suggests a universal mechanism for maintaining functional NBD-TMD coupling.

In summary, this thesis provides new insights into ABC transporter function by describing (novel) molecular determinants that regulate the BmrA activity.

II. Zusammenfassung

Mitglieder der Membranprotein-Superfamilie der *ATP-binding cassette transporter* (ABC-Transporter) sind für den aktiven Transport verschiedener exogener und endogener Substanzen durch biologische Membranen in allen lebenden Organismen entscheidend. Obwohl verschiedene ABC-Transporter im Prinzip ähnlich arbeiten, unterscheiden sie sich in bestimmten Aspekten in ihrer Funktionsweise. Der Kern eines ABC-Transporters besteht aus vier Einheiten: zwei Nukleotid-Bindungsdomänen (NBDs) und zwei Transmembrandomänen (TMDs). Die ATP-Bindung und -Hydrolyse findet an den hochkonservierten NBDs statt, während die strukturell vielfältigen TMDs die Substratbindung und -translokation vermitteln. Dies erfordert eine perfekt synchronisierte NBD-TMD-Kommunikation hinsichtlich der verschiedenen Transportschritte. Da ABC-Transporter eine Schlüsselrolle bei der Nährstoffaufnahme und Multidrogenresistenz (eng.: *multidrug resistance* (MDR)) spielen und mit mehreren menschlichen Krankheiten in Verbindung stehen, ist das Verständnis ihrer molekularen Mechanismen von großem Interesse.

In dieser Arbeit wird der bakterielle ABC-Transporter *Bacillus multidrug resistance* ATP (BmrA) aus *Bacillus subtilis* untersucht, der seit über zwei Jahrzehnten als Modellprotein für die Untersuchung der Struktur und Funktion von ABC-Transportern und ihrer Rolle bei der Multidrug-Resistenz (MDR) dient. Hier werden die Auswirkungen der Membranumgebung sowie strukturelle Elemente, wie inter- und intramolekulare Wechselwirkungen, die für die Funktion von BmrA wichtig sind, untersucht.

Der erste Teil dieser Arbeit zielte darauf ab, den Einfluss spezifischer Lipide und Membraneigenschaften auf die Funktion von BmrA aufzuklären, da der Einfluss der nativen Lipidumgebung auf die Struktur und Funktion von Membranproteinen häufig vernachlässigt wird. Dazu wurde die *in vitro* ATPase Aktivität von BmrA in verschiedenen Lipidzusammensetzungen systematisch untersucht, und es wurde festgestellt, dass drei lipidabhängige Parameter seine basale ATPase Aktivität modulieren: (i) die hydrophobe Dicke der Membran, (ii) die negative Oberflächenladung und (iii) die Lipidpackungsdichte. Diese Studie unterstreicht die Bedeutung einer sorgfältigen Auswahl der Lipidzusammensetzung in *in vitro*-Studien von Membranproteinen und liefert wertvolle Erkenntnisse darüber, wie eine bestimmte Lipidzusammensetzung die basale ATPase-Aktivität von BmrA beeinflussen kann.

Im zweiten Teil dieser Arbeit wurde die Funktion der C-terminalen α-Helix von BmrA analysiert. Das distale Ende der Helix ist entbehrlich und hochflexibel, was durch systematische Alanin- und Cystein-Mutagenese nachgewiesen wurde. Das erste Segment der C-terminalen α-Helix ist hingegen entscheidend für die Funktion von BmrA, wahrscheinlich aufgrund der Etablierung von

Kontakten mit Strukturelementen, die an der ATP-Erkennung, -Bindung und/oder -Hydrolyse beteiligt sind.

Der letzte Teil dieser Arbeit beschreibt die Identifizierung einer neuartigen intermolekularen Salzbrücke zwischen einer Kopplungshelix und der Linkerregion von BmrA mittels Mutationsanalyse der relevanten Regionen und funktioneller und struktureller Charakterisierung der jeweiligen Alanine-Varianten. Diese Salzbrücke scheint die NBDs relativ zu den TMDs korrekt zu positionieren und dadurch die Wechselwirkung zwischen NBD und TMD zu stabilisieren. Die Konservierung dieses Strukturelements in bakteriellen und menschlichen ABC-Transportern deutet darüber hinaus auf einen universellen Mechanismus zur Aufrechterhaltung der funktionellen NBD-TMD-Kopplung hin.

Zusammenfassend liefert diese Arbeit neue Erkenntnisse über die Funktion von ABC-Transportern, indem sie (neue) molekulare Determinanten beschreibt, die die BmrA-Aktivität regulieren.

III. Publications

Parts of this thesis were already published during the course of this thesis (‡ = equal contribution):

- Osten, V. and [redacted] (2025) Membrane properties control the ATPase activity of the ABC transporter BmrA, *Biochim. Biophys. Acta – Biomembranes*, 1867, 184430.
- Osten V.‡, [redacted] (2025) The C-terminal α-helix is crucial for the activity of the bacterial ABC transporter BmrA, *J. Biol. Chem.*, 301 (2):108098.

The format of these articles was adapted to the style of this thesis. No content was changed. All articles are licensed under a Creative Commons CC BY 4.0 license (https://creativecommons.org/licenses/by/4.0/).

The following manuscript was prepared for submission during the course of this thesis:

- Osten, V., [redacted] (2025) A salt bridge pre-arranges the BmrA structure for proper NBD dimerization, *in preparation*.

1 Introduction

1.1 Biological membranes

A key feature of biological life is the existence of a highly regulated and dynamic membrane. Membranes define the inside and outside of cells, thereby acting as a barrier between the cell and its environment. Inside a eukaryotic cell, they form compartments, creating distinct microenvironments that allow different metabolic reactions to occur simultaneously. One of the main functions of membranes is to regulate the exchange of molecules between two separate aqueous compartments[1]. Composed of a lipid bilayer, membranes typically allow small hydrophobic molecules to diffuse through the membrane while preventing or limiting the diffusion of charged and/or larger molecules. In combination with specific transport systems, membranes provide selective permeability, thus controlling which substances remain inside the cell (or the compartment) or are expelled, and which remain outside or can be taken up[2]. Despite their separating properties, membranes also serve as a platform where lipids and proteins interact[3]. Embedded or peripherally attached membrane proteins function as pumps, channels, receptors, energy transmitters, or enzymes, fulfilling essential functions in various cellular processes, such as membrane transport, intercellular communication/signaling, cell-cell recognition, cell identity, energy transduction, etc[4].

Membranes mainly consist of lipids, proteins, and sugars (covalently attached to lipids or proteins)[2]. In 1972, Singer and Nicolson proposed the famous fluid mosaic model, which describes the structural organization of biological membranes as a dynamic fluid mosaic of membrane proteins alternating the lipid bilayer composed of a variety of lipid molecules, in which both are laterally mobile[5]. Both lipids and membrane proteins play central roles in numerous cellular activities that involve the membrane and will be discussed separately[3].

1.1.1 Lipids in membranes

The lipids of biomembranes are typically classified into phospholipids, glycolipids, and sterols[2]. As shown in Figure 1A, lipids have a hydrophilic and a hydrophobic part. This amphipathic character allows the formation of a bilayer in aqueous solution, with the hydrophilic region interfacing with the aqueous phase and the hydrophobic regions facing each other[1]. In the case of phospholipids, the hydrophobic part consists of two (un)saturated fatty acid chains attached to the *sn*-1 and *sn*-2 positions of a glycerol backbone, followed by a phosphate group at the *sn*-3 position and a polar head group attached to the phosphate group. The most abundant phospholipid in eukaryotic membranes is the zwitterionic phosphatidylcholine (PC)[6]. However,

membranes are composed of a structurally diverse set of lipids. The diversity ranges from different acyl chain lengths and degrees of saturation to different head groups. Phosphatic acids (PA) are negatively charged, as are phosphatidylserines (PS), phosphatidylglycerols (PG), cardiolipins (CLs, diphosphatidylglycerol), and phosphatidylinositols (PI) (Figure 1B). The latter can be mono- or polyphosphorylated[3]. On the other hand, lipids can be zwitterionic as PC and phosphatidylethanolamines (PE). Furthermore, the glycerol backbone can be replaced by sphingosine (Figure 1C), resulting in sphingophospholipids. Glycolipids are based on either glycerol or sphingosine to which a glycosyl moiety is directly esterified (Figure 1A). Different sugar moieties on lipids (and proteins) play an important role, as they are often recognized by antibodies and thus involved in immune responses[2]. In contrast, sterols are structurally very different from phospho- and glycolipids. The hydrophilic region is a small hydroxyl group, and the bulky hydrophobic region consists of a rigid steroid structure and a floppy short hydrocarbon side chain (Figure 1A). Because of the proportions, sterols in particular regulate membrane fluidity, packing, phase behavior, etc[3]. However, sterols are not present in most bacterial membranes and,

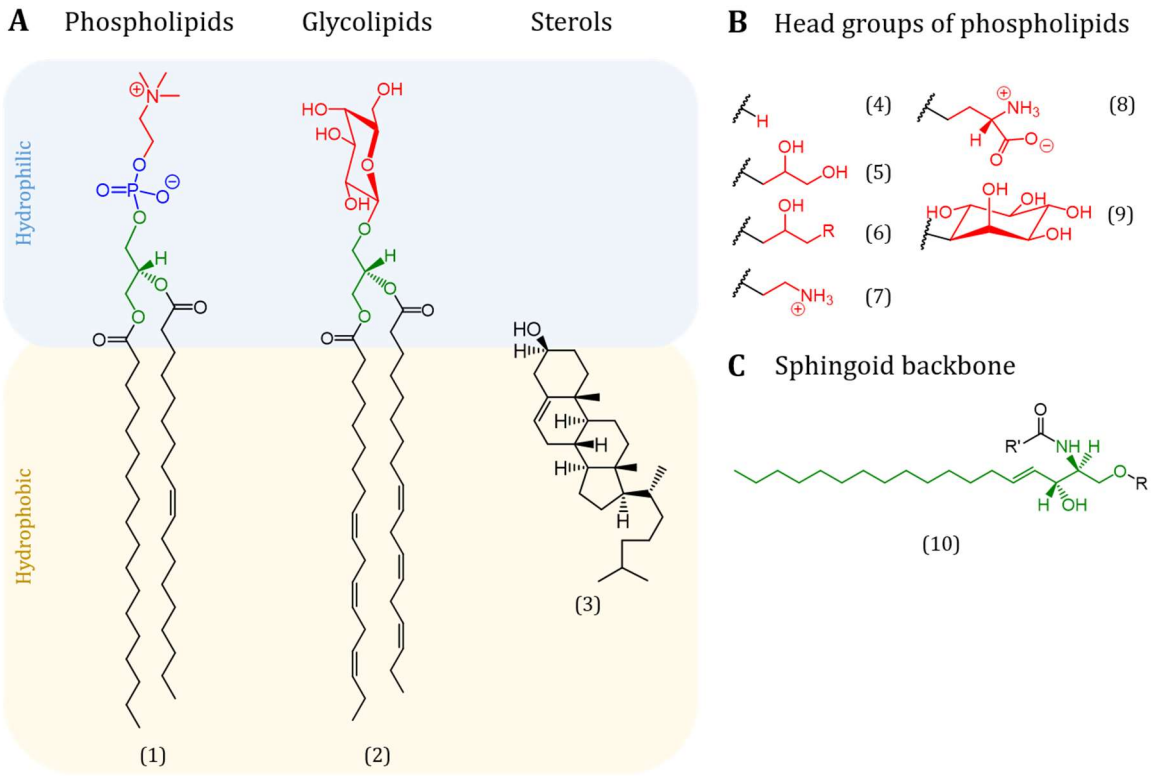

Figure 1: Typical membrane lipids.

(A) The three major classes of membrane lipids. Shown are the chemical structures of (1) 1-stearoyl-2-oleoyl-sn-glycero-3-phosphocholine, a (glycero)phospholipid, (2) monogalactosyldilinolenoylglycerol (MGDG), a (glycero)glycolipid and (3) cholesterol, a sterol. Hydrophilic regions are framed in blue and hydrophobic regions are framed in yellow. The glycerol backbone is highlighted in green, the phosphate group in blue and the head group in red. **(B)** Typical head groups of phospholipids: (4) H (no extra head group), (5) glycerol, (6) phosphatidylglycerol, (7) ethanolamine, (8) serine, and (9) inositol. **(C)** The (10) sphingoid backbone (green) replaces the glycerol backbone in phospholipids and glycolipids resulting in sphingophospholipids and sphingoglycolipids. Structures were drawn using Chemdraw.

together with glycolipids, are beyond the scope of this work and will not be discussed further.

The above-described formation of a lipid bilayer is only one potential assembly of lipids. They have the ability to adopt several different phases, a phenomenon called polymorphism, which is highly dependent on the structural shape (Figure 2). PC, PG, and PI are bilayer-forming lipids and have a similar cross-sectional area of the head group and the acyl chains, resulting in an overall cylindrical shape. In an aqueous solution, they spontaneously form lamellar phases like bilayers[7]. However, lipids with a higher or lower head-to-tail ratio prefer tubular structures and are referred to as non-bilayer-forming lipids. Conical-shaped lipids have a smaller head group compared to their acyl chains, such as MGDG, PS, PE, PA, or CLs, and tend to form structures with a negative curvature. For example, the hexagonal II (HII) phase or the cubic phase. On the other hand, lipids with an inverted-conical shape, such as lysolipids or detergent molecules, where the area of the head group is larger than that of the single acyl chain, prefer to form inverted hexagonal I (HI) phase structures or spherical micelles[8].

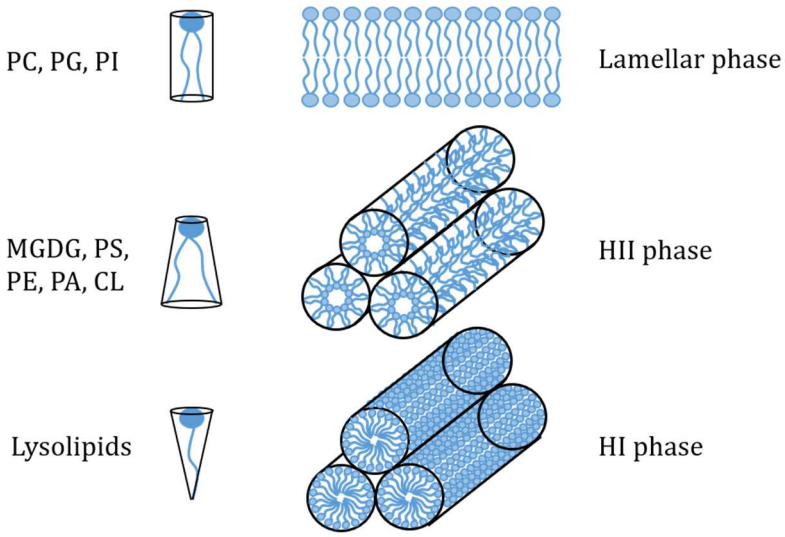

Figure 2: Polymorphism of phospholipids.

Lipids such as PC, PG and PI have a similar subtended area for the head group and the acyl chains and have an overall cylindrical shape. They form a lamellar phase in aqueous solutions. Conical lipids such as MGDG, PS, PE, PA, and CL have smaller head groups compared to the acyl chains and form structures with a negative curvature, as the HII phase. In contrast, lipids with an inverted-conically shape, e.g. lysolipids, with a bulky head group and an acyl chain, form HI phase structures with positive curvature. The figure is based on Jouhet *et al.* (2013)[8].

Since a biological membrane is composed of more than 1000 different lipids, each membrane is a complex macrostructure with different characteristics and biochemical and biophysical properties[3]. For example, the acyl chain's length, saturation level, and lipid tilt angle all contribute to the thickness of a membrane. Membrane fluidity and lipid packing are influenced by the presence of conical-shaped lipids or sterols, as well as the degree of saturation, among other

factors[7]. This in turn can influence the permeability of membranes[9]. Another important aspect is the lateral pressure within a membrane, which is closely related to membrane curvature. Due to the preference of non-bilayer-forming lipids to form curved structures, the tendency to curl is frustrated in a lipid bilayer structure[10]. In an ideal bilayer containing solely cylindrical-shaped lipids, the repulsive lateral pressure, especially in the chain region, the repulsive/attractive forces in the head group region, and the interfacial tension between both are balanced. However, an imbalance leads to an excess of one of these forces, which is stored in the respective bilayer and affects other components of the membrane[10]. A more obvious property is the electrostatics of the membrane surface resulting from the assembly of different lipid head groups. In general, negatively charged lipids dominate the electrostatics of biomembranes and thus affect the membrane phase behavior, phase separation into microdomains, and specific interactions between lipids and proteins[3]. Although less pronounced in bacterial membranes, biological membranes are characterized by lipid asymmetry between the two leaflets. In eukaryotes, anionic lipids, e.g. PS and PE, are mainly found in the inner leaflet, and PC and sphingomyelin in the outer leaflet[2]. Exposure of PS on the outer leaflet is often a sign of injury and leads to recognition of apoptotic cells by phagocytes or activation of blood coagulation[7]. In contrast, in bacterial membranes the lateral lipid asymmetry is more relevant. Lipid (micro)domains (sometimes referred to as lipid rafts) with a distinct lipid and/or protein composition are in particular association platforms for specific membrane proteins and are involved in their regulation[2,7]. By controlling the lipid composition, cells have a powerful tool to regulate various (membrane) proteins and cellular processes. Either the cell provides or removes essential lipids for specific interactions with proteins, or it assembles a membrane with certain collective physical properties that affect (membrane) proteins in a specific way[11]. In response to environmental conditions, cells do not only up- or down-regulate the expression of membrane proteins but also adjust their lipid composition[3]. For example, bacteria growing at low temperatures increase the amount of branched side chains to retain the membrane fluidity[12].

1.1.2 Membrane proteins

However, discussing the importance and the role of lipids in biological membranes without considering the impact of membrane proteins is like telling only one side of the story. In fact, we have to keep in mind that the weight ratio of lipids to proteins in membranes is variable, and proteins can even be the major membrane component[13]. Genome sequence analysis of several organisms showed that approximately 30% of all genes code for integral membrane proteins[14]. In addition, about 50% of all therapeutic drugs target integral membrane proteins[15]. Taken together, functional and structural studies of membrane proteins are highly relevant and of great interest. However, they are numerically underrepresented compared to the entire proteome, with only

1.5% of the protein structures deposited in the Protein Data Bank (PDB, as of April 2025) being membrane proteins. Membrane proteins are involved in numerous cellular processes, such as control and maintenance of cell integrity, inter- and intracellular signaling, control and regulation of substrate transport across membranes, facilitation of biochemical reactions, cell recognition, cell adhesion, etc[2,16,17]. Due to the enormous quantity of membrane proteins and their functions, in the following, only membrane transport proteins and the substrate transport across membranes will be discussed.

1.1.3 Transport across membranes

Small hydrophobic molecules are able to diffuse freely through membranes. However, to overcome the extremely low diffusion rates of polar substances across the lipid bilayer, transport systems have evolved. These transport systems can be divided into passive and active transport. Diffusion of molecules can be classified as either free or facilitated. The latter is part of passive transport, relying on existing concentration gradients and integral membrane proteins that act as channels and carriers. Channels are pore-forming proteins that facilitate the diffusion of specific molecules. Examples are highly selective aquaporin channels, which dramatically increase water permeability of membranes, even though water molecules can actually pass the membrane[18]. Carriers bind specific substrates and release them on the opposite side of the membrane after a series of conformational changes, as e.g., observed for insulin-independent glucose transporters (GLUTs)[19]. In contrast, active transport allows molecules to move against their concentration gradient and therefore requires energy. Primary active transport is mediated by pumps, typically adenosine triphosphatase (ATPase) proteins. They use the energy of adenosine triphosphate (ATP) hydrolysis to transport molecules against their concentration gradient. Such ATPase proteins are, for example, ATP-binding cassette (ABC) transporters, which control the import or export of various substrates[20]. Another mechanism does not require ATP directly but instead uses an existing concentration gradient of one molecule and couples it to the transport of another molecule against its concentration gradient. This secondary active transport is mediated by syn- or antiporters[21]. A prominent example is the Na^+/glucose cotransporter (SGLT). Here, the transport of one molecule of glucose/galactose from the intestinal lumen into enterocytes of the intestinal mucosa against its concentration gradient is coupled with the transport of two Na^+ ions along its concentration gradient[22]. Whereby the concentration gradient of Na^+ is maintained by the Na^+/K^+-ATPase under ATP consumption[23].

Taken together, the assembly of different sets of channels, carriers, pumps, and syn-/antiporters in cells results in a selective membrane permeability and thus constantly controls the uptake and release of "right" molecules (e.g., nutrients *vs.* toxins)[24]. These molecules are structurally very diverse, which explains why a significant portion of the proteome is dedicated to the transport of

these molecules. In particular, the ABC transporter superfamily plays a central role in active transport, as its substrates can include smaller molecules, such as ions, sugars, and lipids, as well as larger molecules, such as antibiotics and anticancer drugs[25].

1.2 ABC transporter

Members of the large superfamily of ABC transporters are integral membrane proteins and are ancient and present in all phyla of life[26–28]. These ATP-driven transporters import or export a wide range of substrates against their chemical gradient across biological membranes. The fact that all transporters have an ATP-binding domain ultimately led to their designation as "ATP-binding cassette" transporters[29]. They are one of the largest protein superfamilies known in bacteria, with 1-3% of the total microbial genomes coding for ABC transporters[30]. In bacteria, ABC transporters are involved on the one hand in the import of essential nutrients (e.g., mono-/oligosaccharides, amino acids, vitamins) and on the other hand in the export of various molecules (e.g., lipids, hydrophobic drugs, toxins) and are thus essential for viability, virulence, and pathogenicity[31]. In contrast, eukaryotic members were thought to be only exporters, which at least is true for human ABC transporters. By exporting hormones, lipids, peptides, xenobiotics, etc., they play essential physiological roles in lipid homeostasis and cellular detoxification[32]. However, in plants, besides exporters, importers are also present that contribute to detoxification, phytohormone transport, and plant-microbe interactions[26,33].

The research focus on ABC transporters is particularly important due to their involvement in multidrug resistance (MDR) in bacteria and cancer cells[34]. In addition, mutations in human ABC-transporter encoding genes lead to a series of different diseases, such as cystic fibrosis, Stargardt, Tangier, and Alzheimer's disease[20,35–39].

1.2.1 Structure

The general architecture of ABC transporters includes four entities: two membrane-embedded transmembrane domains (TMDs), which provide the translocation pathway for the substrate, and two cytosolic nucleotide-binding domains (NBDs), where ATP binding and hydrolysis occur. Typically for bacterial exporters, one NBD is fused to one TMD, forming a so-called "half-transporter", and two of these either homo- or heterodimerize to generate the functional "full-transporter". This is also true for some eukaryotic family members, although here often all four domains are expressed on a single polypeptide chain[36]. However, each domain can also be expressed as an individual polypeptide chain.

1.2.1.1 Classification

Initially, ABC transporters were classified into three main classes based on sequence alignments of bacterial proteins[40]. Class 1 comprises transporters with fused TMDs and NBDs, class 2 contains non-functional proteins consisting only of NBDs, and class 3 contains mainly importers with individually expressed NBDs and TMDs that additionally depend on substrate-binding proteins (SBPs)[31]. Human ABC transporters also have their own classification based on NBD/TMD sequence homology and domain order, which will be addressed in detail in chapter 1.2.3[41,42]. However, a revised classification of ABC transporters (Figure 3) has been proposed in 2020, which combines the phylogenetic analysis of TMDs and the emerging large number of high-resolution structures[43]. According to Thomas *et al.* (2020), types I-III are exclusively classified as importers based on their different TMD architecture[43]. Typically, importers rely on SBPs to capture the substrate and deliver it to the appropriate transporter[44]. Type IV transporters include mostly exporters and some importers and are a very diverse group. The most prominent member is

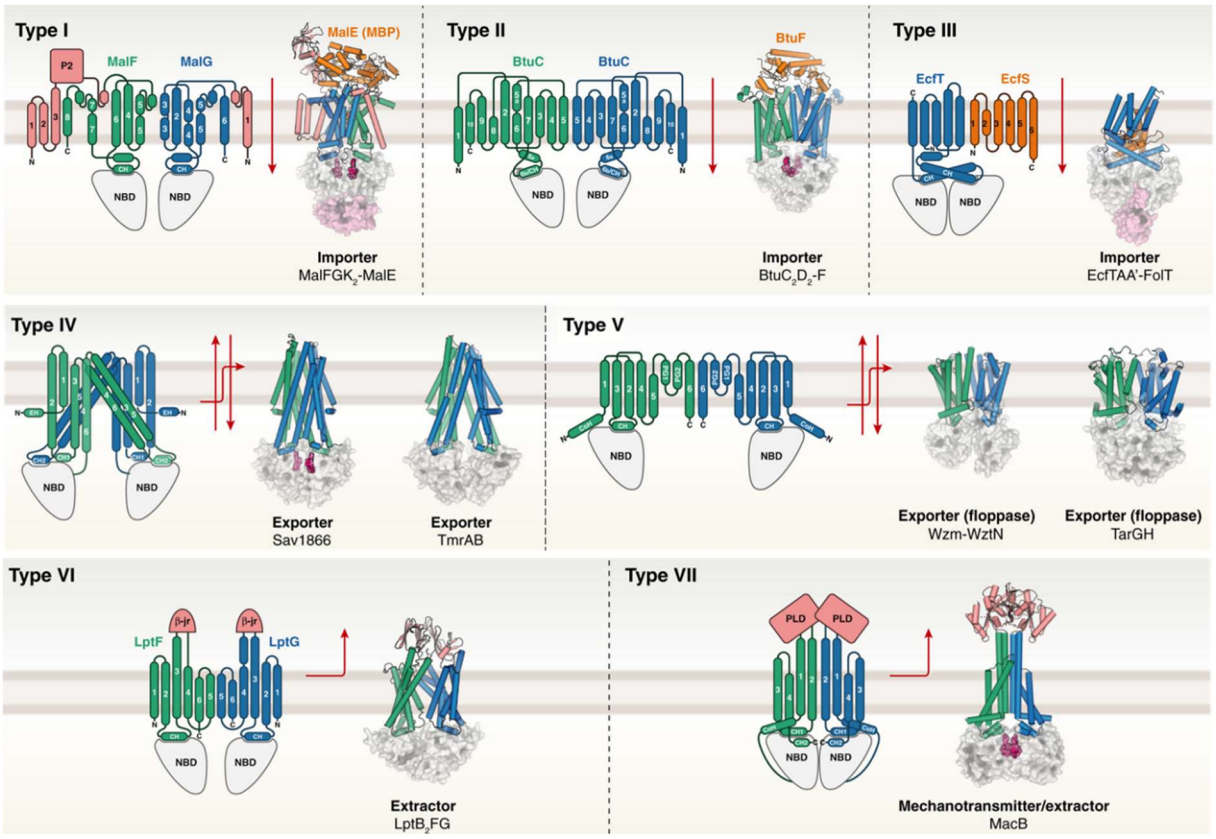

Figure 3: Classification of the ABC transporter superfamily into type I-VII based on their TMD fold.

Each ABC transporter type shows a unique folding of the TMD, illustrated by a topology diagram on the left side. On the right side, the two TMDs are shown as cartoons in blue/green and the surface representation of the corresponding NBDs are shown in gray. For type I-III the SBPs, auxiliary domains and additional helices are shown in orange, red and salmon, respectively. The transport direction is indicated by red arrows. PDBs: $MalFGK_2$-MalE [2R6G][45], $BtuC_2D_2$-F [4FI3][46], EcfTAA'-FolT [4HUQ][47], Sav1866 [2HYD][48], TmrAB [5MKK][49], Wzm-WztN [6OIH][50], TarGH [6JBH][50], $LptB_2FG$ [5X5Y][51], MacB [5LJ7][52]. The figure is modified and taken from Thomas *et al.* (2020)[43].

*Sav*1866 from *Staphylococcus aureus* (*S. aureus*)[48]. It is characterized by its 6+6 TMD helix organization, in which some transmembrane helices (TM) are swapped between the two TMDs. A similar helix organization, but without domain swapping, is found in type V transporters, which are equally diverse. This class is characterized by the presence of amphipathic N-terminal helices and periplasmic gate helices. Although type VI and type VII transporters share TMD similarities with type V, important features are different or missing completely: type VI transporters lack the amphipathic N-terminal helix as well as the extracellular reentrant helices, whereas type VII transporters have only four proper TM helices and contain an additional coupling helix[43].

1.2.1.2 The nucleotide-binding domain

The NBD is highly conserved, both structurally and at the sequence level, among different ABC transporters. NBDs of bacterial and eukaryotic exporters share 30-50% sequence similarity, suggesting similar folding and a conserved mechanism[29,53,54]. Two nucleotide-binding sites (NBS) are formed from conserved regions and residues of both NBDs upon NBD dimerization in a head-to-tail fashion, which is the key element for all ABC transporters[25]. In a symmetrical NBD dimer, two Mg-ATP molecules are "sandwiched" at the NBD-NBD interface and are hydrolyzed there. This requires a number of crucial residues and loops. Both the Walker A and Walker B motifs, which are essential for ATP binding and hydrolysis, are found in the RecA-like domain of the NBDs[25,55]. The glycine-rich Walker A motif (or P-loop, Figure 4, blue) has a characteristic sequence (GXXGXGKS/T; X = arbitrary amino acid). The glycine residues interact with the phosphoryl moieties of the nucleotide through hydrogen bonding and are important for the loop flexibility, while the basic residue is catalytically active during the phosphoryl transfer and the serine/threonine coordinates the catalytic Mg^{2+} ion[25,56]. Mutational analyses have shown that the catalytic lysine is essential, as mutation of this lysine results in completely abolished ATPase activity[57,58]. Equally essential for catalysis are the conserved glutamate and aspartate residues of the Walker B motif (Figure 4, red), which follow a series of hydrophobic amino acids (ϕϕϕϕDE)[55,59]. During ATP hydrolysis, the glutamate is directly responsible for the cleavage of the β-γ-phosphodiester bond[60]. In addition to the residues of the Walker A and B motifs of one NBD, residues of the ABC signature sequence (Figure 4, purple) of the opposite NBD are also required to coordinate one ATP molecule[61–63]. The ABC signature sequence (LSGGQ), sometimes referred to as the S-sequence or C-loop, is located in the α-helical subdomain of the NBDs and is involved in the transduction of the energy released during ATP hydrolysis into conformational changes in the TMDs[25,64,65]. Preceding the ABC signature motif, the X-loop (Figure 4, dark gray), which is only present in type IV ABC transporters (see chapter 1.2.1.1), interacts with residues of the coupling helices (CHs; see chapter 1.2.1.3) and is thus involved in the TMD-NBD cross-talk[48].

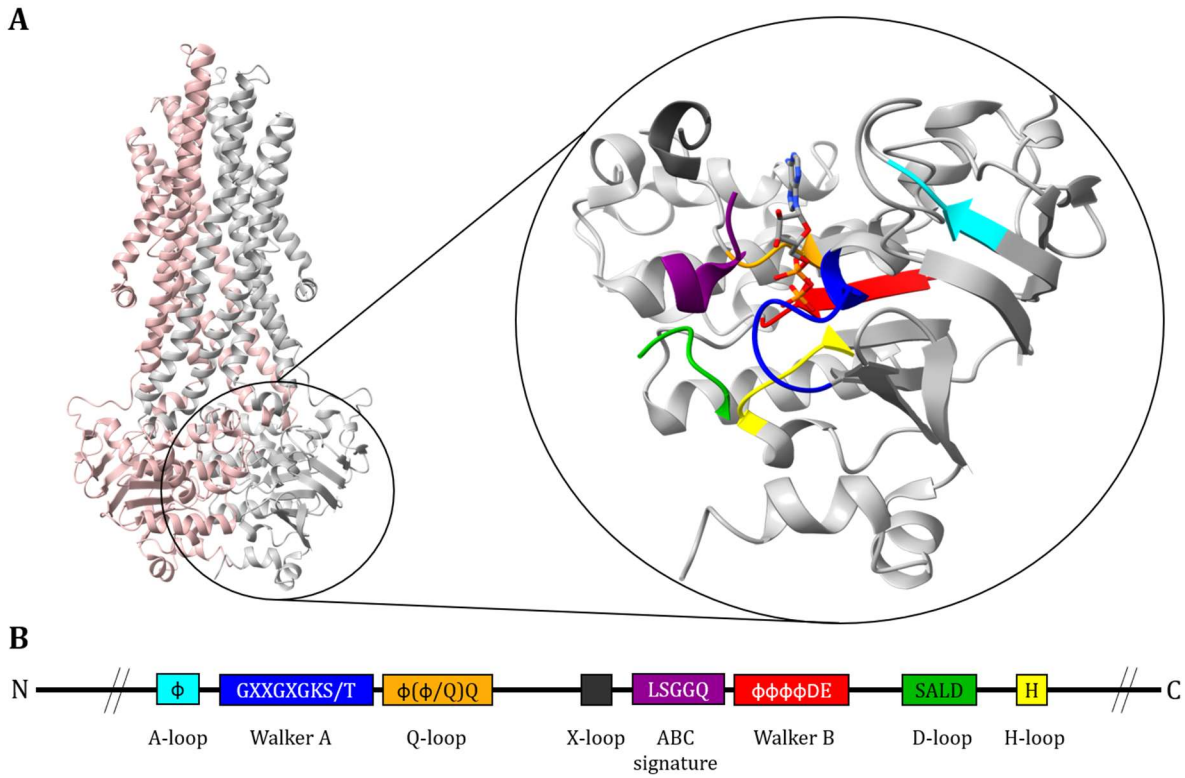

Figure 4: Conserved motifs of ABC transporter NBDs exemplified by the *Sav*1866 NBDs.

(A) Secondary structure of the homodimeric exporter *Sav*1866. PDB: [2HYD][48]. The monomers are shown in rose and gray. On the right, an enlarged view on the NBDs with bound adenosine diphosphate (ADP) in stick representation is given. Conserved motifs are highlighted: A-loop (cyan), Walker A (blue), Q-loop (orange), X-loop (dark gray), ABC signature sequence (purple), Walker B (red), D-loop (green) and H-loop (yellow). The X-loop, the ABC signature sequence, and the D-loop of the opposite NBD (rose monomer) are shown as short segments. Within the gray NBD, these sequences are not highlighted. **(B)** Amino acid sequences and approximate positions on a polypeptide chain of the conserved motifs shown in (A) with the same color scheme. X = arbitrary amino acid; ϕ = hydrophobic amino acid.

Communication between the CH and the NBD is also mediated by the Q-loop (ϕ(ϕ/Q)Q)[60,66,67]. The conserved glutamate directly interacts with the γ-phosphate of the nucleotide, and since the loop is highly flexible and undergoes conformational changes during the catalytic cycle, the loops appear to be involved in NBD-TMD communication[68,69]. Located between the NBD-NBD interface, the D-loops (Figure 4, green, consensus sequence SALD) of both NBDs are in close proximity to each other, as well as to the Walker A motifs[70]. This arrangement is supposed to play an important role in NBD-NBD communication and NBD dimerization, and possibly the NBD-TMD cross-talk, although the latter is still under debate[71–73]. Additionally, residues of the D-loop interact with residues of the H-loop (Figure 4, yellow), suggesting that the H-loop also contributes to inter-domain communication[71,74]. On the other hand, the eponymous and nearly invariant histidine of the H-loop stabilizes the coordination/binding of ATP by the catalytically active glutamate (Walker B motif) via correctly positioning the base[59,75,76]. Finally, based on resolved structures of ABC transporters[77], the A-loop (Figure 4, cyan), although first localized at the N-terminus, has

been identified to interact hydrophobically (π-π) with the adenine ring of the nucleotide base via the conserved aromatic residue in the sequence.

1.2.1.3 The transmembrane domain

In contrast to the NBDs, the TMDs show only little amino acid sequence similarity between different transporters. Structurally, the TMDs consist of multiple TM α-helices[53]. Most half-transporters contain six to ten TM helices and full-transporters 12 to 20[28,78]. However, the exact number of helices and their arrangement varies between different transporters, as described in chapter 1.2.1.1. The combined helices exhibit a molecular two-fold axis, forming two TMDs. In between the two entities, a translocation pathway is formed through which the mediated import or export occurs. During the transport cycle (will be discussed in chapter 1.2.2), the TM helices undergo large movements that enable the translocation of a substrate. Figure 5 shows the different positions that the TM helices of an exporter can adopt for two distinct conformations:

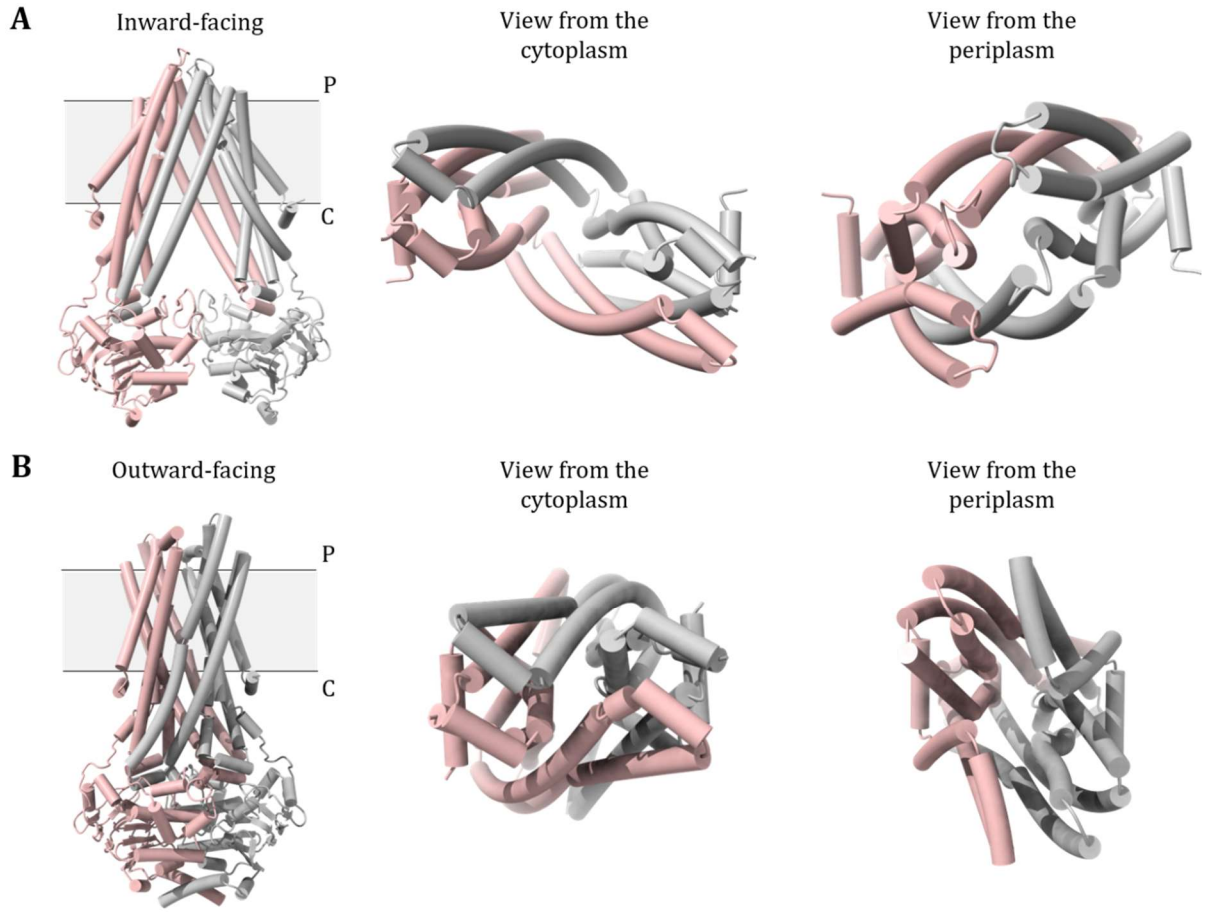

Figure 5: TM helices arrangement of BmrA in the IF and OF conformation.

Tubular representation of the structure of the homodimeric exporter BmrA in the **(A)** IF (PDB: [8QOE][79]) and **(B)** OF conformation (PDB: [7OW8][80]). Monomers are colored in rose and gray. The left panel shows the respective structures with an approximate position of the membrane. The positions of the periplasm (P) and the cytoplasm (C) are indicated. The middle panel shows the view of the TM helices from the cytoplasm and the right panel shows the view from the periplasm. For clarity, the structures of the NBDs are not shown in the middle and right panel.

inward-facing (IF) and outward-facing (OF) (the impact of conformational switches will be discussed in chapter 1.2.2). In the IF conformation, as viewed from the cytosol, the two bundles of TM helices are separated to allow substrate entry from the cytoplasmic (or the membrane) side, and on the other side of the membrane, the helices are in close proximity (Figure 5A). In direct comparison, in the OF conformation, the helices are open on the periplasmic side to release the substrate, and on the cytosolic side, the helices are tightly packed (Figure 5B). As the substrate is transported through the entire TMD region, the substrate specificity is achieved by the TMDs, which explains the lack of sequence conservation[25,81]. Residues interacting with a substrate were identified in almost all TM helices, and the corresponding side chains are directed towards the TM pathway[82,83]. Note that some ABC transporters are highly specific for a particular substrate, such as the maltose transporter $MalFGK_2$ or the bacterial heme transporter BhuT, both are typical importers[84,85]. On the other hand, polyspecific transporters are often exporters involved in MDR, e.g. *Sav*1866, and mediate the transport of various hydrophobic drugs[86].

The communication between NBDs and TMDs is mainly mediated by the CHs (or 'EAA' motifs in importers[87]). This unique architectural feature of the TMDs is part of the NBD-TMD interface, and - compared to the rest of the TMD structure - the CHs show a certain conservation. Residues of the CHs interact with residues of the Q-loop (and X-loop) in the NBDs, and, as a consequence, ATP binding/hydrolysis in the NBDs is coupled to conformational changes in the TMDs[58,68,81].

Since this work focuses on a specific type IV ABC transporter, some additional structural features of this transporter type will be described in more detail. As mentioned in chapter 1.2.1.1, the type IV transporters exhibit a domain intertwining of the TMDs, with TM4-TM5 of one protomer protruding the opposite TMD[43]. With respect to the CHs, this implies that in a fully assembled transporter, an NBD-TMD interface in the IF conformation consists of one NBD, the CH1 of the same monomer, and the CH2 of the opposite monomer (compare Figure 3 and Figure 5)[81]. In contrast, in the NBD dimerized (OF) state, CH1 of one monomer interacts with both NBDs, whereas CH2 still mainly interacts with the NBD of an opposing protomer[43,88]. Furthermore, it is characteristic for type IV ABC transporters that TM2-TM6 are significantly prolonged beyond the membrane plane, reaching into the cytosol[81]. Lastly, a short α-helical segment (often referred to as the elbow-helix (EH)) is located at the N-terminus of type IV ABC transporters and lies perpendicular to the membrane. Due to this location and its mostly amphipathic nature, it is putatively interacting with membrane lipids and anchoring the TMDs in the membrane. In addition, the EH appears to be involved in the initiation of the substrate translocation process, as interactions of the EH with substrates have been observed in some studies[89,90].

1.2.2 Transport cycle

Despite many differences among ABC transporters in their domain topology, (TMD) structure, substrate specificity, translocation direction, and physiological function, most of them pass certain pivotal states during a transport cycle. These are (i) ATP binding and hydrolysis, (ii) ADP and P_i release and (iii) nucleotide-dependent structural changes of the NBDs[68]. Substrate binding to the TMDs occurs in the IF state, which has a high affinity for the substrate. Substrate translocation and substrate release, on the other hand, occur in the OF state with low affinity to the substrate. Switching between the high and low affinity states involves large conformational changes of the TMDs that are directly coupled to structural changes within the NBDs[91,92]. Based on the resolved three-dimensional structures of *Sav*1866 and MsbA, which show two distinct conformations of

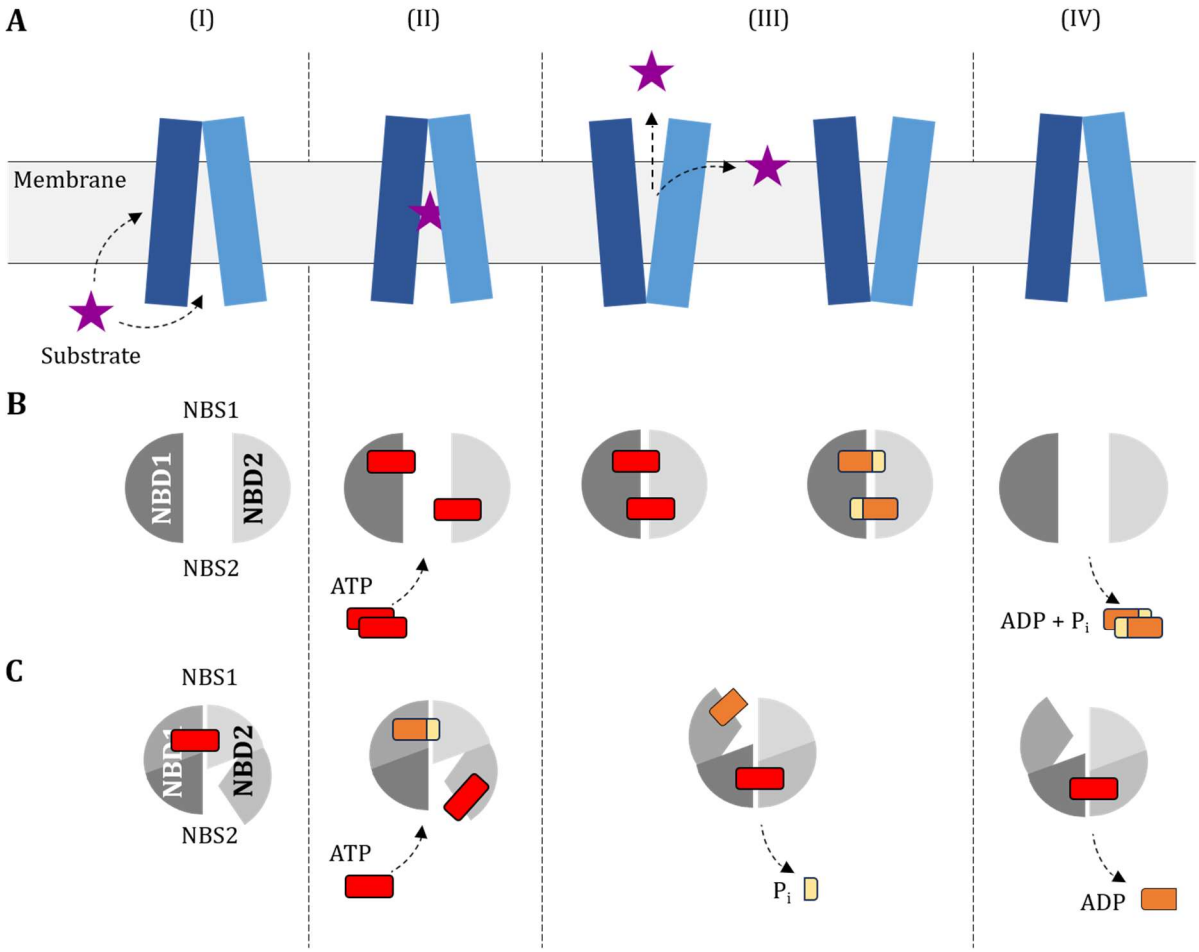

Figure 6: The two main ABC transport cycle models.

(A) Movement of TMDs within a membrane during a transport cycle. Individual TMDs are colored in light and dark blue. The substrate is shown as a purple star. **(B)** Motion of two NBDs (light and dark gray) without constant NBD contact during a transport cycle. This includes dimerization and dissociation/full separation of the NBDs. ATP (red) binding and hydrolysis to ADP (orange) and inorganic phosphate (yellow) and their release are indicated. **(C)** Motion of two NBDs (each monomer is divided into two parts and colored in different shades of gray) with constant NBD contact during a transport cycle. ATP (red) binding and hydrolysis to ADP (orange) and inorganic phosphate (yellow) and their release are indicated. **(A-C)** Different steps are grouped chronologically (I-IV). The figure is modified and taken from Szöllősi *et al.* (2018)[91].

the exporters, a general mechanism known as the switch or alternating access model has been proposed[48,93,94]. These two conformations are (i) the OF conformation with closed NBDs that bind two ATP (analogues) between their NBD-NBD interface, and their TMDs forming an extracellular-facing "V" shape (see Figure 5B), and (ii) the IF conformation, where the NBDs are widely separated and the TMDs form an intracellular-facing inverted "V" shape (Figure 5A)[95]. When the protein is in the IF conformation, substrate binds within the TMDs, while ATP binding takes place in the NBDs. This induces a transition to the OF conformation, involving substrate transport to the extracellular membrane surface. ATP hydrolysis resets the transporter, which then switches back to the IF conformation. Figure 6 illustrates the movement of the TMDs during this transport cycle and shows the switch between the IF (I, II, IV) and OF (III) states. Substrate binding occurs at the high-affinity substrate-binding cavity in the IF state from either the cytosolic side or from within the membrane[96]. However, the mechanistic details can be as diverse as the structures, and in the more than 40 years of ABC transporter research, several models describing the transport cycle have been proposed. For simplicity, the different models are discussed below from the perspective of an exporter.

In general, all models can be categorized into two groups. The first group includes the ATP switch model[97], the processive clamp model[76,98,99] and the tweezers-like model[100], and they all have in common that the NBDs are predicted to separate completely during the transport cycle. In contrast, the alternating sites model[101], the constant contact model[102] and the nucleotide occlusion model[103–105] all propose that at least one NBS is constantly present throughout the transport cycle as a consequence of the constant contact of the NBDs. It should be noted that the ATP switch model and the processive clamp model are mainly supported by experimental data gained in analyses of bacterial ABC transporters, whereas data from mammalian ABC transporters mainly support the alternating site, constant contact, or nucleotide occlusion model[91]. Importantly, all these models differ mainly in their view on how NBDs are associated during the transport cycle, while the movement of TMDs is generally accepted and has already been discussed above and in chapter 1.2.1.3.

In the ATP switch model, substrate binding is the initial step of the transport cycle and precedes the power strokes to avoid futile energy loss[106]. The actual power stroke is assumed to be the NBD dimerization upon ATP binding, whose activation energy is reduced by substrate binding[97]. Binding of two ATP molecules occurs in a cooperative manner, and, depending on the transporter itself, binding of the first ATP can either occur statistically or one NBS has a higher ATP binding affinity[107,108]. The respective conformational changes of both NBDs, after the formation of a closed NBD dimer, lead to conformational changes in the TMDs, followed by the release of the substrate. Finally, ATP is hydrolyzed, and the sequential release of ADP and P_i leads to dissociation of the NBDs and restoration of the basal transporter conformation[97]. The processive clamp model is very similar to the ATP switch model and was proposed based on experiments with Rad50, a

mechanoenzyme involved in DNA repair that also possesses an ATPase domain and shows similarities to ABC transporters[109,110]. Both models involve a complete separation of the NBDs during the transport cycle, as shown in Figure 6B. The same applies to the tweezer-like model originally proposed for $MalFGK_2$, which describes the transport cycle of mainly importers, including their respective SBPs. In the ground state, the NBDs are semi-open dimers, and the translocation pathway is open from the cytosolic side[91,100]. Binding of a loaded SBP to the ABC transporter triggers major conformational changes in the TMD and NBD, facilitating substrate transfer to the transporter and additionally stimulating ATP hydrolysis in the now fully closed NBDs. Finally, the SBP dissociates from the transporter through a rocking motion, opening the substrate-binding cavity on the cytosolic side. Thus, the NBDs play a direct role in substrate translocation[93].

Another model that has been proposed for the transport of ABC transporters is the alternating site model. This model was first proposed for the well-studied permeability glycoprotein (P-gp) in 1995[101]. The unique feature of this model is that the NBDs operate alternately. One NBD undergoes ATP hydrolysis only after ATP has been bound to the other NBD, and *vice versa*[93,101]. Consequently, the NBDs are constantly associated and do not completely dissociate from each other, as shown in Figure 6C. This requires that the resulting reaction intermediates should be asymmetric to provide some "memory" of which site was last catalytically active[105]. The constant contact of the NBDs is also the core of the constant contact model proposed on the basis of molecular dynamic (MD) simulations of NBD dimers[102]. Here, nucleotides in different states during hydrolysis continuously occupy the NBDs during substrate transport. The nucleotide occlusion model goes one step further. In this model, after ATP has bound to an NBD dimer, a rapid transition occurs and an ATP molecule is completely occluded at the NBS. The consequences of the asymmetric occlusion are conformational changes that are transmitted to the TMDs[103–105].

1.2.3 Human ABC transporters

The human genome encodes 48 putative ABC transporters that are evolutionarily highly conserved between species. Based on gene structure, sequence homology, and domain order, they are classified into seven subfamilies ranging from A to G[41]. However, the classification given in chapter 1.2.1 is still valid, and it has been suggested to use the subfamily nomenclature as subcategories of type IV (subfamilies B–D) and type V (subfamilies A and G)[43]. Members of the ABCA subfamily are full-transporters and are among the largest known ABC transporters. They are primarily involved in lipid/cholesterol homeostasis[32,38]. Probably the most divergent group is the ABCB subfamily, which includes full- and half-transporters that transport diverse substrates. These transporters are therefore involved in various cellular processes, such as cellular detoxification, antigen presentation, and iron metabolism[32,41,42]. The members of the ABCC

subfamily are all full-transporters. Almost all of them transport multiple hydrophobic drugs, and ABCC transporters are therefore collectively classified as MDR-associated proteins (MRPs)[111]. However, three members are (non-)directly involved in ion transport[32,42]. A unique feature of the ABCC subfamily is the existence of an additional domain (TMD0). The general function of this domain is still unclear[42]. The subfamily with the fewest members, ABCD, consists of four representatives, from which ABCD1-ABCD3 transport long-chain fatty acids from the cytosol into peroxisomes, and ABCD4 transports cobalamin/vitamin B12 from lysosomes into the cytosol[112,113]. The ABCG half-transporters are structurally unique, as they have an inverted domain arrangement with an N-terminal NBD followed by a C-terminal TMD[32,42]. Physiologically, ABCG members are involved in multidrug transport or sterol/lipid homeostasis[32]. Notably, members of the ABCE and ABCF subfamilies are not transporters, as they lack the transmembrane domains and are instead involved in ribosome modulation[114,115].

Several human ABC transporters are associated with human diseases, but only a few relevant examples will be mentioned here. For example, mutations in the ABCA1-encoding gene involved in cholesterol transport and high density lipoprotein (HDL) biosynthesis lead to Tangier disease, a genetic disorder of lipoprotein metabolism[38]. Another example is ABCB1, which is expressed in several blood-organ barriers and plays an essential role in cellular detoxification[32,116–118]. This full-transporter is polyspecific, *i.e.,* it transports various hydrophobic compounds, including therapeutic drugs, alkaloids, flavonoids, etc., and it provides mainly a protective mechanism against xenobiotics. The protein also known as MDR protein 1 or P-gp has been intensively studied in recent decades due to its contribution to the acquired MDR of cancer cells in response to chemotherapeutic intervention[41,119]. Lastly, the cystic fibrosis transmembrane receptor (CFTR/ABCC7) protein is not a canonical ABC transporter, as it functions as a chloride ion channel[120]. Structurally, it has a unique regulatory domain (R) between the two halves of the protein (TMD1-NBD1-R-TMD2-NBD2) and (de)phosphorylation of the R domain regulates the channel function[32,42]. CFTR plays a role in fluid homeostasis and exocrine secretion[120,121]. Different sets of mutation(s) in the *CFTR* gene result in cystic fibrosis, mainly affecting the lungs and the digestive system[122].

1.2.4 Bacillus multidrug resistance ATP (BmrA)

In 2003, the gene *YvcC* was identified to code for a multidrug-like ABC transporter, among 38 other genes encoding putative ABC transporters in the Gram-positive bacterium *Bacillus subtilis* (*B. subtilis*)[123,124]. It is closely homologous to *Lactococcus* multidrug resistance ATP (LmrA) and both halves of the human P-gp[124,125]. Because of the relation to LmrA, the transporter was renamed to *Bacillus* multidrug resistance ATP (BmrA). The coding gene is constitutively expressed in the *B. subtilis* wild-type (wt) strain[123,124]. Physiologically, BmrA contributes *in vivo* to the resistance to

cervimycin C, an antibiotic produced by *Streptomyces tandæ* against Gram-positive bacteria[126]. In contrast, from a pathological perspective, BmrA may be involved in MDR and antibiotic resistance in pathogenic strains[123,124]. Yet, BmrA transports several hydrophobic drugs across membranes, including Hoechst 33342, ethidium, doxorubicin, 7-aminoactinomycin D, and mitoxantrone (an analog of vinblastine)[123,124].

Over the last 20 years, BmrA has become an excellent model to study the structure and function of ABC transporters and their role in MDR. Especially in recent years, a series of structural and biophysical studies using single-particle cryo-electron microscopy (cryo-EM), X-ray crystallography, nuclear magnetic resonance (NMR) spectroscopy, H/D exchange coupled with mass spectrometry (HDX-MS), electron paramagnetic resonance (EPR) spectroscopy, small-angle neutron scattering (SANS), etc. have given structural and mechanistic insights into the function of ABC transporters like BmrA. Due to its broad substrate spectrum, BmrA exhibits intrinsic structural plasticity throughout the transport cycle. This is the key element to adapting to the available substrate. Based on cryo-EM and MD simulations, a detailed model of the BmrA

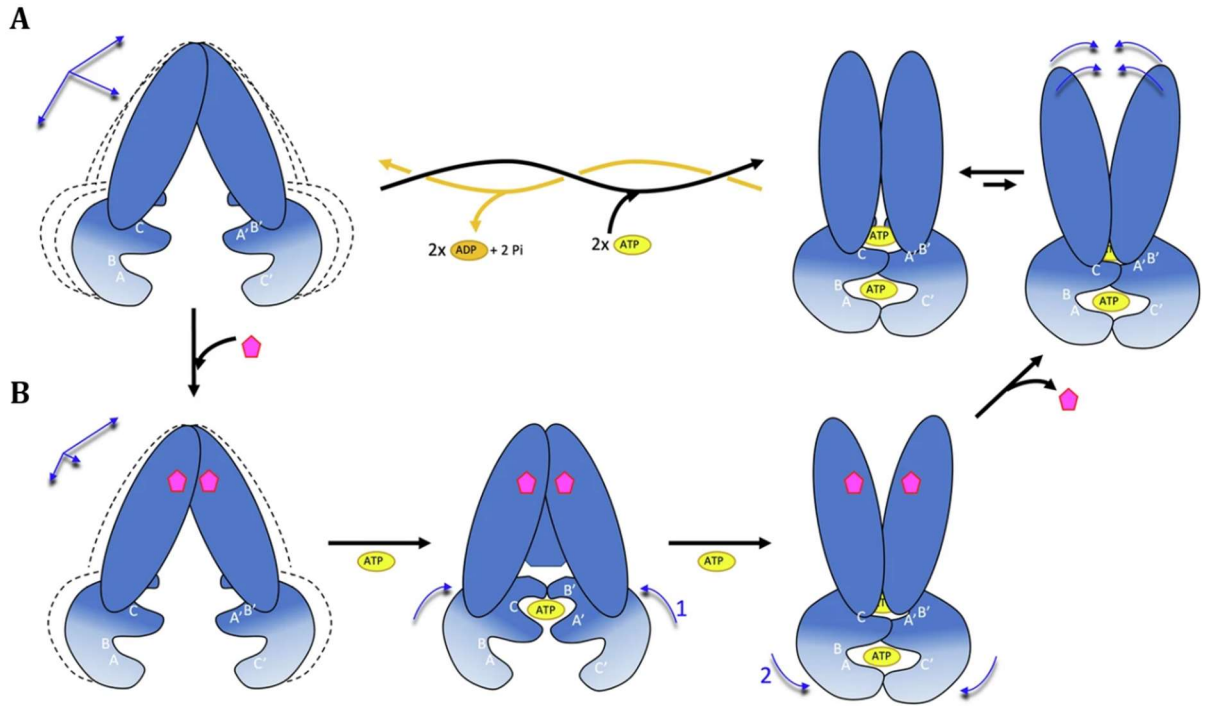

Figure 7: Substrate transport by BmrA.

(A) The IF conformation of BmrA is highly flexible in the absence of substrate, indicated by blue arrows. Binding of two molecules of ATP (yellow) between the Walker A (A/A') and Walker B (B/B') motifs of one monomer and the ABC signature motif (C/C') of the opposite monomer leads to the transfer of the structural plasticity to the outer part of the TMDs. ATP hydrolysis to ADP (orange) and inorganic phosphate (P_i) brings the transporter back to the (flexible) IF conformation. **(B)** In the presence of a substrate (pink), the flexibility of the transporter in the IF conformation is reduced. ATP binding occurs in an asymmetric, cooperative manner, and after binding of the second ATP molecule, the OF conformation is reached. Substrate release is achieved by the structural changes of the external part of the TMDs. ATP hydrolysis is used to set the transporter back to the IF conformation. The figure is modified and taken from Gobet *et al.* 2025[127].

transport mechanism was proposed in early 2025[127], which is shown in Figure 7. In the absence of a bound substrate, BmrA is in the IF conformation and structurally flexible, especially in the NBDs, as e.g., observed by NMR spectroscopy, HDX-MS, and SANS studies[128–130]. This structural plasticity allows the transporter to adopt different conformations in order to bind different substrates. After binding a substrate, the NBDs move closer together as the flexibility of the transporter is allosterically reduced. Consistent with solid-state NMR spectroscopy results, an NBS is first formed, and a molecule of ATP is bound between the two NBDs, followed by the binding of a second molecule in a positive cooperative manner, and finally the OF conformation is reached[131]. Structural changes of the external part of the TMDs lead to substrate release without the need of ATP hydrolysis, which has also been proposed for other ABC transporter[80,132,133]. Finally, ATP hydrolysis returns the transporter to the IF conformation. Importantly, this model includes that the allosteric effect of substrate binding to ATP-Mg^{2+} binding depends on the ATP concentration. At high ATP concentrations, ATP binding and hydrolysis are mainly uncoupled from substrate transport, allowing the transporter to rapidly switch between the IF and OF conformations. Thus, if a drug has been bound during the transport cycle, it will be translocated (Figure 7A). However, at low ATP concentrations, e.g., *in vivo* during starvation or sporulation[134,135], allosteric stimulation of the ATPase activity by substrate-binding helps to efficiently cope with limited ATP availability (Figure 7A)[127,136].

2 Objectives of this thesis

ABC transporters play a significant role in the highly regulated transport of molecules across biological membranes. Understanding the molecular mechanisms underlying their structure and function helps to better understand the fundamental principles of membrane transport and is of great clinical and biomedical relevance. For example, malfunctions of human ABC transporters are associated with diseases, such as cystic fibrosis and Alzheimer's disease[20,35–39]. Furthermore, an overexpression of ABC transporters in cancer cells and pathogenic bacteria contributes to MDR[41,119,123,124].

The bacterial exporter BmrA of *B. subtilis* shares structural similarity with the clinically relevant homolog P-gp and serves as a well-established model system for studying type IV ABC transporters[123–125]. Within the scope of this work, BmrA was studied to gain deeper insight into specific molecular determinants that regulate the transporter function, including the influence of the lipid environment, the role of defined helices, and the mechanisms of interdomain communication.

1) Influence of the lipid environment

It is well known that lipids and membrane properties can influence the structure and activity of membrane proteins. However, the impact of the native membrane environment is often neglected in *in vitro* studies. In the case of BmrA, different basal ATPase activities are observed in different membrane environments. This indicates that the physico-chemical properties of the lipid environment critically affect the protein's function.[40,124,137,138]. Thus, a systematic *in vitro* analysis of BmrA reconstituted into proteoliposomes with defined lipid compositions was performed to identify lipid- and membrane-specific effects.

2) Functional role of the C-terminal α-helix

A prerequisite for a functional transport cycle is the dimerization of the NBDs upon ATP binding. In some ABC transporters, the stability of the NBD-NBD dimer is believed to be supported by α-helices located at the C-terminal ends, among other factors[92,139,140]. However, the precise structural and functional role of these C-terminal helices remains unclear. This study aimed at investigating the C-terminal α-helix of BmrA via site-directed mutagenesis of the coding gene to assess its importance for transporter function.

3) Identification of structural elements stabilizing the NBD-TMD interface

The cytosolic linker of BmrA connecting the NBD and TMD is in the immediate vicinity of both CHs of BmrA. For many ABC transporters, the CH(s) are known to be key elements in NBD-TMD cross-

talk during the transport cycle[88,90,141–144] However, the stabilization of the CHs in the transporter's structure and their interaction with the transporter's remaining parts remain poorly understood. Through a combination of mutational analysis of the linker region and functional assays, we assessed the linker region's impact on stabilizing the NBD-TMD interface. Additionally, cryo-EM analyses were performed to study the structural alterations of a BmrA variant.

3 Materials and Methods

3.1 Materials

3.1.1 Chemicals

All chemicals used during the course of the thesis were either purchased from AppliChem GmbH (Darmstadt, GER), Carl Roth GmbH + Co. KG (Karlsruhe, GER), Merck KGaA (Darmstadt, GER), New England Biolabs (Ipswich, MA, USA), Thermo Fisher Scientific Inc. (Waltham, MA, USA), or VWR International GmbH (Darmstadt, GER).

3.1.2 Phospholipids

The *Escherichia coli (E. coli)* polar lipid (EPL) extract and all phospholipids were purchased from Avanti Polar Lipids, Inc (Birmingham, AL, USA). EPL contains 67.0% PE, 23.2% PG and 9.8% CL.

Table 3.1: IUPAC nomenclature and abbreviation of phospholipids used in this study.

IUPAC nomenclature of phospholipids	Abbreviation
1,2-dioleoyl-sn-glycero-3-phosphocholine	DOPC (18:1PC)
1,2-dioleoyl-sn-glycero-3-phospho-(1'-rac-glycerol)	DOPG (18:1PG)
1,2-dioleoyl-sn-glycero-3-phospho-L-serine	DOPS (18:1PS)
1,2-dioleoyl-sn-glycero-3-phosphoethanolamine	DOPE (18:1PE)
1',3'-bis[1,2-dioleoyl-sn-glycero-3-phospho]-glycerol	CL
1,2-dimyristoleoyl-sn-glycero-3-phosphocholine	14:1PC
1,2-dipalmitoleoyl-sn-glycero-3-phosphocholine	16:1PC
1,2-dieicosenoyl-sn-glycero-3-phosphocholine	20:1PC
1,2-dierucoyl-sn-glycero-3-phosphocholine	22:1PC
1-palmitoyl-2-oleoyl-glycero-3-phosphocholine	POPC (16:0-18:1PC)

3.1.3 Buffers, solutions, and media

All buffers, solutions, and media were prepared with deionized water, unless otherwise stated.

Table 3.2: Composition of the buffers, solutions, and media used in this study.

Buffer/solution/media	Composition
Buffer	

6x DNA loading dye	0.2% Bromophenol blue (w/v) 0.2% Xylencyanol (w/v) 50% Glycerol (v/v)
TAE buffer	40 mM Tris-(hydroxymethyl)-aminomethane-hydrochloride (Tris-HCl) 20 mM Acetic acid 1 mM Ethylenediamine tetraacetate (EDTA)-Na_2 pH = 8.3
5x B7 reaction buffer	15 mM $MgCl_2$ 5 mM Deoxynucleoside triphosphates (dNTPs) Enhancer Stabilizer
1.33x Gibson assembly mix	26.7% (v/v) 5x Isothermal reaction mix 25 U/ml Phusion®HF Deoxyribonucleic acid (DNA) polymerase 4 U/ml T5 exonuclease 4 U/ml *Taq* DNA ligase
5x Isothermal reaction mix	500 mM Tris-HCl 50 mM $MgCl_2$ 1 mM dNTPs 50 mM Dithiothreitol (DTT) 250 mg/mL Polyethylene glycol (PEG)-8000 5 mM Oxidized nicotinamide adenine dinucleotide (NAD^+) pH = 7.5
Tris-A buffer	50 mM Tris-HCl 5 mM $MgCl_2$ 1 mM DTT 1 mM Phenylmethylsulfonyl fluoride (PMSF) pH = 8.0
Tris-B buffer	50 mM Tris-HCl 1.5 mM EDTA-Na_2 1 mM DTT 1 mM PMSF pH = 8.0
Tris-C buffer	20 mM Tris-HCl 300 mM Sucrose 1 mM EDTA-Na_2 pH = 8.0
Tris-T buffer	20 mM Tris-HCl 1 mM EDTA-Na_2 pH = 8.0
Phosphate buffer	50 mM Na_2HPO_4/NaH_2PO_4 150 mM NaCl 10% Glycerol (v/v) pH = 8.0
NBD-washing buffer	50 mM Na_2HPO_4/NaH_2PO_4 10 mM Imidazole
NBD-elution buffer	50 mM Na_2HPO_4/NaH_2PO_4 400 mM Imidazole
Salt-free phosphate buffer	50 mM Na_2HPO_4/NaH_2PO_4 10% Glycerol (v/v) pH = 8.0

High-salt phosphate buffer	50 mM Na_2HPO_4/NaH_2PO_4 1 M NaCl 10% Glycerol (v/v) pH = 8.0
Solubilization buffer	5% Dodecyl-β-D-maltoside (DDM) (w/v) 50 mM Na_2HPO_4/NaH_2PO_4 150 mM NaCl 10% Glycerol (v/v) pH = 8.0
Washing buffer 1	50 mM Na_2HPO_4/NaH_2PO_4 150 mM NaCl 10% Glycerol (v/v) 10 mM Imidazole pH = 8.0
Washing buffer 2	50 mM Na_2HPO_4/NaH_2PO_4 150 mM NaCl 10% Glycerol (v/v) 35 mM Imidazole pH = 8.0
Washing buffer 3	50 mM Na_2HPO_4/NaH_2PO_4 150 mM NaCl 10% Glycerol (v/v) 45 mM Imidazole pH = 8.0
Elution buffer	50 mM Na_2HPO_4/NaH_2PO_4 150 mM NaCl 10% Glycerol (v/v) 400 mM Imidazole pH = 8.0
5x SDS-polyacrylamide gel electrophoresis (SDS-PAGE) sample buffer	0.25 M Tris-HCl 10% Sodium dodecyl sulfate (SDS) (w/v) 0.2% Bromophenol blue 50% Glycerol (v/v) 0.5 M DTT pH = 6.8
SDS running buffer	25 mM Tris-HCl 0.2 M Glycine 0.1% SDS (w/v) pH = 8.3
Coomassie staining solution	0.125% Coomassie Brilliant Blue R-250 (w/v) 40% Ethanol (v/v) 2% Phosphoric acid (v/v)
Coomassie destaining solution	30% Ethanol (v/v) 2% Phosphoric acid (v/v)
4x Blue native-polyacrylamide gel electrophoresis (BN-PAGE) sample buffer	50 mM Bis-(2-hydroxyethyl)-amino-tris-(hydroxymethyl)-methane (BisTris) 6 N HCl 50 mM NaCl 10% Glycerol (w/v) 0.001% Ponceau S (w/v) pH = 7.2
Coomassie sample additive	5% Coomassie Brilliant Blue R-250 (w/v)
Cathode buffer	50 mM BisTris 50 mM Tricine

	pH = 6.8
Anode buffer	50 mM BisTris 50 mM Tricine 0.02% Coomassie Brilliant Blue R-250 (w/v) pH = 6.8
Fixation buffer	40% Methanol (v/v) 10% Acetic acid (v/v)
Coomassie N-staining solution	0.02% Coomassie Brilliant Blue R-250 (w/v) 30% Methanol (v/v) 10% Acetic acid (v/v)
Coomassie N-destaining solution	8% Acetic acid (v/v)
Reconstitution buffer	50 mM Tris-HCl 300 mM NaCl 0.5 mM DDM pH = 8.0
Rehydration buffer	50 mM Tris-HCl pH = 8.0
Reaction buffer	50 mM 4-(2-hydroxyethyl)-1-piperazineethanesulfonic acid (Hepes)-KOH pH = 8.0
Reaction-D buffer	50 mM Hepes-KOH 5 mM DDM pH = 8.0
Labeling buffer	50 mM Hepes-KOH 50 mM DTT pH = 8.0
Stock/working solutions	
Ampicillin solution	100 mg/mL Na_2-Ampicillin in 50% ethanol (v/v)
IPTG solution	1 M Isopropyl-β-D-thiogalacto-pyranoside (IPTG)
PMSF solution	0.1 M PMSF in 2-propanol
EDTA solution	1 M EDTA-Na_2 pH = 8.0
ATP solution	100 mM Na_2-ATP pH = 8.0
Orthovanadate solution	100 mM Na_3VO_4 pH = 10.0
$MgCl_2$ solution	500 mM $MgCl_2$
DTT solution	500 mM DTT
Triton™ X-100 solution	1% Triton™ X-100 (v/v)
SDS solution	4% SDS
SNAP-Surface substrate stock solution	1 mM SNAP-Surface® Alexa Fluor® 488 in Dimethyl sulfoxide (DMSO)
SNAP-Surface substrate working solution	250 µM SNAP-Surface® Alexa Fluor® 488 in DMSO
SNAP-Cell substrate stock solution	1 mM SNAP-Cell® 647-SiR in DMSO
SNAP-Cell substrate working solution	250 µM SNAP-Cell® 647-SiR in DMSO

NADH solution	14 mM Reduced nicotinamide adenine dinucleotide (NADH) in 0.1 M Tris-HCl buffer pH = 8.0
PEP solution	60 mM Phosphoenolpyruvate (PEP)
PhEtOH solution	100 mM 2-Phenylethanol (PhEtOH)
Laurdan solution	0.01 mg/mL Laurdan in $CHCl_3$
Hoechst solution	0.1 mM 2'-[4-ethoxyphenyl]-5-[4-methyl-1-piperazinyl]-2,5'-bis-1H-benzimidazole (Hoechst 33342)
ThT solution	50 µM Thioflavin T (ThT)
Media	
Lysogeny broth (LB)-medium	1% Tryptone (w/v) 0.5% Yeast extract (w/v) 1% NaCl (w/v)
LB^{Amp}-medium	100 µg/mL Na_2-Ampicillin in LB medium
LB-agar	1.5% Agar (w/v) in LB medium
LB^{Amp}-agar	1.5% Agar (w/v) in LB^{Amp} medium
Tryptic Soy Broth (TSB)-medium	10% PEG4000 (w/v) 5% DMSO (v/v) 2% 1 M $MgCl_2$ (v/v) 1% Tryptone (w/v) 0.5% Yeast extract (w/v) 0.5% NaCl (w/v)

3.1.4 Bacterial strains

Table 3.3: Bacterial strains used in this study and their genotype and manufacturers.

Bacteria	Genotype	Manufacturer
E. coli NEB Turbo	F' *proA⁺B⁺ lacI^q ΔlacZM15 / fhuA2 Δ(lac-proAB) glnV galK16 galE15 R(zgb-210::Tn10)*Tet^S *end*A1 *thi-1 Δ(hsdS-mcrB)5*	New England Biolabs GmbH (Ipswich, MA, USA)
E. coli C41(DE3)	F^- *ompT hsdS$_B$ (r_B-m_B-) gal dcm* (DE3)	Merck KGaA (Darmstadt, GER)

3.1.5 Plasmids

All plasmids used in this study are summarized in Table 3.4. For the overexpression of proteins in *E. coli,* the pET303 vector was used, which contains an ampicillin resistance cassette. The vector cards of pET303-CT/His-BmrA-wt and pET303-CT/His-BmrA-SNAP-tag are shown in Figure A1/A2 and were created with the Benchling software.

Table 3.4: Plasmids used in this study.

Plasmid	Origin
pET303-CT/His	Invitrogen (Carlsbad, CA, USA)
pET303-CT/His-BmrA-wt	[redacted] (2022)
pET303-CT/His-BmrA-NBD	AG Schneider
pSNAP-tag (T7)-2 vector	New England Biolabs GmbH (Ipswich, MA, USA)
pET303-CT/His-BmrA-SNAP-tag	This work
pET303-CT/His-BmrA-K4A-K5A-K7A-K9A-K11A-K13A-R20A-R21A (8xM)	This work
pET303-CT/His-BmrA-ΔCT	[redacted] (2022)
pET303-CT/His-BmrA-ΔCTh	[redacted] (2022)
pET303-CT/His-BmrA-L569A	[redacted] (2022)
pET303-CT/His-BmrA-Y570A	[redacted] (2022)
pET303-CT/His-BmrA-R571A	[redacted] (2022)
pET303-CT/His-BmrA-D572A	[redacted] (2022)
pET303-CT/His-BmrA-F573A	[redacted] (2022)
pET303-CT/His-BmrA-A574V	[redacted] (2022)
pET303-CT/His-BmrA-E575A	[redacted] (2022)
pET303-CT/His-BmrA-Q576A	[redacted] (2022)
pET303-CT/His-BmrA-Q577A	[redacted] (2022)
pET303-CT/His-BmrA-L578A	[redacted] (2022)
pET303-CT/His-BmrA-K579C	[redacted] (2022)
pET303-CT/His-BmrA-M580C	[redacted] (2022)
pET303-CT/His-BmrA-N581C	[redacted] (2022)
pET303-CT/His-BmrA-A582C	[redacted] (2022)
pET303-CT/His-BmrA-D583C	[redacted] (2022)
pET303-CT/His-BmrA-NBD-L239A	AG Schneider
pET303-CT/His-BmrA-NBD-Y240A	AG Schneider
pET303-CT/His-BmrA-NBD-R241A	AG Schneider
pET303-CT/His-BmrA-NBD-D242A	AG Schneider
pET303-CT/His-BmrA-NBD-F243A	AG Schneider
pET303-CT/His-BmrA-NBD-A244V	AG Schneider
pET303-CT/His-BmrA-NBD-E245A	AG Schneider
pET303-CT/His-BmrA-NBD-Q246A	AG Schneider
pET303-CT/His-BmrA-NBD-Q247A	AG Schneider

pET303-CT/His-BmrA-NBD-L248A	AG Schneider
pET303-CT/His-BmrA-E323A	This work
pET303-CT/His-BmrA-E324A	This work
pET303-CT/His-BmrA-E325A	This work
pET303-CT/His-BmrA-E326A	This work
pET303-CT/His-BmrA-D327A	This work
pET303-CT/His-BmrA-T328A	This work
pET303-CT/His-BmrA-K109A	This work
pET303-CT/His-BmrA-K217A	This work
pET303-CT/His-BmrA-R389A	This work
pET303-CT/His-BmrA-R414A	This work
pET303-CT/His-BmrA-E326D	This work

3.1.6 Oligonucleotides

All oligonucleotides used in this study for cloning are listed in Table 3.5 and were purchased from Merck/Sigma-Aldrich Chemie GmbH (Taufkirchen, GER).

Table 3.5: Oligonucleotides used in this study. Fw=forward, re=reverse.

Primer	5‘-Sequence-3‘
Cloning of pET303-CT/His-BmrA-SNAP-tag	
pET303-CT/His-BmrA-fw	GCAGGCGGATCCCCCGGGCTCGAGGTTAATGAATTCC ACCACCACCAC
pET303-CT/His-BmrA-re	CTTAGAAAACAAAGCCGGGGGTGGAAGTGACAAAGAT TGCGAAATG
pSNAP-tag (T7)-2-fw	AACAAAGCCGGGGGTGGAAGTGGAGGATCAGACAAA GATTGCGAAATGAAAC
pSNAP-tag (T7)-2-re	ATCTCAGTGGTGGTGGTGGTGGAATTCATTAACC TCGAGCCCGGGGGATCC
Cloning of pET303-CT/His-BmrA-8xM	
K4A-fw	CTAGAATGCCAACCGCCGCCCAAGCCTCTGC
K4A-re	GCAGAGGCTTGGGCGGCGGTTGGCATTCTAG
K5A-fw	GCCAACCAAGGCCCAAGCCTCTGCC
K5A-re	GGCAGAGGCTTGGGCCTTGGTTGGC
K7A-fw	CAACCAAGAAACAAGCCTCTGCCAGTGCC
K7A-re	GGCACTGGCAGAGGCTTGTTTCTTGGTTG
K9A-fw	CAAGAAACAAAAATCTGCCAGTGCCTTGGCCC
K9A-re	GGGCCAAGGCACTGGCAGATTTTTGTTTCTTG

K11A-fw	CAAAAATCTAAAAGTGCCTTGGCCCCCTTTTTTG
K11A-re	CAAAAAAGGGGGCCAAGGCACTTTTAGATTTTTG
K13A-fw	CTAAAAGTAAATTGGCCCCCTTTTTTGCCTTAG
K13A-re	CTAAGGCAAAAAAGGGGGCCAATTTACTTTTAG
R20A-fw	CTTTTTTGCCTTAGTAGCCCGGACCAATCCTTC
R20A-re	GAAGGATTGGTCCGGGCTACTAAGGCAAAAAAG
R21A-fw	CTTTTTTGCCTTAGTAGCCGCCACCAATCCTTCTTATG
R21A-re	CATAAGAAGGATTGGTGGCGGCTACTAAGGCAAAAAAG
Cloning of single mutants	
E323A-fw	GAGATTTTGGCAGCGGAAGAGGAAGATACAGTG
E323A-re	CACTGTATCTTCCTCTTCCGCTGCCAAAATCTC
E324A-fw	GAGATTTTGGCAGAGGCGGAGGAAGATACAGTG
E324A-re	CACTGTATCTTCCTCCGCCTCTGCCAAAATCTC
E325A-fw	GATTTTGGCAGAGGAAGCGGAAGATACAGTGACAG
E325A-re	CTGTCACTGTATCTTCCGCTTCCTCTGCCAAAATC
E326A-fw	GGCAGAGGAAGAGGCGGATACAGTGACAGG
E326A-re	CCTGTCACTGTATCCGCCTCTTCCTCTGCC
D327A-fw	GAGGAAGAGGAAGCGACAGTGACAGGAAAAC
D327A-re	GTTTTCCTGTCACTGTCGCTTCCTCTTCCTC
T328A-fw	GAGGAAGAGGAAGATGCGGTGACAGGAAAAC
T328A-re	GTTTTCCTGTCACCGCATCTTCCTCTTCCTC
K109A-fw	GAAGAAATTAATTGCGCTGCCTGTCTCTTATTTC
K109A-re	GAAATAAGAGACAGGCAGCGCAATTAATTTCTTC
K217A-fw	GAAATCAGACTTGTTGCGGCTTCAAATGCGG
K217A-re	CCGCATTTGAAGCCGCAACAAGTCTGATTTC
R389A-fw	GTTTAAGCTGCTTGAAGCGTTTTATTCTCCGAC
R389A-re	GTCGGAGAATAAAACGCTTCAAGCAGCTTAAAC
R414A-fw	CTTGAATCGTGGGCAGAGCATATCGGGTATGTATC
R414A-re	GATACATACCCGATATGCTCTGCCCACGATTCAAG
E326D-fw	GATTTTGGCAGAGGAAGAGGATGATACAGTGACAGG
E326D-re	CCTGTCACTGTATCATCCTCTTCCTCTGCCAAAATC

3.1.7 Protein and DNA standards

Table 3.6 Protein and DNA standards used in this study.

Marker	Manufacturer

Thermo Scientific™ O'GeneRuler 1 kb DNA Ladder	Thermo Fisher Scientific (Waltham, MA, USA)
Unstained Protein-Molecular Weight Marker	Thermo Fisher Scientific (Waltham, MA, USA)
The Amersham High Molecular Weight Calibration Kit for native electrophoresis	GE Healthcare (Munich, GER)

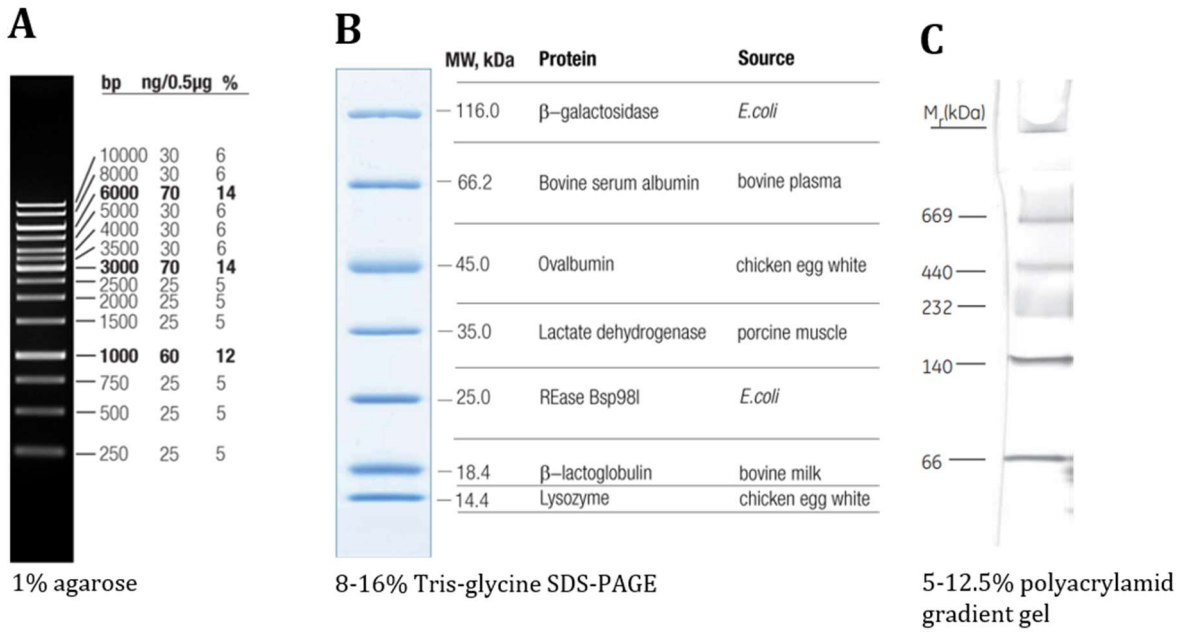

Figure 8: Protein and DNA standards.

(A) Thermo Scientific™ O'GeneRuler 1 kb DNA Ladder Marker. **(B)** Unstained Protein-Molecular Weight Marker. **(C)** Amersham High Molecular Weight Calibration Kit for native electrophoresis. The illustrations were modified and taken from the manufacturers User Guides.

3.1.8 Enzymes and kits

Table 3.7: Enzymes and kits used in this study and their application.

Enzyme/ Kit	Application	Manufacturer
Enzyme		
Biozym B7 High Fidelity DNA Polymerase	Polymerase chain reaction	Biozym Scientific GmbH (Hessisch Oldendorf, GER)
Phusion®HF DNA polymerase	Gibson assembly	New England Biolabs (Ipswich, MA, USA)
T5 exonuclease	Gibson assembly	New England Biolabs (Ipswich, MA, USA)
Taq DNA Ligase	Gibson assembly	New England Biolabs (Ipswich, MA, USA)
*Dpn*I restriction endonuclease	Cloning	New England Biolabs (Ipswich, MA, USA)
Trypsin from bovine pancreas	Limited proteolysis by Trypsin	Sigma-Aldrich Chemie GmbH (Taufkirchen, GER)

Pyruvate kinase/lactic dehydrogenase (PK/LDH) mix	ATPase activity assay	Sigma-Aldrich Chemie GmbH (Taufkirchen, GER)
Kit		
NucleoSpin™ Plasmid kit	Plasmid preparation	Macherey-Nagel™ (Düren, GER)
Pierce™ bicinchoninic acid (BCA) protein assay kit	Determination of protein concentration	Thermo Fisher Scientific (Waltham, MA, USA)
The Amersham High Molecular Weight Calibration Kit for native electrophoresis	Blue native PAGE	GE Healthcare (Munich, GER)

3.1.9 Consumables

Table 3.8: Consumables used in this study

Consumables	Manufacturer
Amicon® Zentricon 30/50 kDa molecular weight cut-off (MWCO)	Merck KGaA (Darmstadt, GER)
Disposable PD 10 Desalting Columns	GE Healthcare (Munich, GER)
Superose 12 10/300 GL column	Cytiva (Freiburg, GER)
Q Sepharose Fast Flow column material	Cytiva (Freiburg, GER)
4 to 16% Bis-Tris polyacrylamide gels	Invitrogen (Carlsbad, CA, USA)
Bio-Beads™ SM-2	Bio-Rad (Munich, GER)

3.1.10 Instruments

Table 3.9: Instruments used in this study.

Instrument	Model	Manufacturer
Circular dichroism (CD) spectrometer	J-1500	JASCO cooperation (Tokyo, JPN)
CD spectrometer temperature controller	MTPC-490S	JASCO cooperation (Tokyo, JPN)
Centrifuge	Avanti J-26XP	Beckmann Coulter (Krefeld, GER)
	Centrifuge 5424	Eppendorf (Hamburg, GER)
	Centrifuge 5415 R	Eppendorf (Hamburg, GER)
	Centrifuge 5810 R	Eppendorf (Hamburg, GER)
	OptimaTM L-100K Ultracentrifuge Sprout	Beckmann Coulter (Krefeld, GER)
	OptimaTM MAX-XP ultracentrifuge	Beckmann Coulter (Krefeld, GER)
Electrophoresis chamber	Mini-Protean 3 Cell	Bio-Rad (Munich, GER)
	PerfectBlue Gelsystem S, M, L	VWR International GmbH (Darmstadt, GER)
	XCell™ SureLock™ Mini-Cell	Invitrogen (Carlsbad, CA, USA)
Electrophoresis power supply	PowerPac Basic	Bio-Rad (Munich, GER)
	PeqPower 300	PeqLab (Erlangen, GER)

Fluorescence spectrometer	FluoroMax-4	Horiba Instruments Inc. (Edison, USA)
Gel documentation	Quantum-ST4 1100/26MX	VWR International GmbH (Darmstadt, GER)
Gel filtration	ÄKTA purifier 10	GE Healthcare (Munich, GER)
Gel scanner	ViewPix 700 Typhoon Trio +	Biostep GmbH (Burkhardtsdorf, GER) Amersham Biosciences (Amersham, GBR)
Heating block	Thermomixer comfort	Eppendorf SE (Hamburg, GER)
High pressure homogenizer	Maximator®	Maximator GmbH (Nordhausen, Germany)
Incubator	B28 Multitron HT	Binder GmbH (Tuttlingen, GER) Infors AG (Bottmingen, CHE)
Overhead shaker	CMV-ROM	Labortechnik Fröbel GmbH (Lindau, GER)
pH-meter	pH211 Microprocessor	Hanna Instruments GmbH (Vöhringen, GER)
Photometer	Cary 3500 Multicell UV-Vis Nanodrop 2000C Ultrospec 10- Cell density meter	Agilent (Santa Clara, CA, USA) Thermo Fisher Scientific Inc. (Waltham, MA, USA) Amersham Biosciences (Amersham, GBR)
Plate Reader	Biotek synergy LX multi-mode reader	Agilent (Santa Clara, CA, USA)
Rotors	JA 25.50 JLA-8.100 Ti 45 MLA-130	Beckmann Coulter (Krefeld, GER) Beckmann Coulter (Krefeld, GER) Beckmann Coulter (Krefeld, GER) Beckmann Coulter (Krefeld, GER)
Stir and heating plate	MR Hei-Standard	Heidolph Instruments GmbH & Co. KG (Schwabach, GER)
Test tube shaker	Vortex shaker	VWR International GmbH (Darmstadt, GER)
Thermocycler	Tgradient 96	Biometra GmbH (Göttingen, GER)

3.1.11 Softwares

Table 3.10: Softwares used in this study.

Software	Application
ChemDraw 16.0	Chemical structures
Microsoft Excel (Office 365)	Data analysis
Origin 2019b	
ImageJ 1.47	
Microsoft PowerPoint (Office 365)	Figure editing
ChimeraX 1.4	Protein structures

Mendeley 1.19.8	Literature management
Clustal Omega	Sequence analysis
Benchling	Vector card visualization
Microsoft Word (Office 365)	Text editing

3.2 Methods

This chapter describes the general procedure for all the methods performed in this thesis. Any modifications are indicated in the relevant chapters. Chapter 3.1 specifies the composition of buffers and solutions and gives the manufactures of the required chemicals, biologicals, and instruments.

The methods performed by the collaboration partner can be found in chapter 6.4.

3.2.1 Molecular biological methods

3.2.1.1 Polymerase chain reaction

To amplify specific DNA fragments for molecular cloning using Gibson assembly (chapter 3.2.1.2) or site-directed mutagenesis (chapter 3.2.1.3), a polymerase chain reaction (PCR) was performed. The composition of a standard PCR sample is listed in Table 3.11. Note that the B7 reaction buffer contains 15 mM $MgCl_2$, 5 mM dNTPs, enhancers, and stabilizers. The PCR temperature program is given in Table 3.12 and was conducted using a Tgradient 96 thermocycler. The exact annealing temperature depends on the primers used and was set 5 °C below their respectively calculated melting temperatures. Amplification was verified by agarose gel electrophoresis. The PCR samples were diluted with 6x DNA loading dye. DNA was separated in TAE buffer on a 1% agarose gel at a voltage of 150 V, stained with ethidium bromide, and visualized under UV light using a Quantum-ST4 1100/26MX.

Table 3.11: Composition of a standard PCR used for site-directed mutagenesis or molecular cloning by Gibson assembly.

Component	Stock concentration	Volume [µL]
DNA template	~100 ng/µL	1
Forward primer	10 µM	2
Reverse primer	10 µM	2
B7 reaction buffer	5x	10
Biozym B7 high fidelity DNA polymerase	2 U/µL	0.5
MP-H_2O		34.5
Total volume		50

Table 3.12: PCR temperature program.

Step	Temperature [°C]	Time [min]	Cycle
Initial denaturation	98	1.0	
Denaturation	98	0.5	

Annealing	50 -72	1.0	17x (site-directed mutagenesis) 30x (Gibson assembly)
Elongation	72	0.5/kb	
Final elongation	72	10	

3.2.1.2 Gibson assembly

The Gibson assembly method was used to generate plasmids with joined DNA fragments from different sources in a single, isothermal reaction[145].

The plasmid pET303-CT-His-BmrA-SNAP-tag, which encodes the BmrA-SNAP-tag fusion protein, was generated by inserting the SNAP-tag sequence from the pSNAP-tag (T7)-2 vector into the target plasmid pET303-CT/His-BmrA between the BmrA and 6xHis-tag sequences. First, the insert and vector sequences were amplified with overlapping ends by PCR using the respective primers. The primers were designed to add an additional short $(GGS)_2$-linker between the BmrA and SNAP-tag sequences. After digesting the amplified PCR products with 0.5 µL *Dpn*I (1 h, 37 °C) the DNA concentration was determined by measuring the absorption at 260 nm using a Nanodrop 2000C. The measured absorption was converted to the DNA concentration using equation 1, pathlength d, and the extinction coefficient of DNA (ε_{DNA}).

$$c_{DNA} = \frac{A_{260\,nm}}{d \cdot \varepsilon_{DNA}} \quad (1)$$

For assembly, 200 ng vector DNA was mixed with the insert DNA at a 1:4 molar ratio and adjusted to 5 µL. Then, 15 µL 1.33x Gibson assembly mix was added, after which the DNA mixture was incubated (30 min, 50 °C). The mixture was then transformed into 200 µL competent *E. coli* NEB Turbos cells, as described in chapter 3.2.2.2. The next day, a single colony was used to inoculate 10 mL LB^{Amp}-medium. The cells were cultivated (6 h, 37 °C, 180 rpm) and finally harvested by centrifugation (2 min, 15,700 g). Plasmids were prepared from the cultivated cells using the NucleoSpin™ Plasmid Kit. Successful cloning was confirmed by DNA sequencing (Eurofins Genomics GmbH (Ebersberg, GER)).

3.2.1.3 Site-directed mutagenesis

BmrA variants carrying single or multiple amino acid replacements were generated by mutating the relevant bases in the pET303-CT/His-BmrA-wt plasmid using site-directed mutagenesis.

First, a PCR was performed using the desired templates and primers. The amplified DNA was then incubated with 0.5 µL *Dpn*I (1 h, 37 °C) to digest the template DNA. Afterwards, 5 µL was used to transform 200 µL competent *E. coli* NEB Turbos cells, as described in chapter 3.2.2.2. Cultivation of a single colony and plasmid preparation were then carried out as described in chapter 3.2.1.2. Successful cloning was confirmed by DNA sequencing (Eurofins Genomics GmbH (Ebersberg, GER)).

3.2.2 Microbiological methods

3.2.2.1 Preparation of chemically competent E. coli cells

Chemically competent *E. coli* cells were prepared according to the protocol of Chung *et al.*[146]. First, the desired *E. coli* cells were plated onto LB-agar plates. A single colony was then used to inoculate 5 mL LB-medium, and the culture was then cultivated (overnight, 37 °C, 180 rpm). The overnight culture was used to inoculate 50 mL fresh LB-medium at a ratio of 1:40 and cultivated (37 °C, 180 rpm) until an optical density at a wavelength of 600 nm (OD_{600nm}) of 0.5-0.6 was reached. Cells were harvested by centrifugation (10 min, 3,220 g) and afterwards resuspended in 5 mL ice-cold TSB-medium. The cell suspension was incubated (on ice, 10 min) and finally, 100 µL aliquots were shock frozen with liquid nitrogen. Competent *E. coli* cells were stored at -80 °C until used.

3.2.2.2 Transformation of competent E. coli cells

The plasmids generated in chapters 3.2.1.2 or 3.2.1.3 were amplified via transformation of *E. coli* NEB Turbo cells with the desired plasmids. *E. coli* C41(DE3) were transformed if heterologous expression of the encoded proteins was aimed for.

Therefore, 1 µL plasmid DNA was added to 100 µL chemically competent *E. coli* cells, and cells were incubated for 10 min on ice. The cells were then heat shocked (90 s, 43 °C) to permeabilize them for DNA uptake and cultured after addition of 500 µL LB medium (1 h, 37 °C, 200 rpm). 200 µL of the bacterial culture was spread onto a LB^{Amp}-agar plate and afterwards incubated (overnight, 37 °C). After successful transformation, bacterial colonies were visible on the LB^{Amp}-agar plate the next day. The plate could be stored at 4 °C for several days.

3.2.2.3 Heterologous expression of BmrA variants

Heterologous overexpression of the recombinant full-length BmrA wt, BmrA variants, soluble NBD wt, or NBD variants was conducted in *E. coli* C41(DE3) cells. Competent cells were

transformed with an expression plasmid encoding the desired protein, as described in chapter 3.2.2.2.

A single transformed colony was used to inoculate 50 mL LB^{Amp}-medium and afterwards the culture was cultivated (overnight, 37 °C, 150 rpm). The overnight culture was then used to inoculate 2 L LB^{Amp}-medium and the fresh culture was cultivated (37 °C, 120 rpm) until an OD_{600nm} of 0.6-0.8 was reached. Protein expression was induced by adding IPTG to a final concentration of 0.7 mM. After induction, the culture was further grown (3-4 h, 37 °C, 120 rpm) and cells were finally harvested via centrifugation (10 min, 4 °C, 1,700 g). If inverted membrane vesicles (IMVs) were to be prepared (chapter 3.2.3.2), the cell pellets were subsequently resuspended in 25 mL Tris-A buffer. For protein extraction and purification (chapter 3.2.3.4), the cells were resuspended in 25 mL phosphate buffer. All cell pellets were stored at -20 °C until use.

3.2.3 Biochemical methods

3.2.3.1 Membrane preparation

The membrane fraction from *E. coli* C41(DE3) cells containing the overexpressed BmrA variants was either isolated to prepare IMVs (chapter 3.2.3.2) or solubilized and purified to produce recombinant proteins (chapter 3.2.3.4).

After heterologous expression, the protease inhibitor PMSF was added to the thawed cells to a final concentration of 0.1 mM. Then, the cells were lysed using a Maximator® by four consecutive passages at 18000 psi. If IMV preparation was intended, a Na-EDTA solution (pH = 8.0) was added to a final concentration of 10 mM. Cell debris and unbroken cells were then removed from the lysate by centrifugation (10 min, 4 °C, 12,075 g). Afterwards the membrane fraction was pelleted from the resulting supernatant by ultra-centrifugation (1 h, 4 °C, 165,000 g). The isolated membrane fraction was either directly used to prepare IMVs (chapter 3.2.3.2) or was resuspended in 10 mL solubilization buffer and stored at -20 °C until the purification process (chapter 3.2.3.4).

3.2.3.2 IMV preparation

The isolated membrane fraction containing the overexpressed proteins was resuspended in 25 mL Tris-B buffer and subsequently pelleted again by ultra-centrifugation (1 h, 4 °C, 165,000 g). The pellet was homogenized using a Potter-Elvehjem homogenizer in 3 mL Tris-C buffer. The total protein concentration of IMVs was determined using a commercially available Pierce™ BCA protein assay kit. Small aliquots were shock-frozen in liquid nitrogen and stored at −80 °C until use.

3.2.3.3 Limited proteolysis by Trypsin

Trypsin proteolysis was conducted on IMVs containing the overexpressed BmrA variants in order to assess the transition from the IF to the OF conformation of the respective variants. In the absence of ligands, BmrA typically adopts the IF conformation, which is characterized by high trypsin accessibility[129,130,147]. In contrast, the OF conformation can be trapped by vanadate in the presence of ligands, resulting in increased resistance to trypsin digestion.

The IMVs were thawed and diluted in Tris–T buffer to a final concentration of 2 µg/µl. Then, the IMVs were incubated in the presence or absence of 2 mM ATP, 1 mM orthovanadate, and 3 mM $MgCl_2$ (15 min, room temperature (= RT)). Prior to proteolysis, a sample was secured and diluted in 5x SDS-PAGE sample buffer. Trypsin digestion was initiated by adding 1 µg of Trypsin per 250 µg IMVs (protein content), and after 2, 5, 15, 30, 60, 120, and 180 min samples for a subsequent SDS-PAGE analysis were taken. Immediately afterwards, Trypsin was inactivated in the SDS-PAGE sample by heating (10 min, 100 °C). Samples were stored at −20 °C until electrophoresis. Digested proteins (16 µg/lane) were separated and analyzed via SDS-PAGE analysis (chapter 3.2.3.6).

3.2.3.4 Purification of BmrA variants

Purification of soluble NBD variants

The cell pellets containing overexpressed wt NBD or variants were thawed, and the protease inhibitor PMSF was added to a final concentration of 1 mM. Then, the cells were lysed using a Maximator® by four consecutive passages at 18000 psi. The lysed cell suspension was then centrifuged to remove cell debris and unbroken cells (10 min, 4 °C, 12,075 g). A volume of 5 mL Ni^{2+}- nitrilotriacetic acid (Ni-NTA) agarose (20% EtOH (v/v)) was equilibrated with phosphate buffer and incubated with the supernatant (1.5 h, RT, overhead agitation). After incubation, the matrix was washed with 25 mL phosphate buffer and 50 mL NBD-washing buffer. The proteins were eluted with 10 mL NBD-elution buffer and then concentrated to a final volume of 2.5 mL using an Amicon® Zentricon (MWCO = 30 kDa). Afterwards, the buffer was exchanged for phosphate buffer using a PD-10 column.

The NBD variants Y240A, R241A, F243A, Q246A, Q247A, and L248A were further purified via size-exclusion chromatography (SEC) using a Superose 12 10/300 GL column on an ÄKTA purifier 10 system. Proteins (500 µL, ~1.5-3 mg/mL) were loaded onto a column equilibrated with phosphate buffer. The flow rate was set to 0.5 mL/min. Main peak fractions were collected and concentrated as described above. Y240A was further purified via anion-

exchange chromatography using a self-packed Q Sepharose Fast Flow column. Salt-free phosphate buffer was used for column equilibration. A volume of 500 µL with a protein concentration of 3-4.5 mg/mL was loaded onto the column. Chromatography was performed at a flow rate of 0.25 mL/min, while the amount of high-salt phosphate buffer was increased stepwise. Protein was finally eluted at a concentration of 100 mM NaCl and concentrated as described above.

Purification of membrane-embedded BmrA variants

Membrane-embedded BmrA variants were extracted and purified from isolated *E. coli* C41(DE3) membranes (chapter 3.2.3.1). First, the frozen membrane pellet in solubilization buffer was diluted with phosphate buffer to a final volume of 50 mL. Membrane proteins were extracted by incubating with the detergent DDM, which was present in the solubilization buffer (1.5 h, RT, overhead agitation). Next, the solubilized proteins were incubated with a volume of 5 mL in phosphate buffer equilibrated Ni-NTA agarose (1.5 h, RT, overhead agitation). After incubation, the Ni-NTA agarose matrix was washed with 25 mL washing buffer 1, 50 mL washing buffer 2, and 35 mL washing buffer 3. Proteins were eluted with 10 mL elution buffer and concentrated using an Amicon® Zentricon (MWCO = 50 kDa) to a final volume of 2.5 mL. Afterwards, the buffer was changed to phosphate buffer using a PD-10 column. For proteoliposome formation, the buffer was exchanged for reconstitution buffer.

After successful purification, proteins were aliquoted and stored at -20 °C until used. Purified proteins and the individual purification steps were analyzed via SDS-PAGE analysis (chapter 3.2.3.6).

3.2.3.5 Determination of protein concentration

The concentration of the purified proteins was determined by measuring their absorption at 280 nm and converting it using the Lambert-Beer law (equation 2), the respective extinction coefficients $\varepsilon_{protein}$, calculated with ExPASy ProtParam[148] (Table 3.13) and the pathlength d.

$$E_{280nm} = \varepsilon_{protein} \cdot c \cdot d \quad (2)$$

Table 3.13: Calculated extinction coefficients and molecular masses of BmrA wt and variants.

Protein	Extinction coefficient [$M^{-1}cm^{-1}$]	Molecular mass [Da]
BmrA wt	38850	65584.27
BmrA-SNAP-tag	60070	86139.79
BmrA 8xM	38850	65071.48
BmrA NBD	15930	29730.69

BmrA TMD	22920	37067.91
BmrA ΔCTh	38850	64727.24
BmrA K579C	38975	65559.24
BmrA M580C	38975	65556.22
BmrA N581C	38975	65573.31
BmrA A582C	38975	65616.33
BmrA D583C	38975	65572.32
BmrA L569A	38850	65542.19
BmrA Y570A	37360	65492.17
BmrA R571A	38850	65499.16
BmrA D572A	38850	65540.26
BmrA F573A	38850	65508.17
BmrA A574V	38850	65612.33
BmrA E575A	38850	65526.24
BmrA Q576A	38850	65527.22
BmrA Q577A	38850	65527.22
BmrA L578A	38850	65542.19
BmrA NBD L239A	15930	29688.61
BmrA NBD Y240A	14440	29638.60
BmrA NBD R241A	15930	29645.59
BmrA NBD D242A	15930	29686.69
BmrA NBD F243A	15930	29654.60
BmrA NBD A244V	15930	29758.75
BmrA NBD E245A	15930	29672.66
BmrA NBD Q246A	15930	29673.64
BmrA NBD Q247A	15930	29673.64
BmrA NBD L248A	15930	29688.61
BmrA E323A	38850	65526.24
BmrA E324A	38850	65526.24
BmrA E325A	38850	65526.24
BmrA E326A	38850	65526.24
BmrA D327A	38850	65540.26
BmrA T328A	38850	65554.25
BmrA K109A	38850	65527.18
BmrA K217A	38850	65527.18
BmrA R389A	38850	65499.16

BmrA R414A	38850	65499.16
BmrA E326A N581C	38975	65515.27
BmrA E326D	38850	65570.25

3.2.3.6 SDS-PAGE

Purified proteins or protein mixtures were separated and analyzed based on their molecular masses in an electric field using an SDS-PAGE[149]. In this study, 10% and 12% SDS-PAGE gels were used to properly analyze full-length BmrA and soluble NBD variants, respectively. The compositions of the separation and stacking gels are given in Table 3.14. Protein samples were diluted in 5x SDS-PAGE sample buffer before electrophoresis. To visualize proteins under non-reducing conditions, DTT was omitted from the sample buffer. Depending on the analysis, 1.5-16 µg of protein were loaded per lane onto the SDS-PAGE gel.

Electrophoresis was performed for 45 min at 200 V in SDS running buffer. After electrophoresis, proteins were stained with Coomassie staining solution (1 h, const. shaking) and subsequently incubated with Coomassie destaining solution (1 h, const. shaking). Typically, the Pierce Unstained Protein MW Marker was used as a protein standard.

Table 3.14: Composition of SDS-PAGE separation and stacking gels.

Ingredient	Separation gel (10%)	Separation gel (12%)	Stacking gel (6%)
H_2O	5 mL	4.5 mL	6
Acrylamid (40%)	2.5 mL	3 mL	1.5 mL
Separation gel buffer	2.5 mL	2.5 mL	-
Stacking gel buffer	-	-	2.5 mL
Ammonium persulfate (APS) (10%)	50 µL	50 µL	50 µL
N,*N*,*N*′,*N*′-Tetramethylethane-1,2-diamine (TEMED)	20 µL	20 µL	20 µL

3.2.3.7 BN-PAGE

Oligomerization of BmrA variants in detergent was analyzed via BN-PAGE. Protein samples were diluted in 4x BN-PAGE sample buffer. For Cys-containing BmrA variants, 0.25 mg/ml of purified proteins was preincubated with a final concentration of 100 µM DTT (30 min, RT). Subsequently, the concentration of DDM in the protein samples was increased to 1%. Immediately before

electrophoresis, the Coomassie sample additive was added to the sample, resulting in a final concentration of 1% Coomassie. 4 µg proteins per lane were separated on 4 to 16% Bis-Tris polyacrylamide gels, with the cathode buffer inside the running chamber and the anode buffer outside. Electrophoresis was initially performed for 30 min at 150 V, followed by 90 min at 250 V. The separated proteins were fixed in fixation buffer (20 min, const. shaking) and stained with Coomassie N-staining solution (1 h, const. shaking). Gels were finally incubated in Coomassie N-destaining solution (1 h, const. shaking). The Amersham High Molecular Weight Calibration Kit for native electrophoresis was used to estimate the molecular weights of protein mono- and oligomers.

3.2.3.8 Proteoliposome formation

(Proteo-)liposomes with different lipid compositions were prepared to study the effect of the membrane environment on the activity of BmrA. In Table 3.15 all analyzed lipid mixtures are summarized.

Table 3.15: Composition of the studied lipids mixtures.

Lipid	**Lipid composition**	
	% studied	% of background lipid
DOPC (18:1PC)	-	background lipid
DOPG (18:1PG)	10-100%	0-90% DOPC
DOPS (18:1PS)	10-100%	0-90% DOPC
DOPE (18:1PE)	10-70%	30-90% DOPC **or** const. 30% DOPG + 0-70% DOPC
CL	10-70%	30-90% DOPC
14:1PC	100%	-
16:1PC	100%	-
20:1PC	100%	-
22:1PC	100%	-
POPC (16:0-18:1PC)	10-100%	0-90% DOPC
EPL	100%	-

An amount of 1.25 µmol of pure lipids or lipid mixtures (dissolved in $CHCl_3$) was dried under a gentle nitrogen flow in a reaction tube. The remaining solvent was then removed under vacuum overnight. Dried lipids were solubilized in rehydration buffer to a final concentration of 5 mM (30 min, 37 °C, const. shaking). The lipid suspension was then subjected to four freeze-thaw cycles

in liquid nitrogen. The liposomes were destabilized by the addition of a 1% Triton™ X-100 solution. The required amount depends on the exact lipid mixture and was experimentally determined (Table S1).
Subsequently, the destabilized liposomes were incubated at a lipid:protein molar ratio of 333:1 with 1 mg/mL purified protein in reconstitution buffer (30 min, 37 °C, const. shaking). All detergent molecules were then slowly removed to ensure proteoliposome formation. To do so, the protein-liposome mixture was incubated four times in succession with 25 mg (for 500 µL proteoliposome dispersion) of fresh Bio-Beads SM-2 (30 min, 1 h, overnight, and again 1 h, 4 °C, overhead agitation). Large liposomal structures and potentially aggregated proteins were removed from the formed proteoliposomes by centrifugation (10 min, 13,000 g). Proteoliposomes were collected by ultra-centrifugation (1 h, 285,000 g) and finally resuspended in reaction buffer. The total protein concentration was determined using a commercially available Pierce™ BCA protein assay kit. For an accurate determination, proteoliposomes were dissolved by adding an SDS solution to a final amount of 2% to the proteoliposomes before the measurement. Proteoliposomes were kept at 4 °C for up to two days, until the ATPase activity measurements or the SNAP-tag labeling were performed. Proper proteoliposome formation was monitored via analyzing individual steps of the reconstitution process via SDS-PAGE (chapter 3.2.3.6).

3.2.3.9 Analysis of protein orientation in proteoliposomes

The final orientation of the proteins in the liposomal membrane after proteoliposome formation was analyzed using the chimeric BmrA-SNAP-tag fusion protein. The SNAP-tag is a variant of the DNA repair protein O^6-alkylguanine-DNA alkyltransferase that is specifically designed to covalently label itself with synthetic probes via enzymatic reactions[150]. By using a membrane-permeable SNAP-tag substrate (SNAP-Surface® Alexa Fluor® 488), which labels all proteins in different orientations, and an impermeable SNAP-tag substrate (SNAP-Cell® 647-SiR), which exclusively labels outside-oriented proteins, the actual orientation of a reconstituted protein can be determined.

Three samples of BmrA-SNAP-tag-containing proteoliposomes were diluted in labeling buffer to a final concentration of 0.25 mg/mL. The samples were either labeled with a 2x molar excess of SNAP-Surface substrate or SNAP-Cell substrate, or with both sequentially (each labeling: 1 h, RT, dark). Samples that were labelled only once were incubated simultaneously with the same volume of labeling buffer. To each sample, 5x SDS-PAGE sample buffer was then added to a final concentration of 1x SDS-PAGE sample buffer, and the samples were stored at −20 °C. 2.5 µg labeled proteins were separated on a 10% SDS-PAGE gel. Immediately after electrophoresis (chapter 3.2.3.6), the in-gel fluorescence of the SNAP-Surface substrate (blue excitation, 526 nm-

short pass emission filter) and afterwards of the SNAP-Cell substrate (green excitation, 670 nm-bandpass emission filter) was analyzed with the Typhoon Trio+. Fluorescence signals were quantified using ImageJ[151]. Gels were afterwards stained with Coomassie brilliant blue R520, as described in chapter 3.2.3.6. The protein orientation was estimated by setting the signal of all labeled proteins with the SNAP-Cell substrate to 100% and subtracting the signal of only inside-oriented protein and the background signal.

3.2.4 Biophysical methods

3.2.4.1 ATPase activity assay

The *in vitro* ATPase activity of BmrA wt and variants was either analyzed in DDM detergent micelles or after reconstitution into liposomes in the absence of detergent, using an ATP regenerating system.

The purified proteins were diluted to a final concentration of 0.2/0.76/1.0 µM (13/50/65 µg/mL), respectively, in 100 µL reaction-D buffer. Whereby, proteoliposomes were diluted to a final concentration of 0.76 µM (50 µg/mL) in 100 µL reaction buffer. Separately, a reaction mix containing 3.5 mM Na_2-ATP, 10 mM $MgCl_2$, 0.28 mM NADH, 2 mM PEP, 6-10 units/mL pyruvate kinase, and 9-14 units/mL lactate dehydrogenase was prepared in a total volume of 100 µL. After incubating both (5 min, 25 °C), the protein or proteoliposome solution and the reaction mix were rapidly mixed, and the NADH consumption was immediately followed via measuring absorbance changes at 340 nm over 5 min at 25 °C using a Cary 3500 Multicell UV-Vis spectrophotometer. The decrease in NADH absorption was finally converted into the ATPase activity in [µmol/min·mg] via equation 3 using the extinction coefficient of NADH (ε_{NADH} = 6220 $M^{-1}cm^{-1}$) and a pathlength of d = 1 cm.

$$ATPase\ activity = -\frac{\Delta A_{340\,nm}}{\Delta t} \cdot \frac{1}{d \cdot \varepsilon_{NADH} \cdot c_{Protein}} \quad (3)$$

Where indicated, purified or membrane-reconstituted proteins were pre-incubated with 0, 1, 2, 4, 8, or 12 mM PhEtOH or with 25 mM DTT (30 min, 25 °C) prior to the measurement.

3.2.4.2 Laurdan fluorescence spectroscopy

The fluorophore probe Laurdan was used to monitor the membrane fluidity of BmrA proteoliposomes in the presence of increasing concentrations of PhEtOH[152]. When incorporated

into lipid bilayers, Laurdan exhibits distinct fluorescence emission properties depending on the polarity of its environment[153].

Proteoliposomes containing Laurdan in a molar ratio of 1:500 (Laurdan:lipid) were prepared using DOPC/DOPG (50/50), as described in chapter 3.2.3.8. The Laurdan-containing proteoliposomes were then incubated with 0, 1, 2, 4, 8, or 12 mM PhEtOH (30 min, 25 °C). Subsequently, Laurdan fluorescence emission spectra of 0.25 mM proteoliposomes (lipid concentration) were measured in triplicate using a FluoroMax-4 fluorescence spectrometer at 25 °C. Spectra were recorded between 400 and 550 nm upon excitation at 350 nm. The excitation and emission slits were set to 1 nm and 5 nm, respectively. Changes in the Laurdan fluorescence emission spectra were quantified by calculating the Generalized Polarization (GP) value via equation 4 using Laurdan's fluorescence emission at 440 and 490 nm[153].

$$GP\ value = \frac{I_{440} - I_{490}}{I_{440} + I_{490}} \quad (4)$$

3.2.4.3 Hoechst 33342 transport activity assay

The transport activity of BmrA variants overexpressed in IMVs was analyzed via fluorescence spectroscopy using the fluorescent substrate Hoechst 33342[124].

For each measurement, 50 µg of IMVs were diluted and incubated in 200 µL transport buffer (5 min, 25 °C). First, the fluorescence emission was monitored using a FluoroMax-4 fluorometer for 50 s. The excitation and emission wavelengths were set to 355 and 457 nm, respectively, with slit widths of 3 and 2 nm. After adding Hoechst 33342 to a final concentration of 2 µM, the fluorescence emission was further measured for 50 s.
Subsequently, 2 mM ATP was added, and the fluorescence emission was monitored for additional 200 s. The transport activity [1/s] was calculated via determining the initial decrease in Hoechst 33342 fluorescence after the addition of ATP.

3.2.4.4 CD spectroscopy

CD spectroscopy was performed to analyze the secondary structure and the thermal stability of purified BmrA wt and variants.

CD spectra of 0.25 mg/mL purified BmrA wt and variants or 0.4 mg/ml purified NBD wt and variants in phosphate buffer were recorded using a JASCO J-1500 CD spectrometer and an MPTC-490S temperature-controlled cell holder. The instrument settings were as follows: spectral range

200-250 nm, scan rate 100 nm/min, 1 mm cell length, 1 nm steps, 1 nm bandwidth, 1 s data integration time, and 6-time accumulation at 25 °C. Three independent purifications of each protein variant were typically analyzed, each in triplicate.

When testing the thermal stability at temperatures between 20 to 88 °C (2 °C steps with a heating rate of 1 °C/min), only one spectrum was measured using the same settings. Single spectra were smoothed using the Savitzky–Golay filter implemented in the instrument's software. For each protein, three samples from three independent purifications were measured, interpolated, averaged, and normalized to yield the final denaturation curve. Using the program Origin (version 9.60), the data points were fitted with an adapted Boltzmann fit (equation 5), and the transition temperature (T_m) at 222 nm was determined. The fit assumes a two-state unfolding mechanism with linear slopes in the plateau areas of the curve.

$$\theta_{222\,nm}(T) = \frac{(T * m_N + \theta_N) - (T * m_D + \theta_D)}{1 + e^{\frac{T - T_m}{dT}}} + (T * m_D + \theta_D) \quad (5)$$

θ_{222nm} = measured ellipticity at 222 nm; T = temperature; θ_N/θ_D = ellipticities of native/denatured protein at plateau regions; m_N/m_D = slopes of plateaus.

3.2.4.5 ThT fluorescence measurements

The formation of amyloid-like structures upon thermal denaturation of the isolated NBD (chapter 3.2.4.4) was monitored using fluorescence spectroscopy together with the fluorescence probe ThT. ThT exhibits enhanced fluorescence upon binding to amyloid-like fibrils and is therefore commonly used to test for amyloid formation[154].

ThT was dissolved in water and filtered through a 0.2 µM filter. The concentration was determined by measuring the absorbance at 416 nm (ε_{ThT} = 22,620 M^{-1} cm^{-1}). Stock solutions of 50 µM were prepared and stored at −20 °C. The isolated wt NBD was heated up to 88 °C (1 °C/min). The preheated and untreated NBD was then incubated at a concentration of 0.4 mg/ml with 1 µM ThT (1 h, RT). Emission spectra were recorded between 465 and 565 nm (slit widths 5 nm) upon excitation at 450 nm (slit widths 5 nm) at 20 °C using a FluoroMax-4 fluorometer.

3.2.5 Bioinformatic analyses

3.2.5.1 Multiple-sequence alignment

Evolutionarily conserved amino acids of BmrA were identified by a multiple-sequence alignment including the amino acid sequences of several bacterial multidrug transporters and the human ABCC family. Sequences of *B. subtilis* BmrA (O06967), *Lactococcus lactis subsp. cremoris* (*L. lactis subsp. cremoris*) LmrA (P97046), *E. coli* MsbA (P60752), *S. aureus* Y1866 (Q99T13) and human ABCC1-ABCC12 (P33527, Q92887, O15438, O15439, O15440, O95255, P13569, O60706, Q5T3U5, Q96J66, Q96J65) were obtained from the Uniprot server (https://www.uniprot.org). Multiple sequence alignment was performed using the Clustal Omega program on the EMPL-API server (https://www.ebi.ac.uk)[155,156]. ESPript 3.0 on the ENDscript server (https://endscript.ibcp.fr) was used to visualize the alignment[157].

4 Results and Discussion

4.1 Membrane properties control the ATPase activity of the ABC transporter BmrA

4.1.1 Publication

The content of this chapter was published during the course of this thesis as:

Osten, V.[a] and [redacted][b] (2025) Membrane properties control the ATPase activity of the ABC transporter BmrA, *Biochim. Biophys. Acta – Biomembranes*, 1867, 184430.

[redacted]

This chapter cites the published article[158] with the following changes:

- The format of this article was adapted to the style of this thesis.
- Abbreviations have been combined with those of the other thesis chapters.
- Figures, tables and citations are rearranged and renumbered in accordance to this thesis.
- The methods section was removed and the performed methods are now included in the general method chapter 3.2 of this thesis.
- The supplementary figures are renumbered and can be found in chapter 6.3.

The Author contributions according to the CRediT taxonomy are listed in Table 4.1.

Table 4.1: Author contribution of the article titled as "Membrane properties control the ATPase activity of the ABC transporter BmrA".

	Application	Author
Conceptualization	Complete study	**V.O.**, [redacted]
Methodology, Investigation,	Figure 9	**V.O.**
Formal analysis, Data	Figure 10	**V.O.**
visualization	Figure 11	**V.O.**
	Figure 12	**V.O.**
	Figure 13	**V.O.**

	Figure S1	**V.O.**
	Figure S2	**V.O.**
Writing	Original draft	**V.O.**, [redacted]
	Review and editing	**V.O.**, [redacted]
Project administration, Funding acquisition, Recourses, Supervision	Complete study	[redacted]

4.1.2 Abstract

The structure and the function of membrane proteins can be affected by the lipid bilayer environment, yet its impact often is neglected in *in vitro* studies where proteins are typically analyzed in membrane mimetics, mostly liposomal systems. It has been observed that the activity of the bacterial ABC transporter BmrA differs when measured in detergent vs. a model membrane environment, indicating that the physico-chemical properties of the membrane environment crucially affect the protein's activity. We now performed a systematic analysis to elucidate the impact of individual lipid/membrane properties on the activity of BmrA and identified three parameters controlling the BmrA activity in lipid bilayers: (i) the hydrophobic thickness of the membrane, (ii) a negative surface charge, and (iii) the packing of lipids in the acyl-chain and head group regions. Our study provides valuable insights into how a specific lipid composition can influence the basal ATPase activity of BmrA and emphasizes that the lipid composition should be carefully selected in *in vitro* studies of membrane proteins.

4.1.3 Introduction

Integral membrane proteins are embedded in a dynamic and highly regulated lipid bilayer whose physico-chemical properties vary depending on the exact lipid composition. In eukaryotes, the exact lipid composition differs between the different cellular membrane systems, and in prokaryotes, the exact lipid composition is strongly regulated by the environment and various stressors[2,159]. Several studies emphasized that the structure and activity of certain membrane proteins are affected by membrane lipids, and it is believed that membrane properties influence/regulate membrane proteins in general[3,160–162]. Individual lipid species can interact with the membrane protein either specifically (e.g., through hydrogen bonding or charge interactions) or non-specifically, due to combined physical bulk properties (membrane thickness, curvature, lateral pressure/stress, and fluidity) if the bilayer is considered as a macrostructure[10,11,163,164]. For example, in the case of the human p24 transmembrane helix dimer, sphingomyelin binds to a specific binding site, which modulates the membrane protein's structure and activity[165,166]. The

structure of the human glycophorin A transmembrane helix dimer also is dramatically affected by the physico-chemical properties of the lipid environment, including the hydrophobic thickness, fluidity, and membrane curvature[167,168].

Depending on the lipid composition, the hydrogen bonding patterns between residues of the membrane protein and the lipid head groups can vary and influence the activity of more complex membrane proteins, as has e.g., been described for the rhomboid protease[169]. Also the activity of the Ca^{2+}-ATPase from the sarcoplasmic reticulum is regulated by different physical properties of the surrounding membrane, such as the hydrophobic thickness, fluidity, and curvature[10]. Despite these (and many other) well-known examples, the native membrane environment is often neglected when the structure and/or activity of membrane proteins is studied. Even though studies in simple systems, such as detergent micelles, can provide important insights into the structure and function of membrane proteins, they typically obscure reality to some extent.

Members of the large superfamily of ABC transporters catalyze the import or export of various substrates into cells, e.g., smaller ions, sugars, lipids, and even larger biomolecules, such as antibiotics and anti-cancer drugs[43,170]. Driven by ATP hydrolysis, they enable substrate transport against a chemical gradient across a membrane[25]. ABC transporters are present in all kingdoms of life, and although diverse in their respective substrate spectrum, they all share a common architecture[25,26]. A functional transporter consists of four entities: two TMDs and two cytosolic NBDs, whereby all four domains can be expressed either on one, two (one NBD is fused to one TMD), or individual polypeptide chains. While a standardized model of the transport mechanism for all ABC transporters remains elusive, and the existence of such a unifying model is highly controversial, the proposed models (ATP-switch, alternating site, and constant contact) share common features[25]. These are that ATP binding occurs at the structurally conserved NBDs followed by their dimerization[25,91,171,172] and that the protein structure undergoes a transition from an "open" state - also called the IF state, where the NBDs are separated and the protein has an overall V-shaped structure[173] - to a "closed" OF state, where the NBDs are in close contact[25]. This structural rearrangement is coupled with the release of a bound substrate.

As the structure of the TMDs within the membrane significantly changes during a transport cycle, and with that the overall conformation of the transporter, the activity of ABC transporters is likely to be influenced by (non-)specific interactions with membranes. In fact, it has been reported that lipid/membrane properties influence the activity and function of different ABC transporters. For example, the basal ATPase activity of the maltose ABC transporter $MalFGK_2$ is decreased drastically in the presence of lipids with long acyl-chains (>C14), possibly due to the lipids affecting the motion of the TMDs[174]. Furthermore, the activity of the "transporter associated with antigen processing" (TAP) is stimulated by the lipid head groups of PI and PE[175]. However, it is difficult to distinguish whether lipids allosterically modulate a transporter function by binding directly to a specific binding site, act as a structural stabilizer of different conformations, change

the bulk membrane properties, or are "simply" a substrate of the transporter, as known for P-gp[36,176]. Yet, the impact of a membrane (systems) on ABC transporters cannot be neglected, as some ABC transporters (e.g., P-gp or human ABCG1) do not exhibit basal ATPase activity in detergents but do in liposomal systems[177,178]. Typically, the ATPase activity of ABC transporters is further stimulated by substrate binding[48,179,180]. The detergent-solubilized BmrA protein has a high basal ATPase activity already in the absence of substrates, yet this activity appears to further increase when the protein is embedded in a lipid environment[40,124,137,138]. Due to this observation, we aimed at elucidating the effect of lipid and membrane properties on BmrA's function. We observed an increased basal ATPase activity of BmrA in membranes with higher hydrophobic thicknesses. Furthermore, high lateral pressure in the acyl-chain region and loose packing of the lipid head groups further stimulate BmrA. Finally, lipids with a negative head group charge significantly stimulate the basal ATPase activity of BmrA. Our observations nicely illustrate that membrane and lipid properties can significantly modulate the BmrA activity. As BmrA has a high, futile ATPase activity even in the absence of substrates, we suggest that its activity is spatio-temporally controlled *in vivo* by its intimate membrane environment.

4.1.4 Results

4.1.4.1 The membrane environment affects the BmrA ATPase activity

While it has been observed that the activity of the bacterial ABC transporter BmrA differs when measured in detergent vs. a model membrane environment[40,124,137,138], indicating that the physico-chemical properties of the membrane environment crucially affect the protein's activity, it still remains unclear which lipid and/or membrane properties exactly control the BmrA activity. Hence, we reconstituted BmrA purified in DDM micelles into liposomes with defined lipid compositions to elucidate in detail the impact of specific membrane lipids and bilayer properties on the (ATPase) activity of BmrA. Since BmrA was heterologously expressed and is highly active in *E. coli* membranes[124,138], we first prepared BmrA-containing proteoliposomes using EPL extract (Figure 9A/B) and determined the ATPase activity of BmrA in DDM-micelles and BmrA reconstituted into EPL liposomes (Figure 9C/D). When dissolved in DDM micelles, BmrA has an ATPase activity of 0.14 ± 0.02 µmol/min*mg (k_{cat} = 0.16 ± 0.02 1/s). In contrast, when BmrA was embedded into an EPL membrane, the ATPase activity increased more than 3-fold to 0.50 ± 0.05 µmol/min*mg (k_{cat} = 0.55 ± 0.06 1/s). Based on these observations, it is obvious that membrane and/or lipid properties control the BmrA activity. Depending on the orientation of the protein within the liposomal membrane, the measured activity might even be underestimated, as proteins with the NBDs localized inside the liposomes would not be able to hydrolyze any ATP added from the outside (compare Figure 9A). Nevertheless, as the NBD is the sole large soluble

protein domain, a preferred orientation with the NBDs oriented outwardly was expected. To experimentally determine the orientation of BmrA, we reconstituted a purified chimeric BmrA protein with a SNAP-tag fused to the C-terminal end of the BmrA NBD into EPL liposomes. A

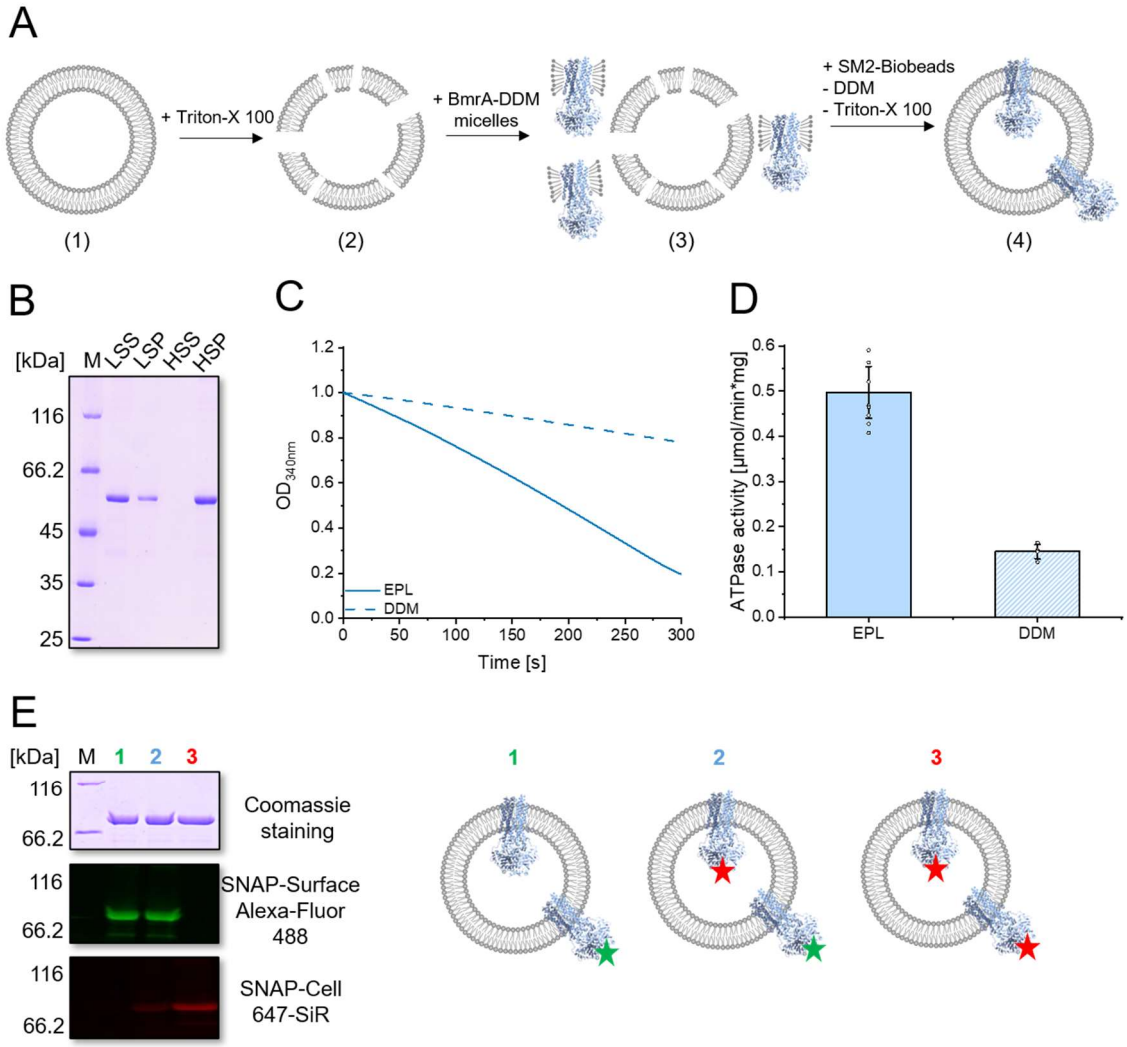

Figure 9: Preparation, ATPase activity, and topology of BmrA in EPL proteoliposomes.

(A) Schematic overview of proteoliposome preparation. Preformed liposomes (1) were destabilized by the addition of Triton-X 100 (2) and afterwards incubated with BmrA in DDM-micelles (3). Slow removal of detergent with SM2-Biobeads led to proteoliposome formation (4). **(B)** SDS-PAGE analysis of the protein during reconstitution. The proteoliposome fraction (LSS = low-speed supernatant) was separated from potentially aggregated protein and multilamellar vesicles (MLVs) by centrifugation (13000 g, 10 min) (LSP = low-speed pellet). Finally, reconstitution was verified by ultra-centrifugation (285000 g, 1 h), where proteoliposomes (HSP = high-speed pellet) were separated from non-reconstituted protein (HSS = high-speed supernatant). M = Marker. **(C)** ATPase activity of BmrA measured in DDM-micelles (dashed line) and reconstituted in EPL liposomes (solid line) via following the NADH consumption at 340 nm. **(D)** Mean ATPase activity of BmrA in DDM-micelles (n = 4, ± standard deviation (SD)) and reconstituted in EPL liposomes (n = 7, ± SD). Single data points of independent proteoliposome preparations are shown. **(E)** Orientation of BmrA-SNAP-tag in EPL proteoliposomes. BmrA-SNAP-tag reconstituted into EPL liposomes was labeled either (1) with the membrane-impermeable SNAP-tag dye (SNAP-Surface® Alexa Fluor® 488), (2) subsequently also with the membrane-permeable SNAP-tag dye (SNAP-Cell® 647-SIR) or (3) only with the membrane-permeable dye. Afterwards, labeled proteins were separated on a 10% SDS-PAGE gel, and the in-gel fluorescence was determined, followed by Coomassie-staining. M = Marker.

membrane permeable plus an impermeable SNAP-tag substrate was used for labeling the different possible orientations of the reconstituted protein, with the membrane-permeable substrate labeling all proteins, whereas the membrane-impermeable substrate exclusively labels BmrA with an NBD_{out} orientation. Based on the fluorescence signals, we calculated that around 93% of all proteins are oriented in an NBD_{out} orientation (Figure 9E), indicating that the measured ATPase activity in EPL proteoliposomes is only slightly underestimated. For each lipid composition tested in this study, the majority of all proteins (93-96%) were oriented NBD_{out} (Figure S1).

4.1.4.2 BmrA is more active in thicker membranes

In contrast to biological membranes, the hydrophobic core of micellar systems is more adjustable to the hydrophobic thickness of a detergent-dissolved membrane protein. The hydrophobic thickness of a membrane depends on the lipid acyl chain lengths, and often a membrane protein's activity is highest when the thickness of the hydrophobic membrane core matches the hydrophobic thickness of the protein[181]. Because of this and as a basis for subsequent analyzes in model membrane systems, we next tested whether the membrane thickness impacts the BmrA activity. For this purpose, BmrA-containing proteoliposomes were prepared using the following PC lipids: 14:1, 16:1, 18:1 (DOPC), 20:1, and 22:1 (Figure S2). Although *B. subtilis* and *E. coli* membranes do not naturally contain DOPC, we still used lipids with a PC head group, since these

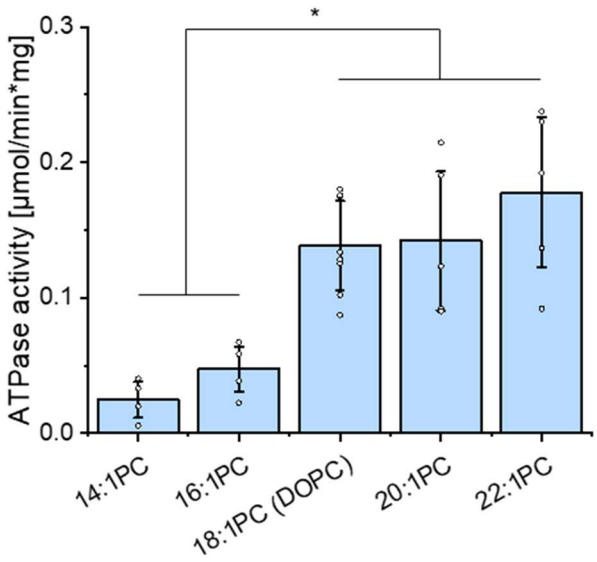

Figure 10: ATPase activity of BmrA proteoliposomes in thinner/thicker membranes.

BmrA was reconstituted into liposomes containing PC lipids with increasing acyl chain length (14:1PC–22:1PC). Shown are the mean ATPase activities and the single data points of independent proteoliposome preparations ($n > 4$, ± SD, two-sample t-test, $p < 0.05$).

lipids were available with different carbon chain lengths (14-22). Importantly, all lipids have transition temperatures far below 25 °C, where the ATPase activity was measured, and *i.e.*, all membranes were in a fluid state. In thinner membranes (14:1PC/16:1PC), BmrA had a low ATPase activity (Figure 10), which was even below the activity measured in DDM micelles (Figure 9C/D). However, when reconstituted into membranes composed of PC lipids with longer acyl chains (18:1-22:1), the ATPase activities significantly increased, reaching the activity measured in DDM micelles (Figure 10). As no differences in the determined ATPase activities were observed between lipids with longer acyl chains (18:1-22:1), BmrA appears to tolerate a certain thickness range. However, when comparing the BmrA ATPase activities determined in C18:1–C22:1PC proteoliposomes with the activity determined in EPL liposomes (Figure 9C/D), it becomes evident that, in addition to the hydrophobic thickness, other membrane properties appear to further stimulate the BmrA activity.

4.1.4.3 Negatively charged lipids modulate the BmrA ATPase activity

Since the lipid species in natural membranes do not only differ in their acyl chain length but also in their head group chemistry, we next analyzed the impact of different lipid species on the BmrA activity. EPL, where BmrA is highly active, contains about 70% PE, as well as 20% and 10% of the negatively charged lipids PG and CL, respectively. Due to its unfavorable head group-to-acyl chain volume ratio, the major lipid species PE is a non-bilayer-forming lipid causing negative curvature stress in biomembranes. As curvature stress can affect a membrane protein´s activity[10,182], we first mixed the non-bilayer-forming lipid PE with the bilayer-forming lipid PC in different ratios and determined BmrA's ATPase activity. Based on our previous results (Figure 10), we chose 18:1PC (DOPC), a typical zwitterionic and bilayer-forming lipid, as a background lipid and varied the relative amount of DOPE. Up to a PE content of 70%, where the lipid bilayers were still stable, no statistically significant changes in the BmrA ATPase activity were detected (Figure 11A), indicating that stored curvature elastic stress does not affect the BmrA activity, at least not in pure PC/PE membranes (compare chapter 4.1.4.4).

Next, we investigated a possible dependence of the BmrA ATPase activity on the negative lipid head group charge, again using C18:1-based lipids with different head groups. In pure DOPC liposomes, BmrA has an ATPase activity of 0.14 ± 0.03 µmol/min*mg (Figure 11B). Yet, when the DOPG content was increased from 0-50%, the ATPase activities constantly increased up to 0.49 ± 0.10 µmol/min*mg, a value similar to the activity determined in EPL proteoliposomes, whereas further addition of DOPG (up to 100%) led to a subsequent decrease in the ATPase activity (Figure 11B). To analyze whether the observed initial activity increase was specific for the DOPG head group or due to the general increase in negative membrane surface charge, we next replaced DOPG by DOPS, a negatively charged lipid not naturally present in *E. coli* or *B. subtilis*

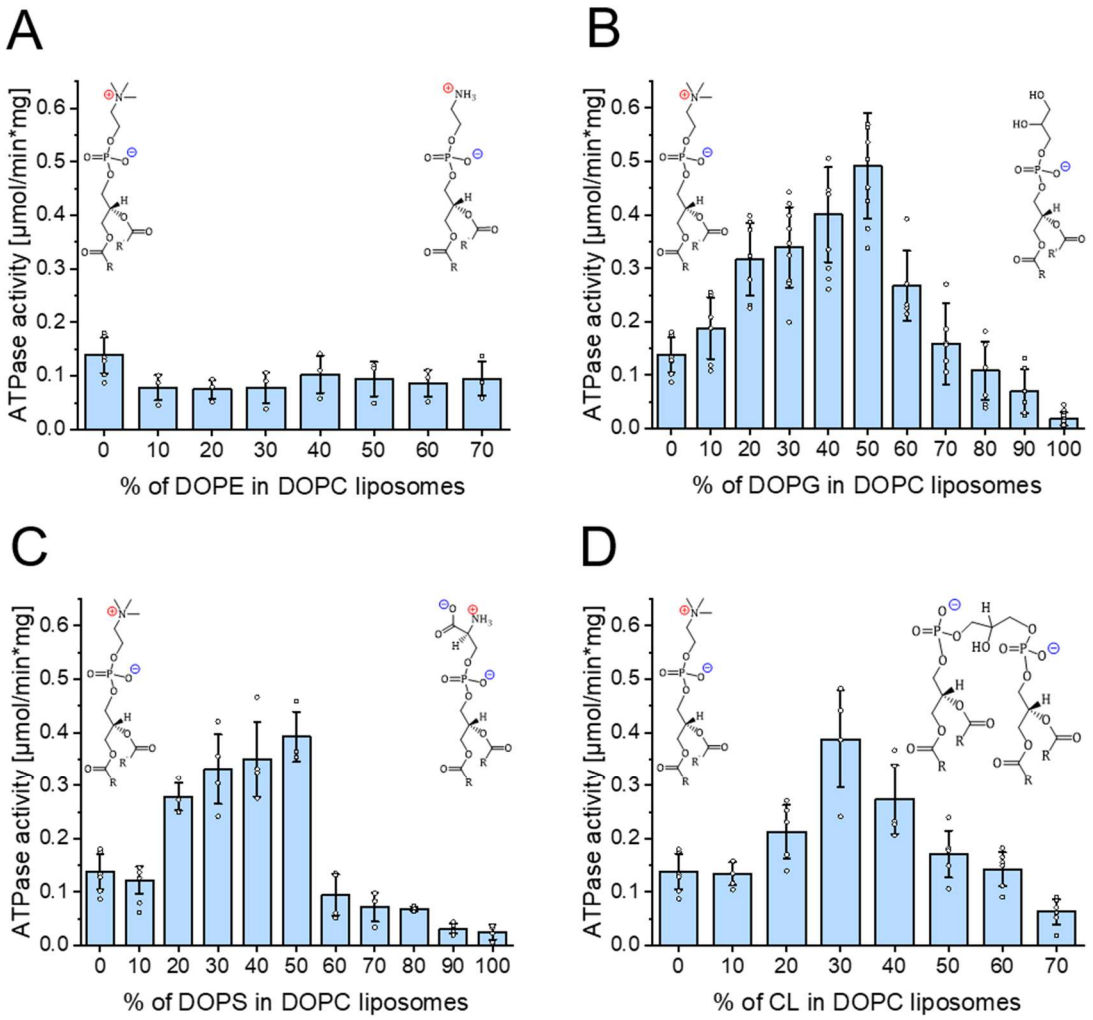

Figure 11: ATPase activity of BmrA in proteoliposomes containing negatively charged lipids.

BmrA was reconstituted into DOPC liposomes with increasing amounts of **(A)** DOPE (0-70%), **(B)** DOPG (0-100%), **(C)** DOPS (0-100%), or **(D)** CL (0-70%). Shown are the mean ATPase activities and the single data points of independent proteoliposome preparations (DOPE/DOPC and DOPS/DOPC: n > 3, DOPG/DOPC: n > 5, and CL/DOPC: n > 4, ± SD). Head group structures of DOPC/DOPE in **(A)**, DOPC/DOPG in **(B)**, DOPC/DOPS in **(C),** and DOPC/CL in **(D)** are also shown. Structures were drawn using Chemdraw.

membranes in significant amounts. Similar to the previous experiment, the ATPase activities increased when the DOPS content was raised from 0-50%, reaching an ATPase activity of 0.39 ± 0.05 µmol/min*mg at 50% DOPS, and the activity was again reduced upon further DOPS addition (Figure 11C). These observations strongly suggest that the ATPase activity is modulated by the negative membrane surface charge. In line with this, when introducing CL, which carries two negative charges, into DOPC liposomes, the highest ATPase activity (0.39 ± 0.09 µmol/min*mg) was already reached when about 30% CL was present, and thereafter the activity decreased again (Figure 11D). Noteworthy, as pure CL membranes are not stable, we determined the BmrA ATPase activities only until a CL content of 70%. Overall, our results clearly suggest that a negative lipid

head group charge modulates the ATPase activity of BmrA, and maximal ATPase activity is reached when BmrA is reconstituted into liposomes containing about 50% lipids with a single negative charge.

When embedded into a membrane, the first N-terminal helix (often referred to as the elbow helix = EH) of BmrA is in direct proximity to the lipid head groups (Figure 12A). The 21 amino acid long elbow helix contains eight positively charged amino acids, which could potentially interact electrostatically with a negatively charged membrane. To test this assumption, we created a BmrA variant lacking all eight positive charges by exchanging them for Ala. Yet, when reconstituted into EPL proteoliposomes, BmrA 8xM displayed a wt-like ATPase activity of 0.44 ± 0.10 µmol/min*mg (Figure 12B). This indicates that the positively charged amino acids of this helix do not modulate the BmrA activity by electrostatic interactions with the membrane.

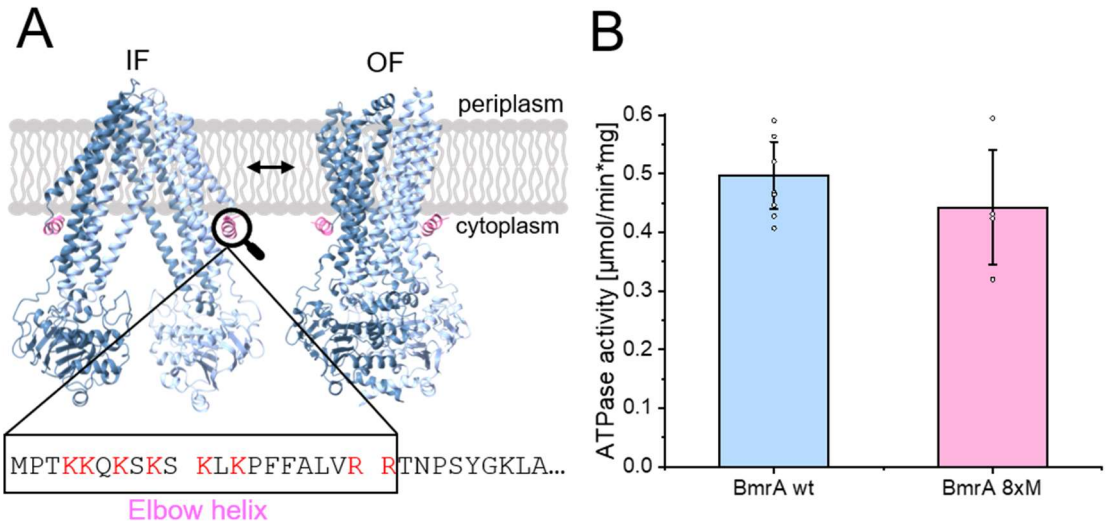

Figure 12: Positively charged amino acids in the elbow helix of BmrA do not cooperate crucially with the negative charged membrane surface.

(A) IF (PDB: [8QOE][79]) and OF (PDB: [7OW8][80]) conformation of a BmrA dimer (single monomers in light and dark blue) in a lipid bilayer. The N-terminal EH (residues 1-21) lies perpendicular below the membrane surface and is highlighted in pink. An enlarged view of the amino acid sequence of the EH is given, and the positively charged amino acids that were exchanged for Ala in BmrA 8xM are highlighted in red. **(B)** Mean ATPase activities of reconstituted BmrA wt (blue, n = 7, ± SD) and BmrA 8xM (pink, n = 4, ± SD) determined in EPL liposomes. Single data points of independent proteoliposome preparations are shown.

4.1.4.4 High lateral pressure in the acyl-chain region and loosely packed lipid head groups stimulate the BmrA ATPase activity

Not only the lipid head group chemistry, but also more global membrane properties, such as the lateral pressure, curvature elastic stress, and/or the membrane fluidity, can significantly affect a membrane protein's function. As PE, the major lipid in *E. coli* membranes, has a conical shape with a small head group, it imposes negative curvature stress to membranes[10,182]. Yet, in the absence of

negatively charged lipids, no changes in the BmrA ATPase activities were observed when the DOPE content was increased (Figure 11A). To further study the potential influence of curvature elastic stress on the BmrA activity, we next selected the bilayer-forming, net-uncharged lipid DOPC together with a constant amount of 30% DOPG as a background lipid to stimulate the ATPase activity of BmrA (Figure 11B). An amount of only 30% of bilayer-forming DOPG ensures that an addition of up to 70% of DOPE, *i.e.*, replacing DOPC by DOPE, can be achieved. Due to the

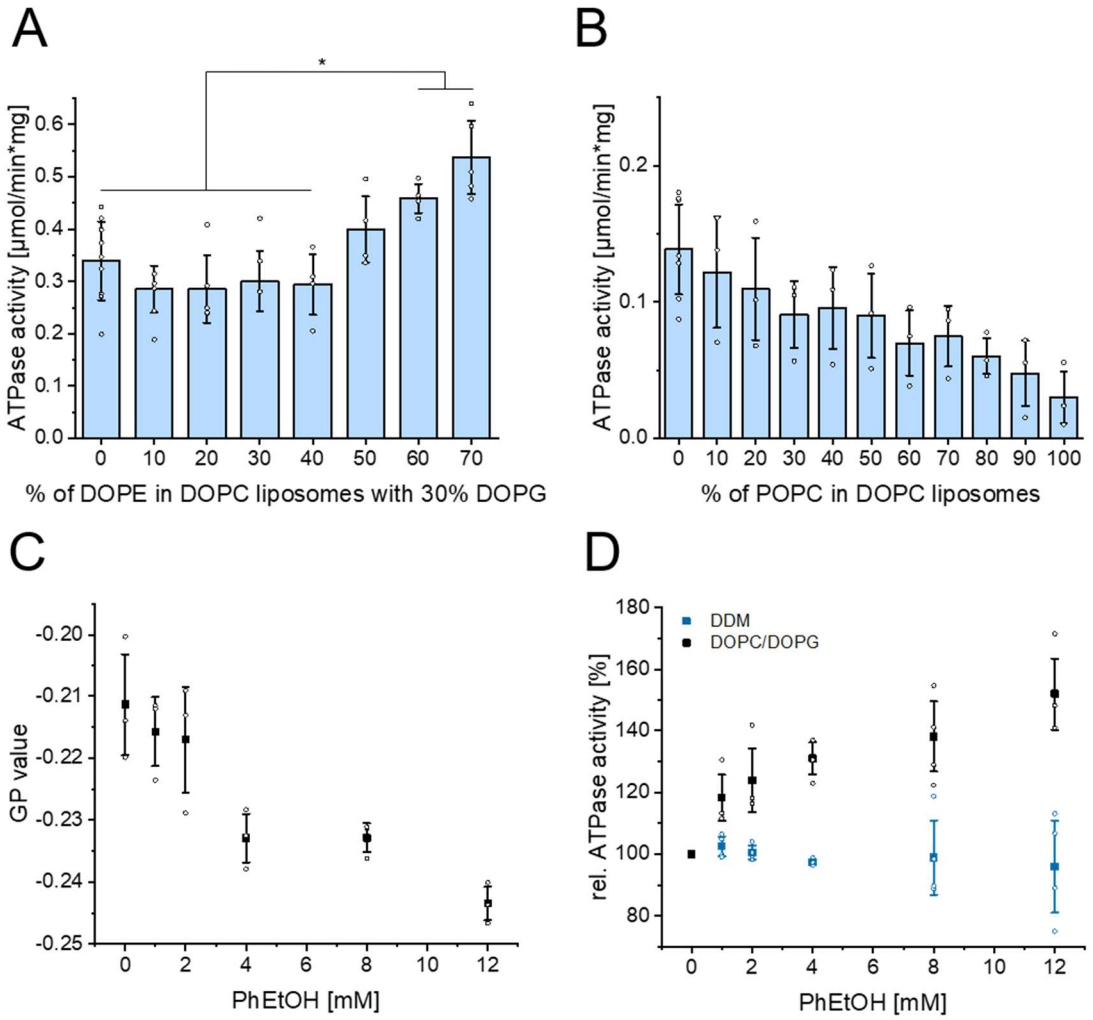

Figure 13: ATPase activity of BmrA proteoliposomes in membranes with varying fluidity.

BmrA was reconstituted into DOPC liposomes containing **(A)** increasing amounts of DOPE (0-70%) and a constant content of 30% DOPG and **(B)** increasing amounts of POPC (0-100%). Shown are the mean ATPase activities and the single data points of independent proteoliposome preparations (DOPE/DOPG/DOPC: n > 4 ± SD, two-sample t-test, $p < 0.05$, POPC/DOPC: n > 3 ± SD). **(C)** Fluidity of DOPC/DOPG (50/50) proteoliposomes containing reconstituted BmrA and the fluorescence probe Laurdan in presence of 0-12 mM PhEtOH. Mean GP values were calculated from the Laurdan fluorescence emission spectra of independent proteoliposome preparations (n = 3, ± SD) and shown with single data points. **(D)** Mean relative ATPase activities of BmrA in DDM-micelles (n > 3, ± SD, blue) and reconstituted in DOPC/DOPG (50/50) liposomes (n > 3, ± SD, black) in presence of 0-12 mM PhEtOH. Additionally single data points of independent proteoliposome preparations or protein purifications are shown.

DOPE structure with a small volume of the head group region relative to the volume of the acyl-chain region, the molecule influences the lateral lipid packing, and lipids are more tightly packed in the acyl-chain region, whereas the relatively small head group causes weak packing in the head group region[182].

When increasing the DOPE content in DOPC/DOPG liposomes from 0-40%, the ATPase activity did not significantly change (Figure 13A). Yet, above 50% DOPE, the ATPase activity increased significantly, reaching the value observed with 50/50 DOPC/DOPG in the previous experiment (Figure 11), indicating a stimulating effect of DOPE on the (pre-stimulated) ATPase activity of BmrA, caused by the increased lateral membrane pressure in the acyl chain region or the reduced packing in the lipid head group region (or both). To separate these packing effects, we next analyzed the impact of acyl-chain packing using BmrA proteoliposomes containing DOPC plus increasing amounts of POPC. The latter contains a saturated and an unsaturated acyl chain, *i.e.*, increasing amounts of POPC led to a reduced lateral pressure in the acyl-chain region whereby the head group regions remained unaffected. With increasing amounts of POPC, the BmrA ATPase activity steadily decreased (Figure 13B), again suggesting that a more tightly packed membrane inhibits the ATPase activity of BmrA. Note that one acyl chain of POPC is shorter (C16) compared to the other acyl chain (C18), which could also influence the activity of BmrA, as we showed in Figure 10.

Next, we focused on the lipid head group packing and examined the (pre)stimulated ATPase activity of BmrA proteoliposomes (DOPC/DOPG: 50/50) upon addition of increasing concentrations of the alcohol PhEtOH (0-12 mM). PhEtOH is known to incorporate into the lipid bilayer at the interface between the polar and the nonpolar membrane regions, which disturbs the membrane organization in the lipid head group region, yet not in the hydrophobic membrane core, resulting in an increased membrane fluidity[152]. At first, we investigated changes in the membrane fluidity upon addition of 0-12 mM PhEtOH to BmrA-containing DOPC/DOPG (50:50) proteoliposomes using the fluorescent probe Laurdan. While the membrane was already quite fluid in the absence of PhEtOH (Figure 13C), further increasing the PhEtOH concentration led to an increased fluidity, as indicated by the decreasing GP value. Also, upon PhEtOH addition, BmrA's ATPase activity in proteoliposomes increased by a factor of 1.5 from zero to the highest PhEtOH concentration studied (Figure 13D, black). Importantly, PhEtOH had no significant impact on the ATPase activity of BmrA in DDM micelles (Figure 13D, blue), indicating that PhEtOH does not directly stimulate the BmrA activity, thus, the observed effect is rather membrane-mediated. Under the assumption that PhEtOH does not differently interact with BmrA in detergent vs. liposomes. Taken together, our results emphasize that both high lateral pressure in the acyl-chain region and weaker lipid head group packing stimulate the ATPase activity of BmrA.

4.1.5 Discussion

The activity of a membrane protein might be controlled by three key features; its (proper) structure, structural dynamics, and the natural environment[161]. Yet, especially the natural membrane environment is often neglected in biochemical and biophysical *in vitro* analyzes of membrane protein structure and activity[183], albeit several recent observations have emphasized the importance of membranes and lipids for proper functioning of some membrane proteins[3,10,161–163,181–183]. However, in most cases the exact impact of a defined lipid environment on the activity of a membrane protein cannot be simply predicted, except when lipids are tightly bound to an integral part of a protein (complex) structure[36,184,185]. Typically, the optimal lipid environment has to be experimentally tested, and the lipid composition of the membrane the protein naturally resides in might be a good starting point. Nevertheless, as the membrane lipid composition might depend on the exact growth conditions, especially in bacteria, there might not be "the one" typical lipid environment, rather, membrane proteins have to function in a certain range of lipid compositions and/or membrane properties. Furthermore, changing the intimate lipid environment might be used by organisms to control the activity of environment-sensitive membrane proteins.

Here, we analyzed in proteoliposomes with defined lipid compositions the impact specific lipids and membrane properties have on the activity of the bacterial ABC transporter BmrA. Of note, additionally to the lipid composition, the chosen membrane model system (liposomes, nanodiscs, etc.) appears also to be important for a transporter function, as the size of nanodiscs was reported to significantly modulate the activity of an ABC transporter by narrowing down the transporter's conformational spectrum[162,186]. When incorporated into EPL liposomes, the BmrA ATPase activity was significantly higher compared to a micellar environment, in line with previous reports[40,58,124]. Yet, the influence of specific lipid and/or membrane properties on the BmrA activity is largely unknown.

A biological membrane provides a defined environment with specific physical properties, including the hydrophobic membrane thickness, the lateral pressure, and the membrane surface charge, which all potentially modulate the structure and/or activity of membrane proteins[3,10,181]. Ideally, the hydrophobic thickness of membranes and the hydrophobic thickness of protein transmembrane regions roughly match, preventing high energy costs for exposing fatty acids and/or hydrophobic protein regions, which either distorts the membrane or the protein, both potentially affecting the protein´s structure and activity[10]. A dramatic impact of a membrane´s hydrophobic thickness has been nicely illustrated using simple model systems, such as the human glycophorin A transmembrane helix dimer[167].

The hydrophobic thickness of BmrA is predicted to be around 31 Å (OPM, as of March 2025[187]). As observed in the present study, BmrA clearly prefers membranes thicker than 16:1 PC

(Figure 10). Yet, BmrA was similarly active in DOPC and 22:1PC membranes with hydrophobic carbon core thicknesses of 27 Å and 34 Å, respectively[188], which indicates a certain flexibility of BmrA in maintaining its activity at different membrane thicknesses.

For several membrane proteins it has been reported that negatively charged lipids modulate the protein structure and/or function[129,160,189]. Our results suggest that also in the case of BmrA, negatively charged lipids stimulate the ATPase activity up to a content of 50% (Figure 11A-D). In fact, the exact chemical nature of the lipid head group appears to play only a minor role, as PS stimulates the BmrA activity essentially as well as PG. Based on the here-presented observations, a membrane surface where approximately 50% of the lipids contain a single negative charge is optimal for the BmrA activity. In perfect agreement, in the case of CL, a lipid containing two negative charges, we observed the highest activity at around 30% of CL (Figure 11D). It is reasonable to assume that the negative surface charge is crucial for the BmrA activity due to interactions and (potentially) stabilization of protein regions containing positively charged residues. Thus, membrane interactions of these regions might be involved in stabilization of an active BmrA conformation. In the case of BmrA, a small N-terminal α-helix, often referred to as the EH (residues 1-21), lies perpendicular to the membrane surface, and in fact this helix contains a high amount of the positively charged residues Lys and Arg. Yet, replacing these residues by Ala did not result in a reduced BmrA activity in EPL proteoliposomes (Figure 12B), and thus interaction of this helix with negatively charged membrane surfaces is not crucial for the BmrA activity, at least not in lipid bilayers. The protein domains critically involved in establishing membrane-protein contacts via ionic interactions thus remain currently elusive.

Furthermore, not only a negative membrane surface, yet additionally changes in the lipid packing (Figure 13) appear to stimulate the BmrA ATPase activity, and both the acyl-chain region (Figure 13A/B) as well as the head group region (Figure 13C/D) contribute. Non-bilayer-forming lipids, such as PE, exert a lateral pressure that leads to negative curvature of a monolayer. This intrinsic tendency to bend becomes frustrated in a lipid bilayer, resulting in curvature stress[8,10]. Since PE is the most abundant phospholipid in *E. coli* membranes, it is obvious that the role of this lipid and the lateral pressure on membrane proteins is of major importance[12,181,190]. However, high lateral pressure in the acyl chain region goes hand in hand with loose packing of lipid head groups. The latter results in local exposure of the hydrophobic tails of membrane lipids and probably enables amphipathic helices to bind better to the membrane surface, which might stabilize defined BmrA structures. The transport cycle of BmrA involves a structural transition from a V-shaped, wide-open IF via an occluded to an OF state, and the thermodynamic equilibrium between these states might control the protein´s ATPase and transport activity[79,80]. A membrane with high positive curvature or high positive curvature elastic stress might (de)stabilize a defined protein structure/state, thereby shifting the equilibrium and resulting in the (here observed) activity changes.

In summary, we here identified three parameters controlling the BmrA activity in lipid bilayers: (i) the hydrophobic thickness of the membrane, being optimal at around 27-34 Å, (ii) a negative surface charge with an optimum at around 50%, and (iii) changes in lipid packing, especially high lateral pressure in the acyl-chain region and loosely packed head groups, which stimulates the BmrA activity.

Interestingly, the *E. coli* membrane contains about 70% of the non-bilayer-forming lipid PE, plus 20% and 10% of the negatively charged lipids PG and CL, respectively[191], *i.e.*, about a negative surface charge of 30% (note that cardiolipin carries two negative charges, which corresponds to a net charge of 40%). Also the thickness of *E. coli* membranes (37.5 ± 0.5 Å[192]) is close to the optimal conditions identified in the present study. This explains the observed high background ATPase activity BmrA has in *E. coli* membranes or when incorporated into EPL liposomes (Figure 9C/D).

Similarly, also the composition and properties of *B. subtilis* membranes (natural environment) can be expected to support the BmrA activity well. The membrane lipid composition appears to highly depend on the exact growth conditions, yet a high amount of negatively charged lipids (up to ~12% CL and ~36% PG) can be naturally present in *B. subtilis* inner membranes[193]. While not further analyzed here, the charges of PG and CL likely cannot simply be added up, and thus probably both *E. coli* and *B. subtilis* offer a membrane surface charge that highly supports the BmrA activity. Furthermore, *B. subtilis* membranes might contain 20-40% of the non-bilayer-forming phospholipid PE, *i.e.*, less than *E. coli* membranes, yet can additionally contain up to 30% of the neutral, non-bilayer-forming lipid diacylglycerol[194]. Thus also *B. subtilis* membranes can have high negative curvature stress, which, as we show here, affects the BmrA activity. On the other hand, the *B. subtilis* membrane appears to be thinner than *E. coli* membranes, as the average lipid acyl chain length of membrane lipids is C16[194,195], which corresponds to a hydrophobic membrane thickness of around 26 Å[188,196], suggesting that BmrA is not optimized for the *B. subtilis* membrane. Yet, as shown for other membranes, the average *in vivo* membrane thickness is not exclusively determined by the lipid acyl chain length but also by membrane-incorporated proteins[192]. Furthermore, other membrane constituents besides the here-studied phospholipids might additionally affect the structure and thickness of the *B. subtilis* membrane. Thus, the thickness of the *B. subtilis* membrane likely differs from the value anticipated solely based on the average acyl chain length, again suggesting that the *B. subtilis* membrane environment stimulates the BmrA activity well.

It is still unclear why the ATPase activity of BmrA is so high in the absence of substrates, resulting in constant futile ATP hydrolysis that is not typical for all ABC transporters. The here-presented observations now show that the intimate lipid environment can control the activity of BmrA. As *B. subtilis* membranes are structured and defined lipid domains with specific lipid compositions appear to exist[197,198], it is feasible to assume that the activity of BmrA is spatio-temporally

controlled in living *B. subtilis* cells by the intimate lipid environment. Activation of the protein by sorting it into or out of membrane regions with an activity-stimulating lipid composition would allow cells to regulate the activity of the protein and prevent futile ATP hydrolysis *in vivo*. Thus, we suggest that the activity of BmrA might be controlled *in vivo* via a dynamic (re)localization of the protein into or out of membrane regions with defined lipid compositions and (potentially) membrane thicknesses.

4.2 The C-terminal α-helix is crucial for the activity of the bacterial ABC transporter BmrA

4.2.1 Publication

The content of this chapter was published during the course of this thesis as:

Osten V.[a,‡], [redacted] (2025) The C-terminal α-helix is crucial for the activity of the bacterial ABC transporter BmrA, *J. Biol. Chem.*, 301 (2):108098.

[redacted]

This chapter cites the published article[199] with the following changes:

- The format of this article was adapted to the style of this thesis.
- Abbreviations have been combined with those of the other thesis chapters.
- Figures, tables and citations are rearranged and renumbered in accordance to this thesis.
- The methods section was removed and the performed methods are now included in the general method chapter 3.2 of this thesis.
- The supplementary figures are renumbered and can be found in chapter 6.3.

The Author contributions according to the CRediT taxonomy are listed in Table 4.1.

Table 4.2: Author contribution of the article titled as "The C-terminal α-helix is crucial for the activity of the bacterial ABC transporter BmrA".

	Application	Author
Conceptualization	Complete study	**V.O.**, [redacted]
Methodology, Investigation,	Figure 14	**V.O.**
Formal analysis, Data	Figure 15	**V.O.**, [redacted]
visualization	Figure 16	**V.O.**
	Figure 17	**V.O.**, [redacted]
	Figure 18	**V.O.**
	Figure 19	**V.O.**
	Figure 20	**V.O.**, [redacted]
	Figure S3	**V.O.**, [redacted]

	Figure S4	**V.O.**
	Figure S5	**V.O.**
Writing	Original draft	**V.O.**, [redacted]
	Review and editing	**V.O.**, [redacted]
Project administration, Funding acquisition, Recourses, Supervision	Complete study	[redacted]

4.2.2 Abstract

ABC transporters are membrane integral proteins that consist of a TMD and an NBD. Two monomers (half-transporters) of the *B. subtilis* ABC transporter BmrA dimerize to build a functional full-transporter. As all ABC exporters, BmrA uses the free energy of ATP hydrolysis to transport substrate molecules across the cell membrane. For substrate transport, a BmrA dimer undergoes major conformational changes. ATP binding drives dimerization of the NBDs followed by the hydrolysis of the nucleotides. Conserved structural elements within the NBD and TMD are crucial for dimerization and the activity of BmrA. In the BmrA structure, an α-helix is present at the C-terminus, which can be subdivided into two smaller helices. As shown here, the very C-terminal helix (fragment) is not crucial for the BmrA activity. In fact, based on Cys-scanning mutagenesis, this region is highly flexible. In contrast, a BmrA variant lacking the entire C-terminal α-helix showed no ATPase and transport activity. Via Ala-scanning, we identified residues in the N-terminal fragment of the helix that are crucial for the BmrA activity, most likely via establishing contacts to structural elements involved in ATP recognition, binding, and/or hydrolysis.

4.2.3 Introduction

ABC transporters are found in all domains of life[31,200]. These transporters either import (mainly in bacteria and plants) or export a broad variety of substrates[78,201]. Structurally, ABC transporters consist of four core domains: two TMDs and two cytosolic NBDs, albeit the exact molecular architecture of these transporters is extremely diverse[53,78,202]. In fact, a transporter can consist of a single polypeptide chain that contains all four domains, or, if one TMD and one NBD are located on a single polypeptide chain, two different such half-transporters heterodimerize, such as the ABC transporter TAP1/TAP2[203], or two identical half-transporters homodimerize (e.g., *Sav*1866[48]) to form an active transporter. Finally, each of the four domains can be individual proteins, which assemble to form a functional ABC exporter[53,204].

The structurally diverse substrates of ABC exporters enter the substrate-binding cavity, which is located in the TMD[28,78], either from the cytoplasmic site of the membrane or from within the

membrane[205,206]. Upon substrate binding, the transporter undergoes major conformational changes, finally resulting in the transport of a substrate against a concentration gradient[48,53,97,132,207]. Substrate transport is fueled by ATP hydrolysis at the NBDs, which are located at the cytoplasmic side. The sequences and topologies of NBDs of different ABC transporters are highly similar, and motifs involved in ATP recognition, binding, and hydrolysis are conserved[29,202,208]. These motifs within the NBDs are located in two different subdomains of the NBD, an α-helical domain with the ABC signature motif and the X-loop, and a RecA-like subdomain with the Walker A and Walker B motifs and the Q-, D-, and H-loops. The ATP-binding sites are formed via interaction of two NBDs, and an ATP molecule is bound between the Walker A motif of one NBD and the ABC signature motif of the opposing NBD[209,210]. Consequently, ATP-binding triggers dimerization of the two opposing NBDs of an ABC transporter[76,98,140,211–213]. The CHs at the cytoplasmic side of the protein are additionally relevant for NBD-TMD communication[48,214,215]. ATP-induced NBD dimerization causes a conformational change of the exporter from an IF via an occluded state to an OF conformation[129]. Now, the substrate cavity within the TMDs is open to the extracellular side of the membrane, and the substrate is released. Substrate release and ATP hydrolysis set the transporter back into the IF conformation, and the transporter is ready for the next translocation cycle[216].

Isolated NBDs have typically no propensity to dimerize in the absence or presence of ATP[64], and, in fact, the TMDs facilitate NBD dimerization upon ATP binding. Occasionally, NBDs of transporters contain additional domains that also stabilize the dimer in the absence of ATP, as, e.g., the C-terminal regulatory domain (of 136 residues) of the ABC importer MalK[217,218]. Furthermore, the NBDs of the tetrameric ABC transporter $ModB_2C_2$ are suggested to be in constant contact, mediated by α-helices at the C-terminal ends that interact to some degree and thereby link the NBDs[92]. Likewise, the homodimeric ABC transporters Atm1[139] and HlyB[74] appear to have interacting helices at their NBDs' C-termini, which were postulated to stabilize the dimer. Since many ABC exporters appear to have such short C-terminal α-helices, this structure might more generally contribute to dimer stability[219]. However, the exact role of these short C-terminal helices in the translocation cycle is still enigmatic, although the C-terminal helices appear to be important for the activity of the heterodimeric ABC exporter called *Thermus thermophilus* multidrug resistance proteins A and B (TmrAB)[49]. Also the homodimeric ABC transporter BmrA of the Gram-positive bacterium *B. subtilis* contains an α-helical segment at its very C-terminus[220,221]. BmrA can extrude a broad variety of substrates out of a membrane, and the protein shows sequence identity with the human P-gp as well as with the bacterial ABC exporters MsbA and LmrA[124]. Not only because of this, BmrA became a paradigm for studying the structure and function of ABC transporters and their role in MDR. The structure of the BmrA exporter in the OF conformation was solved via X-ray crystallography as well as cryo-EM[80]. As can be seen in these structures (Figure 14A/B), the α-helical C-terminal ends of the NBDs are in close distance and thus,

potentially interact. Recently, the IF conformation of wt BmrA was also solved via cryo-EM, and here the C-terminal ends remained in close distance[79].

In the present study, we show that deletion of the entire C-terminal α-helix of BmrA leads to a complete loss of the ABC transporter activity, measured as ATPase activity as well as via quantifying transport of the dye Hoechst 33342 across membranes. However, the C-terminal helix is not continuous, yet in fact is built from two smaller α-helical segments. Deletion of the most C-terminal α-helical fragment did not affect the BmrA activity, whereas the N-terminal helix part is crucial for the BmrA ATPase as well as transport activity. In fact, via Cys-crosslinking, we show that the C-terminal part is rather flexible. In contrast, upon replacing individual residues in the N-terminal fragment of the α-helix, we identified residues that are crucial for the BmrA activity, most likely due to interactions with structural elements crucial for ATP binding and/or hydrolysis.

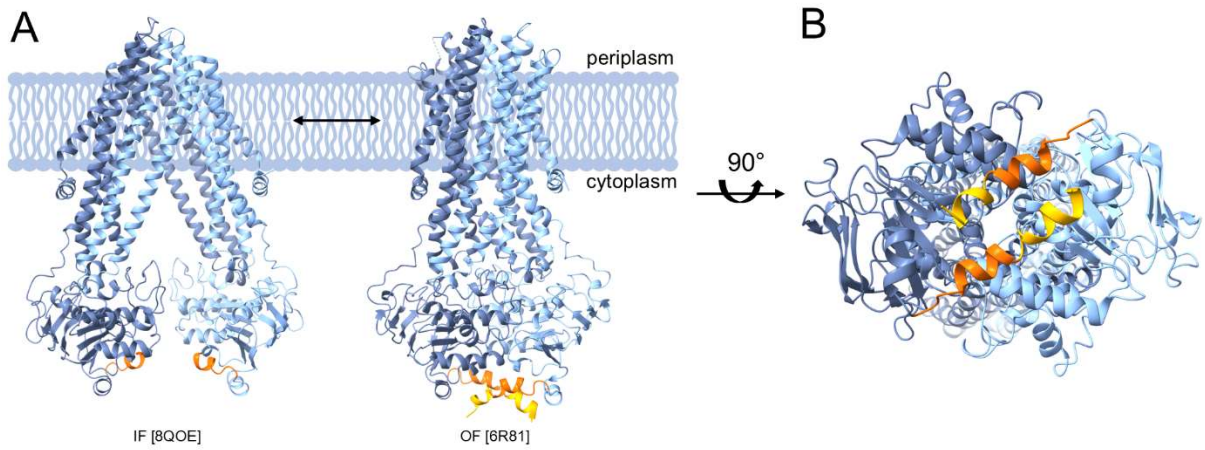

Figure 14: The ABC transporter BmrA in the IF and OF conformation.

(A) A BmrA dimer (half-transporters: light blue and dark blue) in a lipid bilayer with the first C-terminal α-helical segment of the NBDs highlighted in orange and the second segment highlighted in yellow. The IF (PDB: [8QOE][79]) and OF (PDB: [6R81][80]) conformations are shown. **(B)** View of the C-termini from the cytoplasmic side after a 90° rotation of the BmrA dimer in its OF conformation as shown in (A).

4.2.4 Results

4.2.4.1 The BmrA C-terminus is crucial for activity

In the BmrA structure, a short α-helix is located at the very C-terminus[80], and the two C-terminal helices of two interacting monomers (half-transporters) appear to interact in an anti-parallel fashion in the dimer (Figure 14). Based on the previous observations that many ABC exporters contain short α-helices at the C-terminal end, which might contribute to the dimer stability[74,92,139,217–219], it is reasonable to assume that the C-terminal α-helix might also be crucial for the activity of BmrA. Therefore, we analyzed in the present study (i) whether the BmrA C-

terminal helices are crucial for the BmrA activity and (ii) whether the C-termini of adjacent BmrA half-transporters indeed interact.

To investigate the putative role of the C-terminal helix on the BmrA activity, we first analyzed BmrA variants where the C-terminal α-helix was completely absent (residues L569-G589, ΔCT) or solely the very last α-helical region (residues K579-G589, ΔCTh, "h" for half) that forms an independent helix in some structures (Figure 14A/B, 15A).

While the ATPase activity of BmrA ΔCTh was not significantly reduced compared to the wt (Figure 15B), indicating a dispensable function of this region, the ATPase activity was essentially completely abolished when the entire C-terminus was removed. Next, we aimed to quantify the substrate transport activity of the BmrA variants and used IMVs to determine transport of the hydrophobic dye Hoechst 33342 across the membrane. Similar to the above-presented observations, the transport activity of ΔCTh was not significantly reduced compared to BmrA wt, whereas the transport activity of ΔCT was essentially completely abolished (Figure 15C).

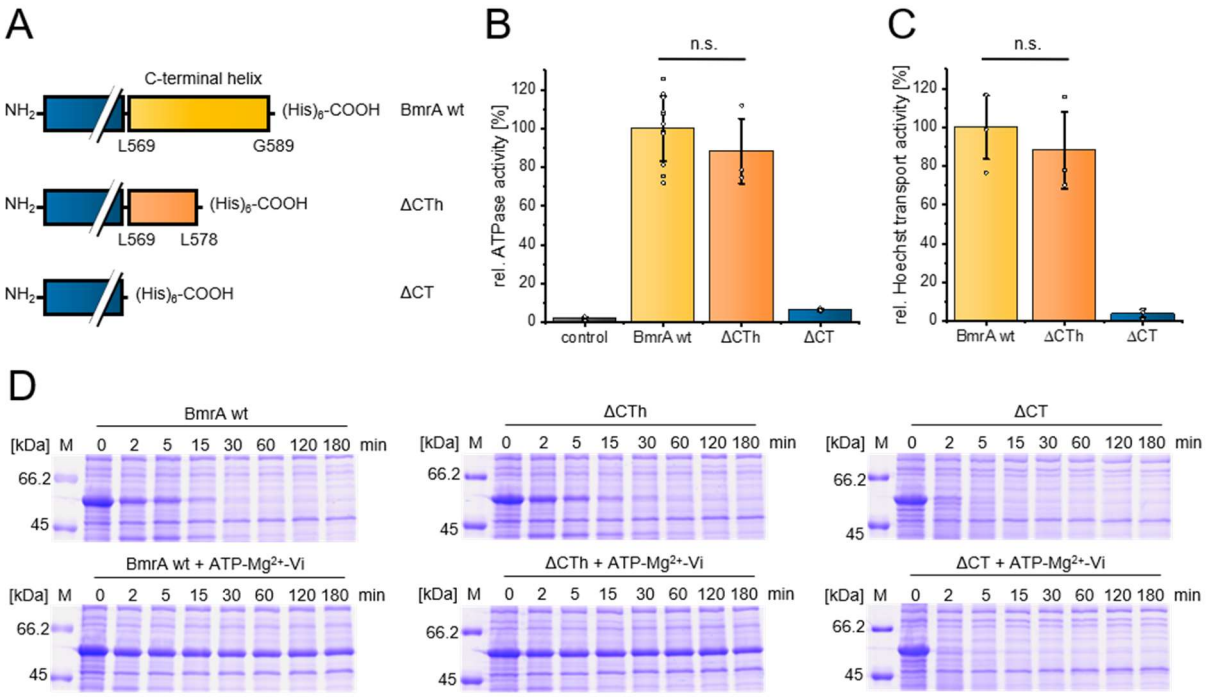

Figure 15: ATPase, Hoechst 33342 transport activities, and limited proteolysis of C-terminally truncated BmrA variants.

(A) Sketch of the C-terminal end showing the ΔCTh and the ΔCT compared to BmrA wt. **(B)** Mean of relative ATPase activity of BmrA wt and variants (n = 10 for the wt, n = 3 for the truncated variants, ± SD, two-sample t-test, p = 0.61). Individual data points are shown and represent independent biological replicates. **(C)** Mean of relative Hoechst 33342 transport activity assay of IMVs containing overexpressed BmrA wt or variants (n = 3, ± SD, two-sample t-test, p = 0.50). Individual data points are shown and represent independent biological replicates. **(D)** SDS-PAGE analysis of IMVs containing overexpressed BmrA wt, ΔCTh, or ΔCT after limited digestion by Trypsin. Samples in the presence or absence of ATP, Mg^{2+} and orthovanadate, which stabilizes the OF conformation, are shown. Samples were treated for the indicated times (0, 2, 5, 15, 30, 60, 120, and 180 min) with Trypsin and subsequently analyzed via SDS-PAGE.

Next, the putative effects of C-termini interactions on protein structure and/or conformational changes (IF vs. OF conformation) were analyzed via limited proteolysis. Therefore, IMVs containing the BmrA variants were digested with a low amount of Trypsin. In the IF conformation, the transporter is more accessible for Trypsin and will be rapidly digested, while in the OF conformation, the transporter is more resistant against Trypsin digestion[147]. In line with this, BmrA wt incorporated in IMVs was digested slower when ATP, Mg^{2+} and orthovanadate were present, which stabilizes the OF conformation (Figure 15D). The proteolytic stability of the truncated variant ΔCT was wt-like, suggesting that the very last C-terminal part is not required for formation and/or stabilization of the OF conformation. In contrast, no increased resistance against Trypsin digestion upon the addition of ATP, Mg^{2+} and orthovanadate was observed when the entire C-terminal α-helix was deleted (BmrA ΔCT). In fact, already in the absence of ATP, Mg^{2+} and orthovanadate, BmrA ΔCTh was more sensitive against Trypsin digestion than the wt (Figure 15D). This indicates that not solely the OF state, yet the overall transporter conformation is destabilized when the full C-terminal BmrA α-helix is deleted. Taken together, the C-terminal residues L569 to L578 are crucial for the BmrA ATPase and transport activity, whereas the amino acids at the very C-terminal end appear to have no direct impact on the ATPase or transport activity of BmrA.

4.2.4.2 Cys crosslinking of C-terminal residues indicates structural flexibility

While the above-presented deletion analysis implied that the last part of the C-terminus (K578-G589) has no impact on the BmrA function, in contrast to the first part of the C-terminal α-helix (L569-L578), we studied putative interactions within the dimer, which might be involved in fine-tuning the BmrA activity. The L569-L578 region is located in close proximity to its counterpart from the interacting monomer. Based on the available BmrA structures in the OF conformation, the C-terminal helices of two protomers appear to form an antiparallel helix dimer, and the two helices cross at residue N581, where the distance between the C_α residues is only about 4.1 Å (Figure 16A). Noteworthy, in other studies this helix part was found to be not highly structured but more flexible[222]. Thus, we aimed at illustrating the interaction of the two helix fragments via crosslinking the two C-terminal helices of BmrA half-transporters and introduced a Cys residue at position N581. Furthermore, to analyze a potential flexibility in this region, we individually replaced also the residues adjacent to N581 (K579-D583) by Cys and tested whether here the formation of disulfide bridges and covalent linkage of two neighboring NBDs is possible also in the absence of ATP. When analyzed via non-reducing BN-PAGE, the wt protein ran as stable monomers and dimers, whereas all Cys-containing variants formed stable dimers in solution (Figure 16B). Yet, in the presence of the reducing agent DTT, the variants also run as monomers and dimers on a BN-PAGE gel, as observed for the wt (Figure 16B). While the C-terminal helices

appear to cross at residue N581 in the solved structure, the capability of all here analyzed variants to form crosslinked dimers strongly indicates a certain flexibility of this region, as no preferentially interacting residue was identified. Furthermore, the observations indicate that the C-terminal helices of the two transporter halves are in close distance even in the absence of ATP, *i.e.*, the two NBDs appear to stay in close distance even when no nucleotides are bound.

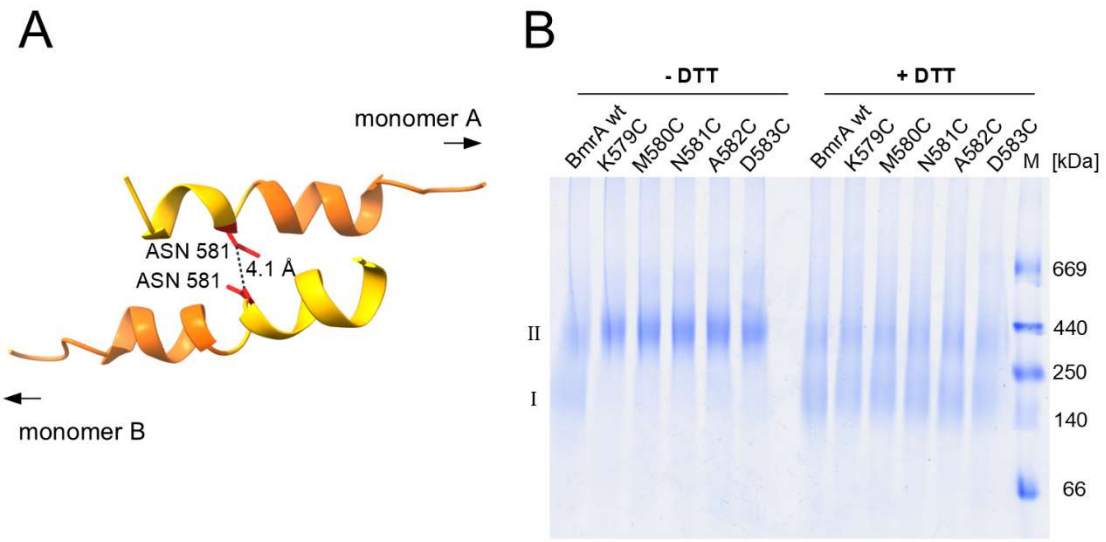

Figure 16: Antiparallel C-terminal helix dimer of BmrA.

(A) The C-terminal helices (L569-L578 in orange, K579-G589 in yellow) of two BmrA monomers (A/B) are in close distance and cross at the amino acid N581 (red). The distance of the C_α atoms of opposing N581 is 4.1 Å (PDB: [6R81][80]). **(B)** BN-PAGE analysis of BmrA Cys variants crosslinked in DDM micelles. Reducing (+ DTT) and oxidizing (- DTT) conditions are indicated. The proteins were separated on a 4 – 16% Bis-Tris gel, and monomers (I) and dimers (II) were observed.

4.2.4.3 Ala scanning of essential C-terminal residues

Based on the results presented above, we next elucidated which amino acids of the essential C-terminal helix fragment (residues L569 to L578) are most critical for the ATPase and transport activity of BmrA. For this purpose, all individual amino acids of this region were replaced by Ala (or Val, when an Ala was naturally present), and the ATPase as well as the Hoechst 33342 transport activities of these BmrA variants were tested (Figure 17). Mutations in the margins of this helical fragment (L569-R571 and Q576-L578) led to strongly reduced (≤ 25%) ATPase activities compared to the wt activity (Figure 17A).

In contrast, the variants carrying mutations in the helix core (D572A-Q576A) displayed only slightly or moderately reduced ATPase activities (≥ 50% remaining). The only exception was the variant F573A that showed significantly reduced ATPase activity (as further analyzed and discussed below). Thus, based on these analyses, most residues in the core of this helical fragment (residues D572-E575) do most likely not establish contacts in the protein that are crucial for

activity, whereas the margin regions L569-R571 and Q576-L578, and potentially F573, are more crucial for the BmrA activity.

Next, we analyzed a putative correlation between the determined ATPase and the relative Hoechst transport activities using IMVs (Figure 17B). The transport activities of five variants (L569A, Y570A, R571A, F573A, and L578A) were less than 25% compared to the BmrA wt activity, whereas the activity of the variants D572A and A574V-Q577A was reduced 'only' to about 50% (40% in the case of Q577A) of the wt activity. Our results show a very good correlation (Figure 17C) between ATPase and Hoechst transport activities in IMVs considering an uncertainty

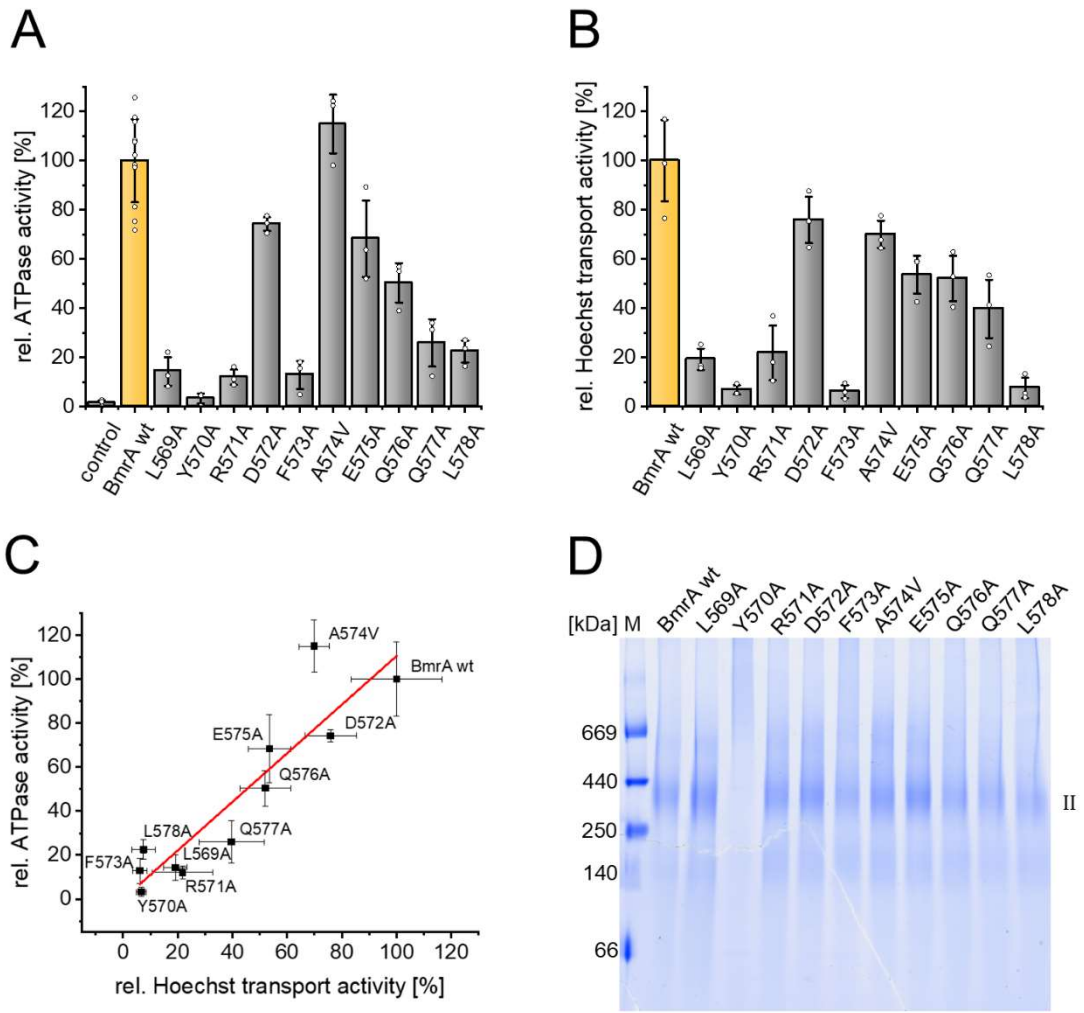

Figure 17: ATPase, Hoechst 33342 transport activities, and dimerization propensities of BmrA wt and variants L569A-L578A.

(A) Mean of relative ATPase activities of the Ala (Val) variants (n = 10 for the wt, n = 3 for the variants, ± SD). Individual data points are shown, representing independent biological replicates. **(B)** Mean of relative Hoechst 33342 transport activities of the Ala (Val) variants overexpressed in IMVs (n = 3, ± SD). Individual data points are shown, representing independent biological replicates. **(C)** Relative ATPase activities versus the relative transport activities. Data points were fitted with a linear fit shown in red (R^2 = 0.93). **(D)** Dimerization tendency of BmrA wt and variants in DDM micelles analyzed via BN-PAGE. The proteins were separated on a 4 – 16% Bis-Tris gel, and the dimer bands are indicated (II).

range of 20%. Since ABC transporters are only functional as homo- or heterodimers, we additionally tested whether the introduced mutations led to an altered dimerization propensity and analyzed dimerization of the BmrA variants via BN-PAGE. As shown in Figure 17D, BmrA wt mainly forms dimers in DDM micelles. All here analyzed BmrA variants showed a wt-like dimerization propensity, except Y570A. In contrast to all other variants, BmrA Y570A appears to aggregate, which explains the observed drastically reduced ATPase and transport activities (Figure 17A/B). However, for the remaining variants, the reduced activities cannot be explained by an impaired dimerization propensity.

4.2.4.4 Thermal stability of the isolated NBD carrying the x-to-Ala mutations

While the amino acids were replaced to disturb putative crucial interactions, it was also possible that the replacements affected the overall stability of the NBD. Therefore, we next analyzed the structure and stability of isolated wt and mutated NBDs. For the sake of simplicity, we leave the amino acid numbering of the variants at that of the full-length protein, even if they are NBD variants. Via CD spectroscopy we aimed at identifying potential altered structures of the BmrA variants to exclude that altered folding and/or stability has caused the observed changes in BmrA activities. As shown in Figure 18A, all proteins were electrophoretically pure after isolation. The CD spectra of the purified variants measured at 25 °C (Figure 18A) revealed that all variants showed a similar CD spectrum typical for mainly α-helical proteins, with characteristic minima at 208 and 222 nm. Yet, with increasing temperatures (20-88 °C), the protein structure changed, visible as changes in the CD spectra characteristics (Figure 18C, shown for NBD wt as an example and for the other variants in Figure S4). The CD intensities of both minima increased to a certain degree, and finally solely a minimum at 217 nm was observed at high temperatures, a value typical for β-sheet structures. Using the fluorescence probe ThT, which changes its fluorescence properties upon binding to amyloid fibrils[154], we observed that its fluorescence emission maximum was significantly increased when the NBD was thermally denatured (Figure S5). The isolated NBD thus appears to form amyloid-like structures at high temperatures, resulting in a high ThT quantum yield at 482 nm.

Plotting the ellipticity at 222 nm against the temperature revealed that in most cases denaturation occurred in a highly cooperative manner, with one transition (Figure 19A). In order to estimate the apparent transition temperature, a modified Boltzmann curve was fitted to the data (Figure 19A). The inflection point represents the transition temperature of a protein and can be used to compare the thermal stabilities of proteins and/or protein variants. Most of the NBD variants examined showed comparable transition temperatures, which were in the range of the wt protein ± 4.2 °C (Figure 19B). Yet, for Y570A and F573A, the transition temperatures were

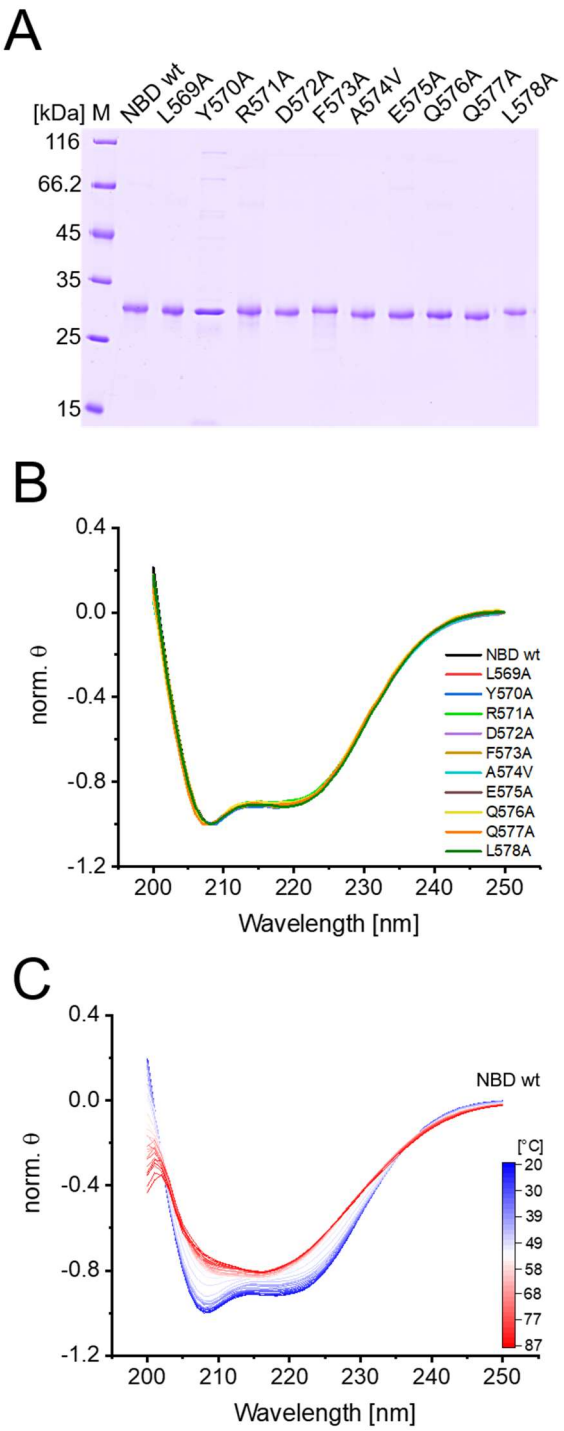

Figure 18: Secondary structure of NBD wt and the variants with Ala (Val) mutations in the C-terminal helix part L569A-L578A.

(A) SDS-PAGE analysis of purified NBD variants after Ni-NTA chromatography and further chromatography steps, if necessary (see methods). The calculated mass for each variant is around 29.5 kDa. M = marker. **(B)** CD spectra of NBD wt (black), L569A (red), Y570A (blue), R571A (light green), D572A (violet), F573A (ocker), A574V (cyan), E575A (brown), Q576A (yellow), Q577A (orange), and L578A (dark green) measured at 25 °C. For better comparison, the mean spectra determined for three independent purifications after normalization are shown. The θ value at 250 nm was set to 0 and the minimum θ value to -1. **(C)** CD spectra of NBD wt recorded at increasing temperatures (20 °C, blue – 88 °C, red). For each temperature the mean value determined using three independent purifications was normalized (θ of 250 nm was set to 0; minimum θ was set to -1).

significantly reduced. For Y570A (T_m = 32.9 ± 2.0 °C) the sigmoidal melting curve showed no plateaus at higher and lower temperatures, and thus, we conclude that the structure and stability of this protein is altered due to the amino acid exchange, in line with our observation that the corresponding full-length protein BmrA Y570A tends to aggregate (Figure 17D). Similar observations were made with the variant F573A, where the transition temperature is significantly reduced (40.7 ± 0.4 °C, Figure 19B). Explaining the reduced ATPase and transport activity of the respective full-length BmrA variant F573A (Figure 17A/B), although this variant ran as the wt protein during BN-PAGE (Figure 17D). It should be mentioned that all activity measurements were carried out at 25 °C, where no significant structural changes were observed via CD measurements (Figure 18C). Taken together, the observations indicate that in the case of Y570A and F573A, the altered structure/stability of the NBD most likely explains the observed reduced activity of the full-length protein. Yet, F573A still has a wt-like tendency to form dimers at lower temperatures, unlike Y570A (Figure 17D). In contrast, in the case of L569A-R571A and L578A, the NBDs had wt-like stability, and likely interactions with other parts of the full-length protein are disturbed.

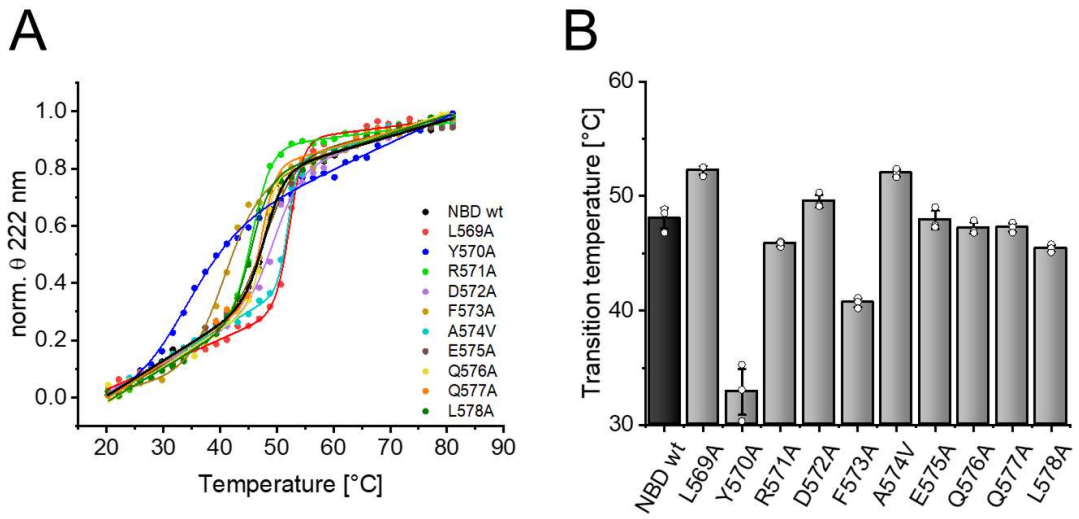

Figure 19: Transition temperatures of NBD wt and the variants with Ala (Val) mutations in the C-terminal helix part L569A-L578A determined via CD measurements.

(A) Normalized θ values at 222 nm of NBD wt (black), L569A (red), Y570A (blue), R571A (light green), D572A (violet), F573A (ocker), A574V (cyan), E575A (brown), Q576A (yellow), Q577A (orange), and L578A (dark green) plotted against the temperature. The means of three independent measurements of three independent biological replicates are shown, which were fitted with an adapted Boltzmann fit (shown as lines, $R^2 > 0.997$). **(B)** Calculated transition temperatures (T_m) of the NBD variants determined via CD spectroscopy. T_m corresponds to the inflection points of the fitted curves and is shown with SD: 48.1 ± 0.9 °C (NBD wt), 52.3 ± 0.4 °C (L569A), 32.9 ± 2.0 °C (Y570A), 45.8 ± 0.2 °C (R571A), 49.5 ± 0.6 °C (D572A), 40.7 ± 0.4 °C (F573A), 52.0 ± 0.3 °C (A574V), 47.9 ± 0.8 °C (E575A), 47.7 ± 0.5 °C (Q576A), 47.3 ± 0.4 °C (Q577A), and 45.4 ± 0.3 °C (L578A).

4.2.5 Discussion

The C-terminus is crucial for the BmrA ATPase and transport activity

ABC exporter-mediated transmembrane substrate transport involves major conformational changes of the transporter structure, from an IF to an OF conformation and backwards. Here, not only are interactions between the TMDs and NBDs crucial, but also interactions between the two NBDs of an ABC transporter to finally form stable dimers resulting in proper ATP hydrolysis and substrate transport. The NBDs of type IV dimeric ABC exporters in the OF conformation are already in quite close proximity[43]. Yet, ATP binding is necessary for proper NBD dimerization[223], whereas ATP hydrolysis is needed for the disassembly of the NBD dimer to reset the translocation cycle[133,224]. Based on the recently published BmrA structures in the OF conformation[80], it is apparent that the C-terminal ends are in close proximity and are oriented to some extent side by side (Figure 14). Consequently, in this study we investigated a putative role of C-terminal helix interactions for the activity of BmrA.

The C-terminal helix of BmrA can be subdivided into two shorter α-helical fragments (Figure 14). When the entire helix was deleted, the switch between the IF and OF conformations was

disturbed, and the ATPase as well as transport activity were completely abolished, indicating a critical role of this helix (Figure 15). Yet, when solely the very C-terminal helix fragment was deleted (Figure 15, ΔCTh), the activity was essentially unaltered. Apparently, this helical region does not establish interactions within or between half-transporters crucial for function (Figure 15). In fact, when we replaced the residues K579-D583 of this fragment individually by Cys, all variants formed stable Cys cross-linked dimers (Figure 16B/C). Thus, the very C-terminal end of BmrA appears to be highly flexible and is possibly not completely α-helical at all times, in excellent agreement with a recent NMR study of the isolated BmrA NBD monomer[222]. Furthermore, in the recently published structures of BmrA in the OF conformation (PDBs: 6R81, 6R72, 7OW8, 7BG4), the very C-terminal region appears to be more flexible and has varying α-helix content. This high flexibility indicates that this region does not establish stable and crucial contacts. Our observations clearly support this assumption, as the very C-terminal region is not necessary for the OF state (Figure 15D). Even in the IF conformation, where the NBDs are separated to some degree, the C-termini of the BmrA monomers still remain in close proximity, in contrast to other ABC transporters that show a large separation of the NBDs, such as MsbA[79]. Close proximity of the NBDs even in the BmrA IF conformation is strongly supported by our results, as our Cys crosslink experiments were carried out in the absence of ATP, *i.e.*, under conditions favoring the IF conformation.

A pair of hydrophobic amino acids stabilize the C-terminal α-helix of BmrA

In contrast to BmrA ΔCTh, the BmrA ΔCT variant showed only a poor ATPase activity, and thus we concluded that some or all amino acids L569-L578 in the C-terminal α-helix are crucial for activity. Based on our mutational analyses, especially the neighboring residues L569-R571 and Q577/L578 are crucial for the overall BmrA function, as well as F573. In contrast, replacement of the remaining core residue of this α-helix fragment (D572, A574-Q576) did not affect the BmrA activity dramatically (Figure 17). As shown by BN-PAGE analysis, all variants, except Y570A, had a wt-like propensity to dimerize (Figure 17D). This indicates that the Ala substitution altered the stability of the dimer solely in case of Y570A. To elucidate whether the reduced activities of the remaining BmrA variants were due to disturbed putative crucial interactions or a reduced protein stability, we determined the thermal stability of the isolated NBD (variants) via CD spectroscopy. Here we used the soluble NBD since it is properly folded, as shown in numerous studies, and is therefore suitable for our approach[131,222,225]. Our observations clearly showed that most variants had a wt-like transition temperature, except the NBD variants Y570A and F573A which both showed a drastically reduced transition temperature (Figure 19). This indicates that both mutations affect the protein stability, possibly due to disruption of the stabilizing effect on α-helices by a pair of two hydrophobic residues in a distance of three or four amino acids at the N-terminus[226]. This nicely explains the observed lowered ATPase and Hoechst 33342 transport

activities of the respective full-length variants (Figure 17). For the other amino acids studied, however, it is more likely that the corresponding effects on protein function are due to disturbed key interactions of the C-terminal helix with crucial structural elements.

Putative crucial interactions of the C-terminal helix

Based on the structures of the BmrA full-length protein (PDBs: 6R81, 6R72, 7OW8, 7BG4, 8QOE), the residues L569-R571 are in close proximity to the Walker A motif of the same monomer (Figure 20). The Walker A motif mediates ATP binding and triggers NBD dimerization[211]. Therefore, it is feasible to assume that mutating the residues L569-R571 individually to Ala affects dimerization and ATP hydrolysis of BmrA. A decreased ATPase activity could also be determined for the variant carrying mutations in Q576-L578 (Figure 17). These amino acids are in close distance (C_α<10 Å) to residues of the H-loop of the same monomer (Figure 20B). This loop recognizes and adjusts ATP and is, consequently, also needed for proper dimerization and ATP hydrolysis by an ABC transporter. *E.g.*, mutations in the eponymous H-loop caused a drastically

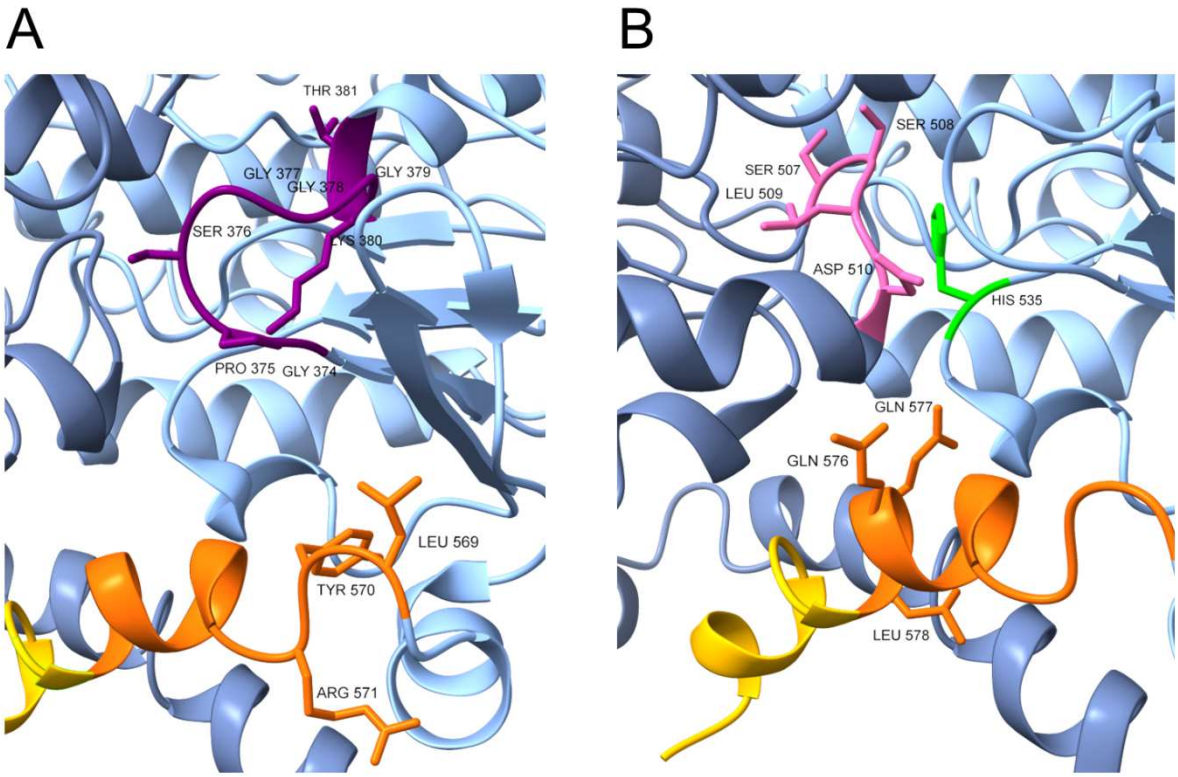

Figure 20: Structure of BmrA with putative interaction partners of crucial residues at the C-terminal end.

View on the C-terminal α-helix of a BmrA dimer, where one monomer is colored in blue and the second in dark blue. Of one monomer the first segment of the C-terminal α-helix (L569-L578) is highlighted in orange and the second segment (K578-G589) in yellow with certain amino acids marked. Additionally, the amino acids residues of **(A)** the Walker A motif (purple), or **(B)** of the H-loop (green) and the D-loop (pink) are shown (PDB: [6R81][80]).

decreased ATPase activity of the ABC transporters HisP, MalK, and HlyB, and substrate transport activities were not observed anymore[74,227,228]. The lack of crucial interaction partners for amino acid residues that directly interact with the conserved (eponymous) His of the H-loop could lead to further malfunctions of this important structural part. Furthermore, the amino acid residues Q576 and Q577 are close to the D-helix of the adjacent NBD (Figure 20B). In line with this, the C-terminal α-helix is crucially involved in dimerization of the eukaryotic ABC transporter TAP1[73]. Thus, interactions between the C-terminal amino acid residues Q576 to L578 and the H-loop of the same monomer as well as the D-helix of the opposite NBD are potentially important for dimerization of BmrA, and thereby for ATP hydrolysis.

In summary, the N-terminal part of the last C-terminal α-helix of BmrA is important for the ABC transporter to be fully functional, likely due to interactions with conserved elements crucial for ATP binding and/or hydrolysis. Especially the proximity of the residues L569-R571 to the Walker A motif and the interactions of Q576-L578 with residues interacting with the H-loop of the same NBD and the D-helix of the adjacent NBD might be crucial for mediating NBD dimerization and thereby regulating the ATPase activity of BmrA.

4.3 A salt bridge pre-arranges the BmrA structure for proper NBD dimerization

4.3.1 Manuscript

The content of this chapter was prepared for submission as part of this thesis:

Osten, V.[a], [redacted] (2025) A salt bridge pre-arranges the BmrA structure for proper NBD dimerization, *in preparation*.

[redacted]

Methods performed by collaboration partners can be found in chapter 6.4.

The Author contributions according to the CRediT taxonomy are listed in Table 4.3.

Table 4.3: Author contribution of the manuscript titled as "A salt bridge pre-arranges the BmrA structure for proper NBD dimerization".

	Application	Author
Conceptualization	Complete study	**V.O.**, [redacted]
Methodology, Investigation,	Figure 21	**V.O.**
Formal analysis, Data	Figure 22	**V.O.**, [redacted]
visualization	Figure 23	**V.O.**, [redacted]
	Figure 24	**V.O.**, [redacted]
	Figure 25	**V.O.**
	Figure 26	**V.O.**, [redacted]
	Figure 27	**V.O.**, [redacted]
	Figure 28	[redacted] **V.O.**
	Figure 29	**V.O.**
	Figure S6	**V.O.**, [redacted]
	Figure S7	**V.O.**
	Figure S8	**V.O.**

Writing	Original draft	**V.O.**, [redacted]
Project administration	Complete study	[redacted]
Funding acquisition, Recourses, Supervision	Complete study	[redacted]

4.3.2 Abstract

ATP-powered ABC transporters mediate the transport of a wide variety of substrates across membranes. Successful substrate translocation relies on the intricate communication between the NBDs and the TMDs. In type IV ABC exporters, such as BmrA of *B. subtilis*, this NBD-TMD communication is facilitated by two intracellular CHs. However, the structural elements that stabilize this interface are not fully understood. Inspection of the available BmrA structures shows that the linker connecting the TMD to the NBD lies adjacent to both CHs, suggesting that this region may provide essential contacts.

Via Ala mutagenesis, we analyzed a crucial part of the linker and characterized the ATPase and transport activities of the respective mutants. We identified Glu326 as being essential for the BmrA activity, and Ala substitution impaired the BmrA transport activity and completely abolished the *in vitro* ATPase activity, although cysteine-cross-linking confirmed that the NBDs themselves remained functional. Cryo-EM analysis of the Glu326Ala variant revealed a disrupted NBD-TMD arrangement, with the CHs spatially uncoupled from the NBDs. Further mutational work on oppositely charged residues identified Lys217 in CH2 as a potential interaction partner. We propose that a conserved salt bridge between Glu326 and Lys217 stabilizes the CH-NBD interface, thereby promoting proper NBD dimerization and functional coupling. This salt bridge motif is conserved across bacterial exporters and members of the human ABCC family, underscoring a previously unrecognized role for the linker region in ABC transporter function.

4.3.3 Introduction

ABC transporters constitute one of the largest protein superfamilies, ubiquitously present across all phyla of life[27,28]. These transporters facilitate the import or export of a diverse range of substrates, including endogenous molecules (e.g., sugars, lipids, metabolites) and exogenous compounds (e.g., drugs), across cell membranes via primary active transport[25,43,170]. A functional ABC transporter comprises four key entities: two highly conserved NBDs and two substrate-binding TMDs[29]. The organizational structure of these domains varies, with three possible configurations: (1) as a single polypeptide chain, (2) as two chains with one NBD fused to one TMD (half-transporter), or (3) as four separate polypeptides. The latter two configurations require homo- or hetero-oligomerization to form a functional full-transporter.

ATP binding and hydrolysis occur at the NBSs, which are formed by dimerization of both NBDs in a head-to-tail orientation. ATP binding engages conserved motifs from both NBDs: the Walker A and Walker B motifs, the A-loop, Q-loop, and H-loop from one NBD, and the ABC signature (S-sequence/C-loop) and D-loop from the opposite NBD (and *vice versa*)[55,67,77,140,209]. In contrast, TMDs exhibit low sequence similarity and high structural diversity, reflecting the broad spectrum of substrate specificities[28,78]. During the transport cycle, TMDs and NBDs undergo significant conformational changes. From an exporter's perspective, the transporter transitions from an IF state, characterized by open TM helices facing the cytosol for substrate entry and separated NBDs, to an OF state. In the OF state, the cytosolic side is closed, and the opposite side opens to release the substrate, while the NBDs are dimerized (Figure 21)[173,229,230]. This process relies on an interface between the domains that senses and converts conformational changes in the NBDs (induced by ATP binding and hydrolysis) into corresponding changes in the TMDs. Residues in the CHs at the cytosolic tips of the TMDs play a crucial role in this bidirectional NBD-TMD communication[68,203].

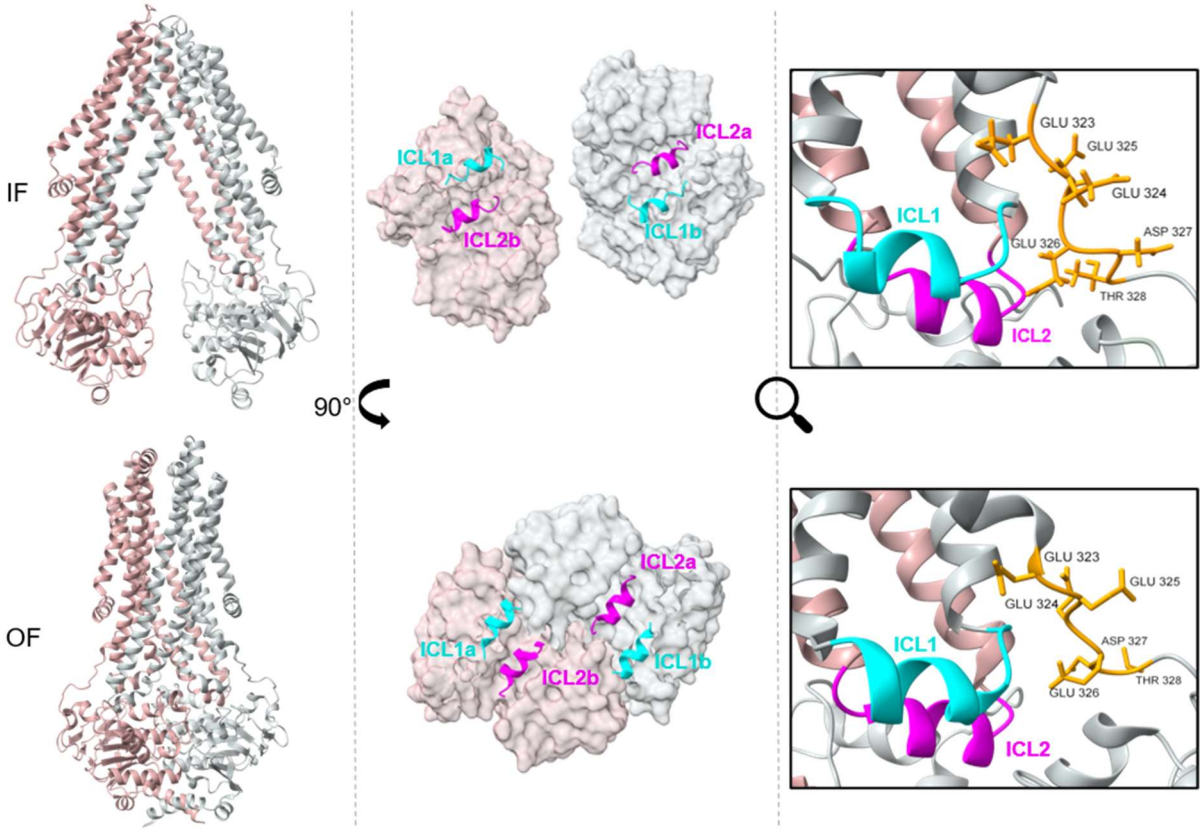

Figure 21: Structure of BmrA in the IF- and OF conformation and the position of the ICLs.

The left panel shows the secondary structure of the BmrA dimer in the IF (PDB: [8QOE][79]) and OF (PDB: [7OW8][80]) conformations, respectively. Individual monomers are colored in rose and gray. The middle panel shows the view on the NBDs from the TMDs. Additionally, ICL1 (cyan) and ICL2 (magenta) of the monomers a and b are shown. The right panel shows an enlarged view of the amino acids (Glu323-Thr328, orange) at the N-terminal segment of the linker. These amino acids are in close proximity to ICL1 (cyan, same monomer) and ICL2 (magenta, opposite monomer).

Type IV ABC transporters, such as BmrA, have a unique TMD arrangement. They possess a preceding amphipathic N-terminal EH on the cytosolic side of the membrane, and two of their six TM helices from each TMD are intertwined in the IF conformation (Figure 21). This unique structure involves TM1-TM2-TM3 and TM6 from one TMD forming a bundle with TM4-TM5 from a different interacting TMD[28,43,88]. The intracellular loops (ICLs) connecting TM2-TM3 and TM4-TM5 are in direct contact with the NBDs, constituting the afore-introduced CHs[231]. Consequently, each NBD interacts with CH1 of the same monomer and CH2 from the opposite monomer (Figure 21). Residues involved in interdomain communication in the NBDs are especially those in the Q-loop and X-loop regions, which precede the ABC signature sequence in type IV ABC transporters[48,60,66,130,141]. In the NBD-dimerized OF state, the NBD-TMD interface is characterized by CH1 (monomer A) interacting with both NBDs, while CH2 (monomer B) predominantly engages with the opposite NBD (monomer A), and *vice versa* (Figure 21)[43,88].

Numerous studies have partially elucidated the molecular mechanism underlying NBD-TMD cross-talk[48,88,128,129,141,232–234], yet the interaction between CHs and the surrounding protein regions in their respective transporters remains poorly understood. In BmrA, residues within the first segment of the domain-connecting linker region are situated in close proximity to both CHs (Figure 21), which suggests that they may play a role in stabilizing the NBD-TMD interface. The linker connects the NBDs to the TMDs via a short, 17-amino-acid sequence. Due to its cytoplasmic exposure, the linker is highly hydrophilic and enriched with negatively charged amino acids (Figure 21).

In the present study, we performed a mutational analysis of the first linker segment (Glu323-Thr328). Our findings pin-point towards the residue Glu326 as being crucial for the overall BmrA function. Mutation to Ala resulted in a complete loss of the ATPase activity and a substantial reduction of the Hoechst 33342 transport activity. ATPase activity, however, could be restored via Cys-crosslinking the C-termini of BmrA E326A. This indicates that the NBDs of BmrA E326A are, in principle, functional. Cryo-EM analysis of the variant revealed an altered domain arrangement with the NBDs detached from the CHs of the TMD. Furthermore, we analyzed four putative interaction partners in the immediate vicinity of Glu326. Three of these are crucial for the BmrA activity, and we discuss their potential to form a salt bridge with Glu326. Based on our results, we propose that a salt bridge forms between Glu326 and Lys217, which is located in CH2. This salt bridge stabilizes the orientation of the NBDs relative to the CHs of the TMDs and is a prerequisite for proper NBD dimerization. Importantly, this structural element appears to be conserved throughout multidrug exporters and the entire human ABC-C family.

4.3.4 Results

4.3.4.1 Glu326 is crucial for the BmrA activity

To identify potential crucial interactions between residues of the linker and the CHs (ICLs), we conducted an Ala scanning mutagenesis on the first linker segment (Glu323-Thr328) and evaluated the resulting Ala variants based on their activity. This involved IMVs from *E. coli* membranes containing the overexpressed BmrA variants and assessing the transport activity of each variant in a native membrane environment using the fluorescence dye Hoechst 33342. Notably, the majority of BmrA variants exhibited a Hoechst 33342 transport activity comparable to the wt, which had a transport rate of 0.49 ± 0.01 1/s. However, the E326A variant exhibited significantly reduced transport activity (0.16 ± 0.01 1/s), as illustrated in Figure 22A/B. This implies that the residue Glu326 is essential for the transporter function, while the chemical nature of the remaining residues appears to be less crucial.

Additionally, we examined the ability of the BmrA variants to transition between the IF and OF conformations in IMVs via Trypsin proteolysis, as previously described[129,130,147]. In the absence of ligands, BmrA adopts an IF conformation, characterized by high Trypsin accessibility. Consequently, all BmrA variants were rapidly digested by Trypsin within 5 minutes (Figure 22C). Yet, the behavior of the BmrA variants differed significantly in the presence of ATP, Mg^{2+}, and orthovanadate. Under this condition, vanadate typically traps transporters in the OF conformation once attained. Unlike the IF conformation, the OF conformation confers increased resistance to Trypsin digestion, as observed for the wt protein (Figure 22C). The E323A and E324A variants exhibited Trypsin resistance similar to the wt, while the E325A, D327A, and T328A variants showed a moderate decline in resistance. Notably, the E326A variant displayed almost no resistance to Trypsin, suggesting an inability to achieve the NBD-dimerized OF conformation. This impairment likely explains the drastically reduced Hoechst 33342 transport activity observed for E326A (Figure 22A/B), implying an inability to bind and hydrolyze ATP.

To test this assumption, we next analyzed the *in vitro* ATPase activity of purified BmrA variants (Figure 23A). As shown in Figure 23B, E323A maintained a basal ATPase activity (0.16 ± 0.03 µmol/min∗mg) comparable to the wt (0.13 ± 0.01 µmol/min∗mg). In contrast, all other Ala variants (E324A-T328A) exhibited reduced ATPase activities. E324A and E325A retained moderate ATPase activities (0.05-0.06 ± 0.02 µmol/min∗mg), sufficient to support wt-like transport (Figure 23). However, D327A and T328A displayed significantly impaired ATPase activities (< 0.02 ± 0.01 µmol/min∗mg), despite exhibiting wt-like Hoechst 33342 transport activities (Figure 22C/D), indicating uncoupling of these activities, at least in part. As expected, the

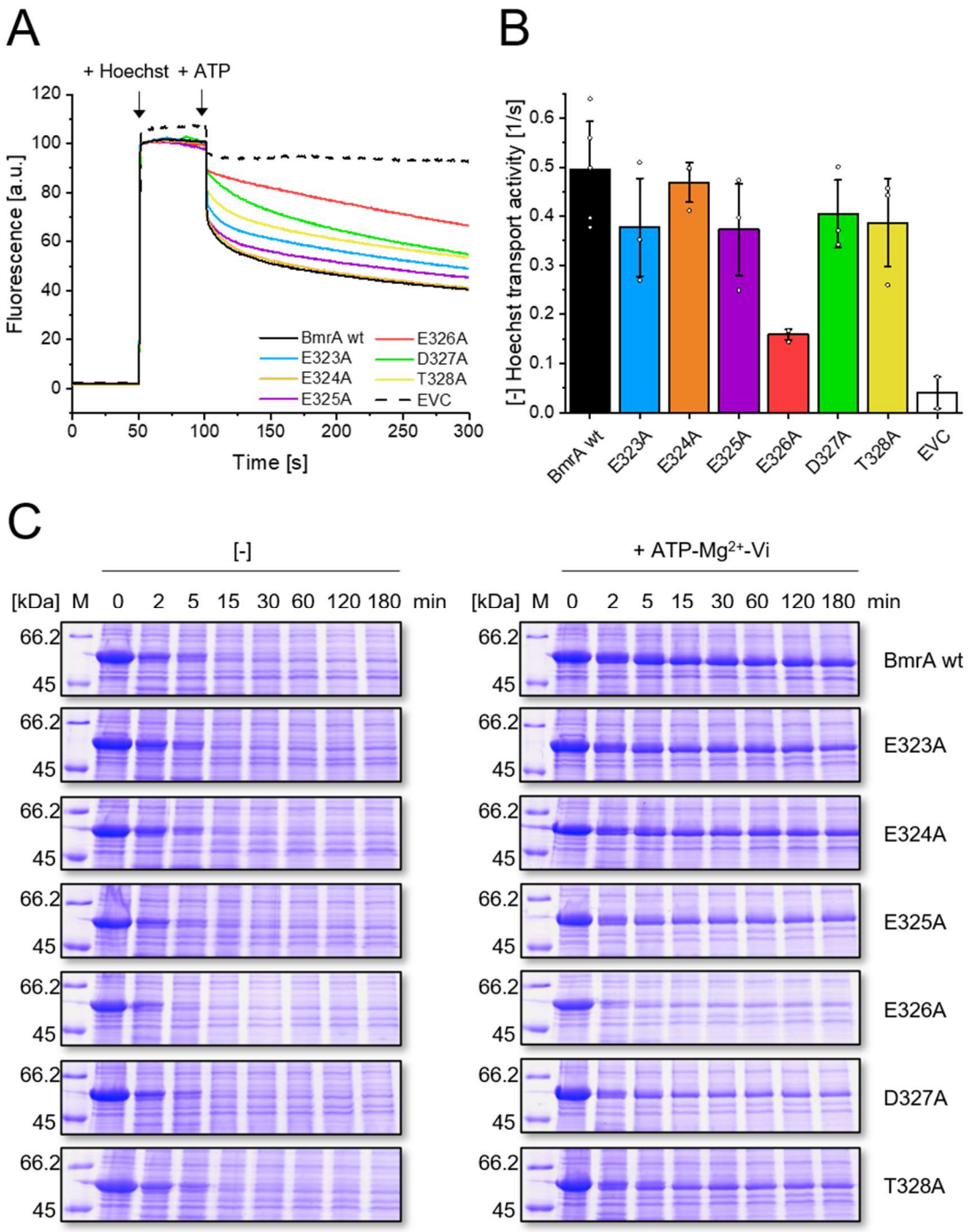

Figure 22: Hoechst 33342 transport activity and limited proteolysis by Trypsin of BmrA wt and variants (E323A-T328A) overexpressed in IMVs.

(A) Fluorescence emission of Hoechst 33342 monitored over 300 s at 457 nm upon excitation at 355 nm in the presence of IMVs containing BmrA wt (black), E323A (blue), E324A (orange), E325A (purple), E326A (red), D327A (green), and T328A (yellow). Addition of Hoechst 33342 and ATP is indicated. EVC = empty vector control (black dashed line). **(B)** Mean Hoechst 33342 transport activities of BmrA wt (n = 5 ± SD), E323A-T328A (n = 3 ± SD), or EVC (white, n = 2 ± SD). Single data points are shown and represent independent IMV preparations. **(C)** SDS-PAGE analysis of IMVs containing overexpressed BmrA wt or the Ala variants after digestion by Trypsin in the absence or presence of ATP, Mg^{2+} and orthovanadate. Samples were analyzed after the indicated times (0, 2, 5, 15, 30, 60, 120, and 180 min). Protein fragments were separated on a 10% SDS-PAGE gel and subsequently stained with Coomassie brilliant blue R250. Experiments were performed in duplicate using two different IMV preparations.

E326A variant showed the most substantial reduction in ATPase activity, with no measurable activity (Figure 23A), supporting the notion that E326A cannot attain an NBD-dimerized state required for ATP hydrolysis.

Notably, the CD spectra of all analyzed Ala variants were similar (Figure S6A), with only slight variations in intensity, confirming proper protein folding. Collectively, these findings highlight the importance of residues Glu324-Thr328, especially Glu326, in maintaining proper ATPase activity and overall transporter function. The impaired IF to OF transport cycle observed in E326A underscores the indispensable role of Glu326 in this process.

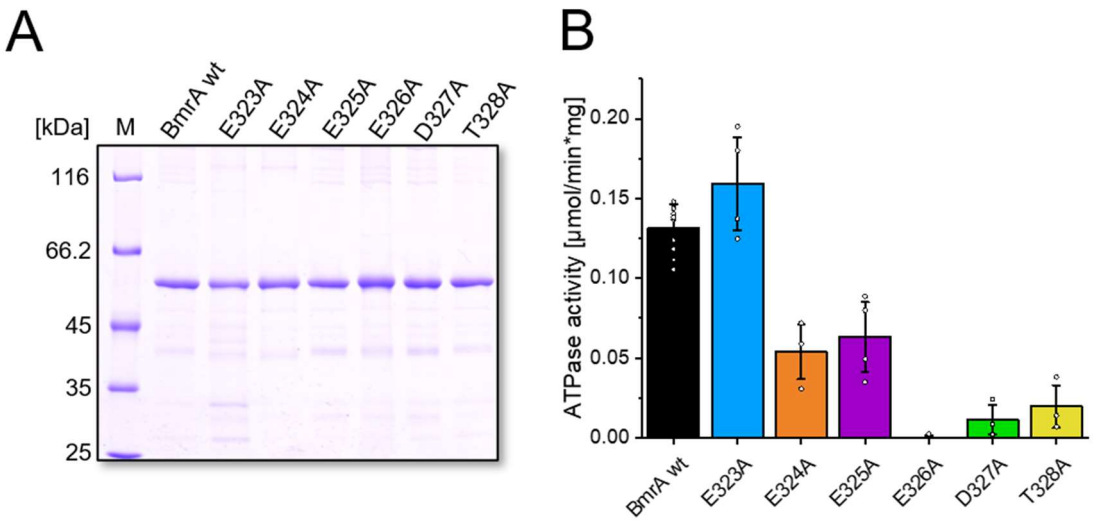

Figure 23: ATPase activity of purified BmrA wt and variants (E323A-T328A).

(A) SDS-PAGE analysis of purified BmrA wt and Ala variants (E323A-T328A) after Ni-NTA chromatography. Each lane contains 1.5 µg of protein. The calculated masses for each variant are around 65 kDa. M = Marker. **(B)** Mean ATPase activities of 1 µM BmrA wt (black, n = 11 ± SD), E323A (blue), E324A (orange), E325A (purple), E326A (red), D327A (green), and T328A (yellow) (n ≥ 3 ± SD). Single data points of independent protein purifications are shown.

4.3.4.2 E326A is able to bind and hydrolyze ATP, when NBDs are artificially dimerized

To gain deeper insights into the molecular basis of the E326A variant's inability to form an NBD dimer, we attempted to dimerize its NBDs artificially. We recently identified a position in the C-terminal helices of BmrA where the introduction of a Cys residue facilitates Cys-crosslinked dimer formation[199], and consequently, we now substituted Asn581 by a Cys residue in the E326A background. This resulted in the E326A/N581C ($E326A_{C\text{-}C}$) variant, which, along with the single-mutant N581C, was assessed for dimerization and ATPase activity under oxidizing and reducing conditions.

Figure 24A shows that both $E326A_{C\text{-}C}$ and N581C formed partial Cys-crosslinked dimers (II) under oxidizing conditions. These dimers could be fully converted to monomers (I) under reducing

conditions. Notably, the dimer-to-monomer ratio was lower for E326A$_{C\text{-}C}$ than for N581C. Under oxidizing conditions, N581C, *i.e.*, the wt protein with artificially dimerized NBDs, exhibited a fourfold increase in ATPase activity (0.53 ± 0.01 µmol/min∗mg) relative to the wt, which was reversible to wt levels upon DTT-induced reduction (Figure 24B). This indicates that the enforced NBD contact results in increased ATP hydrolysis and that removing the forced dimerization (reducing the disulfide bridge) restores wt-like activity.

Strikingly, artificially crosslinking the NBDs of the ATPase-deficient E326A variant at Asn581 restored its ATPase activity to 0.30 ± 0.01 µmol/min∗mg, which was entirely sensitive to the reducing agent DTT (Figure 24B). This finding suggests that the NBDs of E326A are inherently functional and capable of ATP binding and hydrolysis when forcibly dimerized. Consequently, the substitution of Glu326 with Ala appears to disrupt the transporter's conformational landscape by specifically impairing the formation of the NBD-dimerized state.

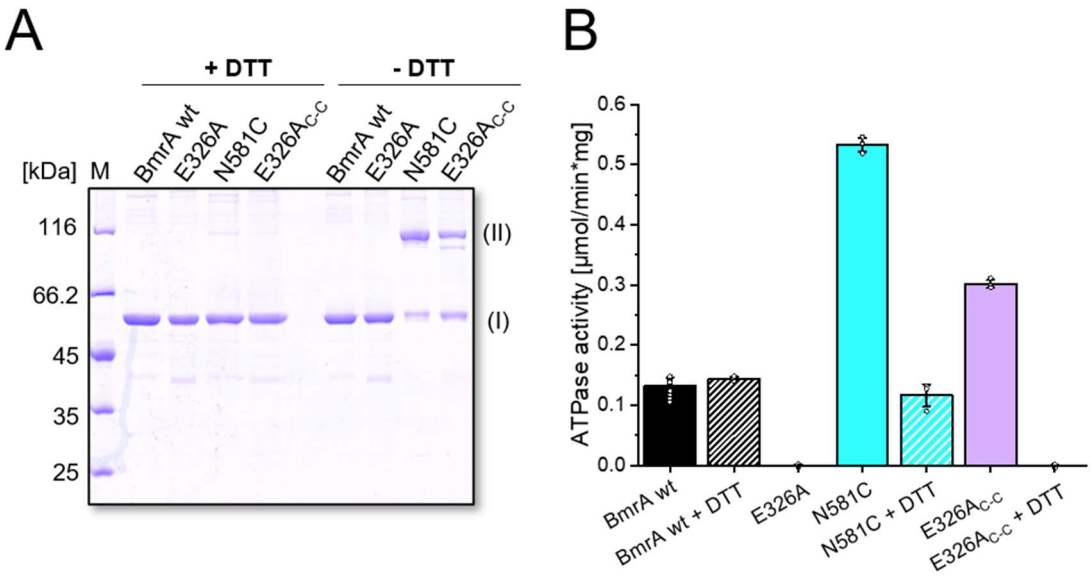

Figure 24: ATP hydrolysis of E326A is restored via artificial dimerization of the NBDs.

(A) SDS-PAGE analysis of purified BmrA wt, E326A, N581C, and E326A$_{C\text{-}C}$ after Ni-NTA chromatography. Reducing (+DTT) and oxidizing (−DTT) conditions are indicated. Each lane contains 1.5 µg of protein. The calculated masses for the monomeric (reduced) forms are around 65 kDa, and for the dimeric (Cys-crosslinked) forms are around 130 kDa, indicated by (I) and (II), respectively. M = Marker. **(B)** Mean ATPase activities of 1 µM BmrA wt (black, n = 11 ± SD), E326A (red), N581C (cyan), and E326A$_{C\text{-}C}$ (lavender) at reducing (+DTT, single-colored) and oxidizing (-DTT, cross-hatched) conditions (n = 3 ± SD). Single data points of independent protein purifications are shown.

4.3.4.3 Positively charged amino acids in proximity to Glu326 are crucial for the BmrA activity

The negatively charged residue Glu326 appears to play a crucial role in BmrA by potentially stabilizing a specific structural conformation. To identify potential electrostatically interacting

partners, we examined the resolved structures of BmrA in the IF and OF conformations[79,80]. Within a 10 Å radius of the Glu326 side chain, four positively charged amino acids (Lys109, Lys217, Arg389, and Arg414) are at an appropriate distance to electrostatically interact with Glu326 (Figure 25). Notably, Lys109 and Lys217, which are located in the ICLs, were of particular interest due to our initial hypothesis of stabilizing interactions between the linker and the CHs (ICLs) (Figure 21). Additionally, we identified two positively charged residues (Arg389 and Arg414) within the NBD that could potentially interact with Glu326.

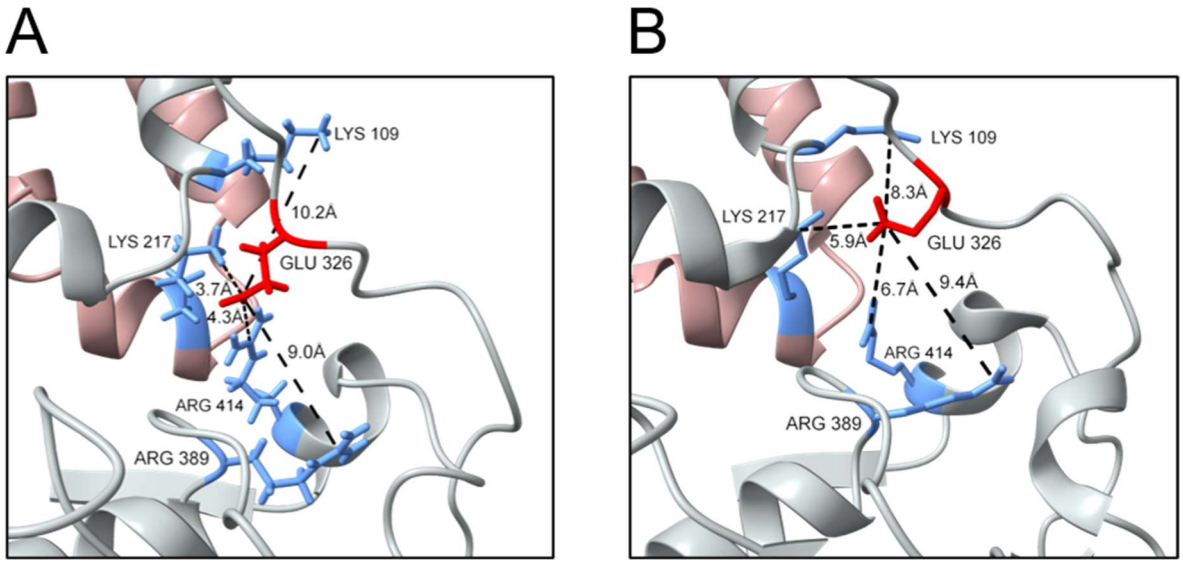

Figure 25: Positively charged amino acids in close proximity to Glu326.

View of Glu326 (red in stick representation) in the **(A)** IF (PDB: [8QOE][79]) and **(B)** OF (PDB: [7OW8][80]) conformations of BmrA. In close proximity (< 10 Å) to Glu326 are four positively charged amino acids (blue in stick representation). On the same monomer (gray) Lys109 is located near CH1, and Arg389 and Arg414 are within the NBD. Lys217 is located at the CH2 of the interacting monomer (rose). Shown are the distances between Glu326 and each positively charged amino acid. For the sake of simplicity, the C-terminal amino acids starting at Val420 are not shown.

To evaluate the functional significance of residues that potentially interact with Glu326, we mutated these residues to Ala and examined the transport and ATPase activities of the resulting variants. As shown in Figure 26A/B, the transport activities of the BmrA variants K217A, R389A, and R414A were significantly impaired, as observed for E326A, with reduced resistance to Trypsin under turnover conditions (+ ATP-Mg^{2+}-Vi) (Figure 26C). In contrast, IMVs containing BmrA K109A exhibited wt-like Hoechst 33342 transport activity, though the resistance to Trypsin was moderately reduced.

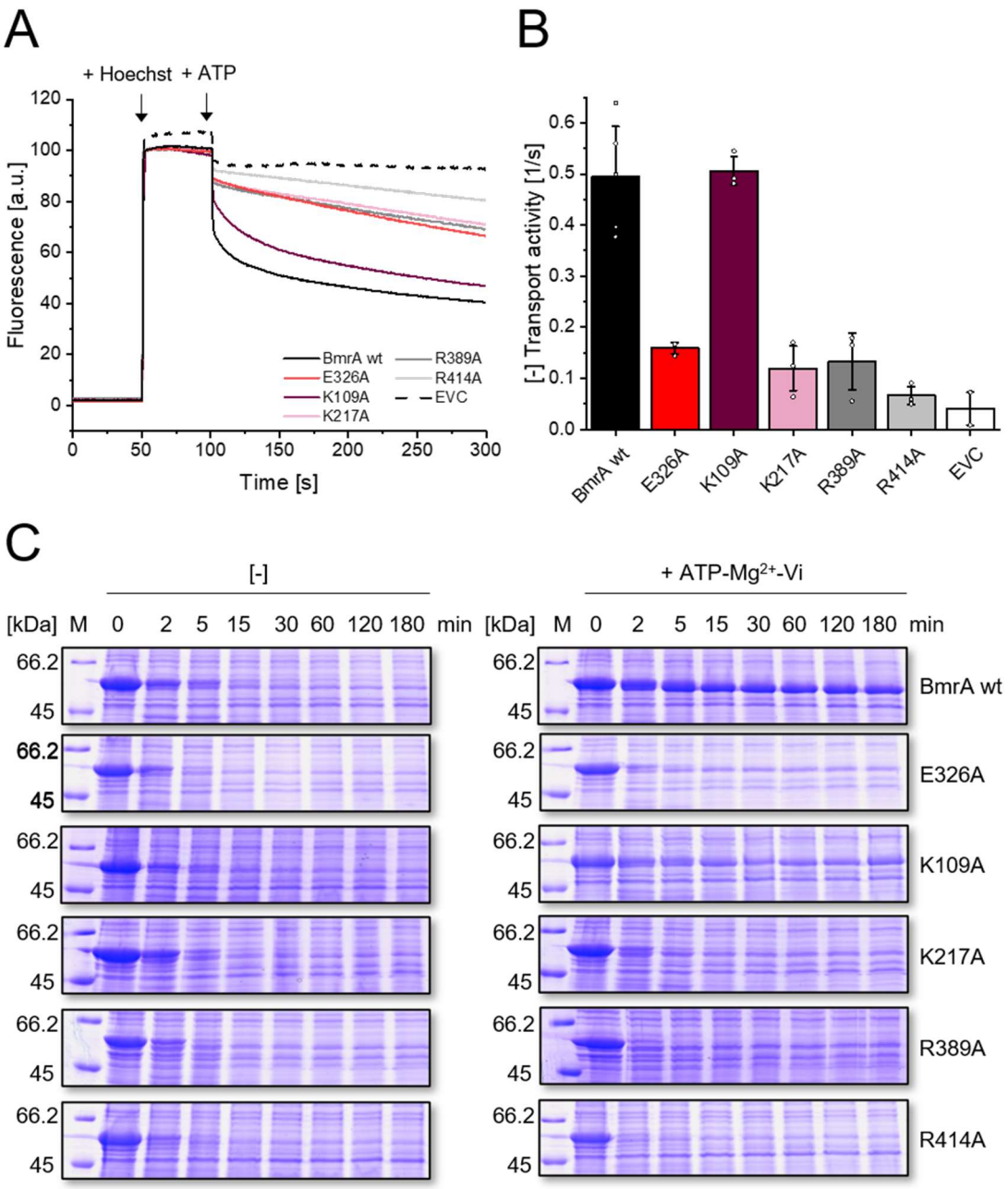

Figure 26: Hoechst 33342 transport activity and limited Trypsin proteolysis of IMV-incorporated BmrA wt and variants (E326A, K109A, K217A, R389A, and R414A).

(A) Fluorescence emission of Hoechst 33342 monitored over 300 s at 457 nm upon excitation at 355 nm in the presence of IMVs containing BmrA wt (black), E326A (red), K109A (dark red), K217A (rose), R389A (dark gray), and R414A (light gray). Addition of Hoechst 33342 and ATP is indicated. EVC = empty vector control (black dashed line). **(B)** Mean Hoechst 33342 transport activities of BmrA wt (n = 5 ± SD), E326A, K109A, K217A, R389A, and R414A (n = 3 ± SD) or EVC (white, n = 2 ± SD). Single data points are shown and represent independent IMV preparations. **(C)** SDS-PAGE analysis of IMV containing overexpressed BmrA wt or Ala variants (E326A, K109A, K217A, R389A, and R414A) after digestion by Trypsin in the absence or presence of ATP, Mg^{2+} and orthovanadate. Samples were taken after the indicated times (0, 2, 5, 15, 30, 60, 120, and 180 min). Protein fragments were separated on a 10% SDS-PAGE gel and subsequently stained with Coomassie brilliant blue R250. Experiments were performed in duplicate using two different IMV preparations.

Next, we analyzed the *in vitro* ATPase activities of the purified BmrA K109A, K217A, R389A, and R414A variants (Figure 27A). Notably, the R389A and R414A samples showed consistent signs of

protein aggregation. This strongly indicated protein misfolding, and, in line with this assumption, also the CD spectra of both variants showed drastically reduced CD intensities (Figure S6B). Thus, the results obtained with these samples must be interpreted with caution.

The ATPase activity of the variants correlated with their respective transport activity. K217A displayed a wt-like ATPase activity (0.17 ± 0.02 µmol/min∗mg), while the remaining variants exhibited drastically reduced ATPase activities, as previously observed with E326A (Figure 27B). Collectively, our functional analysis revealed that Lys217, Arg389, and Arg414 are essential for BmrA's transport function, putatively participating in electrostatic interactions with Glu326, as was initially speculated. Noteworthy, the exact chemistry of the amino acid side chain at position 326 appears to be extremely relevant. Replacing Glu with the also negatively charged amino acid Asp, which has a shorter side chain, cannot establish the putative salt bridge (Figure S7).

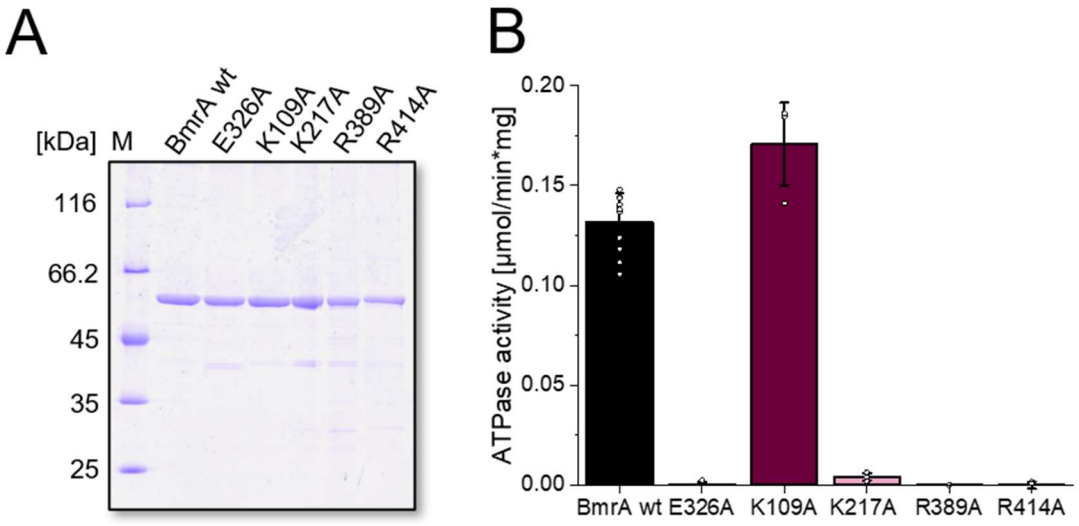

Figure 27: ATPase activities of purified BmrA wt and variants (E326A, K109A, K217A, R389A, and R414A).

(A) SDS-PAGE analysis of the purified BmrA wt and Ala variants (E326A, K109A, K217A, R389A, and R414A) purified via Ni-nitrilotriacetic acid (NTA) chromatography. Each lane contains 1.5 µg of protein. The calculated masses for each variant are about 65 kDa. M = Marker. **(B)** Mean ATPase activities of 1 µM BmrA wt (black, n = 11 ± SD), E326A (red), K109A (dark red), K217A (rose), R389A (dark gray), and R414A (light gray) (n = 3 ± SD). Single data points of independent protein purifications are shown.

4.3.4.4 The NBDs and TMDs are disconnected in BmrA E326A

Our functional analysis of the first linker segment revealed the crucial function of Glu326 in the structure and function of BmrA. Specifically, Glu326 is essential for BmrA's overall function, including transport and ATPase activity. Additionally, this residue likely stabilizes a specific BmrA conformation through electrostatic interactions. To elucidate the role of Glu326 further, we analyzed the structure of BmrA wt and the E326A mutant in detergent via single-particle cryo-EM

analysis. Remarkably, 2D class averages revealed a dimer-of-dimers arrangement in both samples in a non-physiological tail-to-tail orientation. This conformation was rare in the wt dataset (< 5%, Figure 28A) but became the dominant species in the E326A variant (> 90%, Figure 28B). Inherent flexibility and imperfect dimerization prohibited a high-resolution 3D reconstruction. Thus, we employed rigid body fitting, with manually detached NBDs, to generate a tentative assembly model of the E326A variant, guided by the 2D class averages and the low-resolution map. This model illustrates how two BmrA dimers could interact via their TMDs, while the NBDs would be displaced and oriented outwards (Figure 28C). These findings indicate that the E326A mutation destabilizes the TMD-NBD interface, leading to increased uncoupling of the domains.

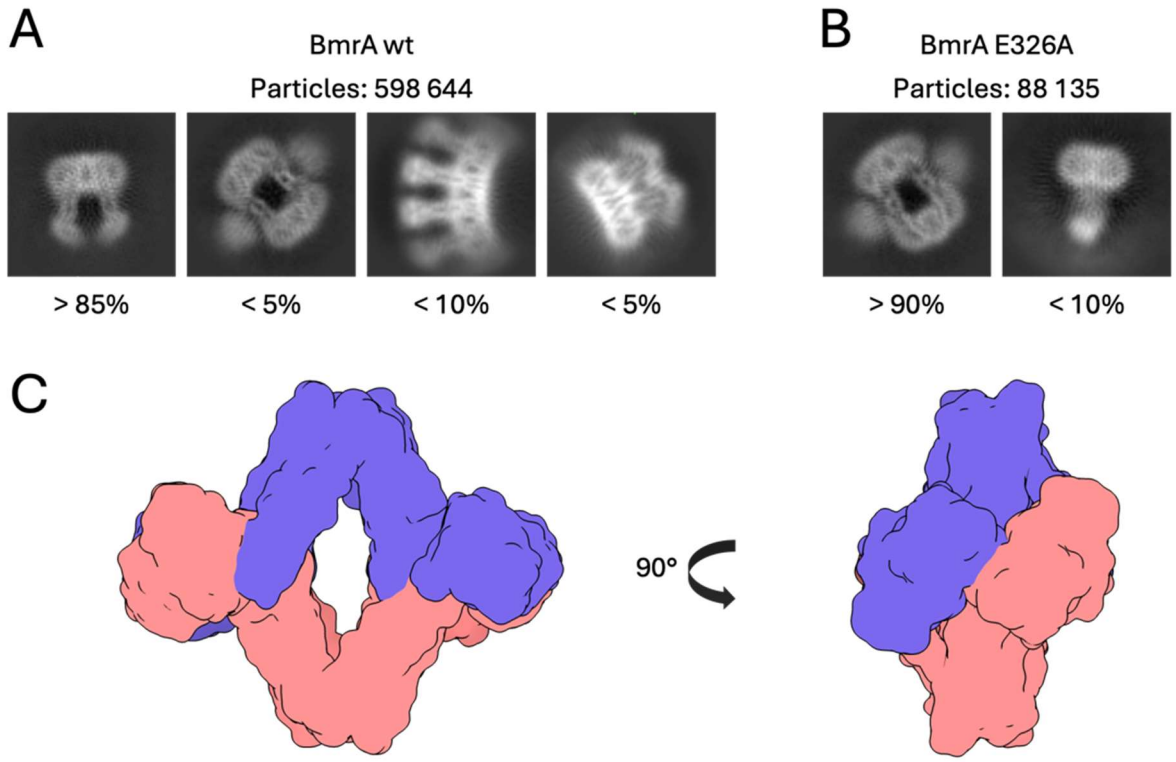

Figure 28: Single particle cryo-EM analysis of purified BmrA wt and E326A.

(A) Representative 2D class averages for BmrA wt, showing the distribution of distinct particle arrangements. Percentages indicate the relative abundance of each species within the dataset, based on classification via CryoSPARC. **(B)** Representative 2D class averages for BmrA E326A, showing the distribution of distinct particle arrangements. Percentages indicate the relative abundance of each species within the dataset, based on classification via CryoSPARC. **(C)** Tentative assembly model of the BmrA E326A variant based on rigid body docking of a modified BmrA structure (PDB: 8QOE[79]) into a low-resolution cryo-EM reconstruction. Data were acquired in collaboration with A. Baier and A. Moeller from the University of Osnabrueck, Department of Biology/Chemistry, Structural Biology section. The relevant methods are described in chapter 6.4.

4.3.4.5 Glu326 is conserved across the human ABC-C transporter family

The presented findings suggest that a putative salt bridge between Glu326 and a positively charged amino acid (pre)arranges the NBDs relative to the CHs of the TMDs. To analyze the conservation of such a pre-arrangement in ABC transporters, we performed a multiple sequence alignment of the linker region across various ABC exporters. This analysis included bacterial multidrug transporters and the human ABCC family, which are collectively classified as MRPs[32,111,121].

The sequence alignment revealed that the negatively charged residue corresponding to Glu326 in the first linker segment of BmrA is highly conserved among the analyzed transporters (Figure 29B). Notably, two transporters, ABCC8 and ABCC9, lack the Glu residue at the aligned positions, yet they possess a Glu residue at the preceding positions. Structural analysis of human ABCC transporters (e.g., ABCC2 and ABCC4) corroborates our findings by showing the conserved Glu residue surrounded by positively charged amino acids, similar to BmrA (Figure 29)[235]. These residues are positioned analogously to those proposed to form a salt bridge with Glu326 in BmrA (Figure 25B). Specifically, most ABCC structures feature a Lys in the CH2 and two Arg residues within the NBD.

Based on these observations, it is reasonable to assume that a salt bridge between Glu326 and a positively charged amino acid (located in either the CH2 or the NBD) is crucial for proper NBD arrangement, dimerization, and transporter movement. Furthermore, this structural element appears to be conserved across the entire human ABCC family and various bacterial ABC transporters.

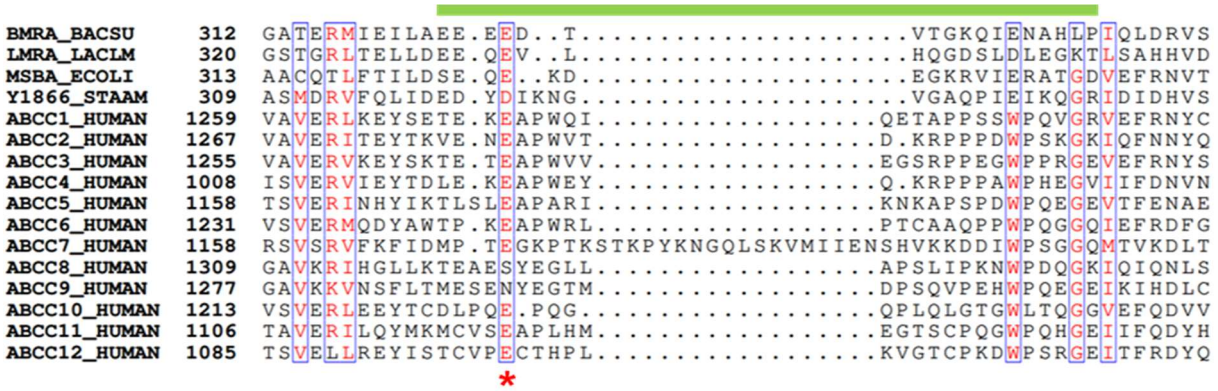

Figure 29: Sequence alignment of the linker region of different bacterial ABC exporters and the human ABCC family.

Amino acids with a high similarity (>70%) are colored in red and are framed in blue. The position of the linker region of BmrA is indicated by a green-colored square, and the BmrA residue Glu326 is marked by a red star. Abbreviations indicate the aligned exporters: BmrA from *B. subtilis* (BACSU); LmrA from *L. lactis* subsp. cremoris (LACLM); *Sav*1866 from *S. aureus* (STAAM); and ABCC1 - ABCC12 from humans.

4.3.5 Discussion

The functional importance of the CHs in ABC transporters for allosteric NBD-TMD communication is well-established and has been analyzed in the past via genetic, biochemical, and structural approaches[88,90,141–144]. Despite their structural and functional diversity, CHs in different ABC transporters interact similarly with the NBDs, primarily via the Q- and X-loops[48,92,141,202,232]. Yet, the interaction of CHs with the transporter's remaining parts remains poorly understood.

Type IV ABC transporters are characterized by a distinct arrangement of the TM helices, in which TM helices 4-5 of one monomer (in dimeric transporters) protrude into the opposite TMD. Consequently, both monomers contribute a CH to the NBD-TMD interface (e.g., Figure 21)[43]. The proximity of the two CHs enables for potential interactions, as discussed for MsbA[88]. It has been proposed that residues of CH1 and CH2 interact via π-stacking to achieve cooperativity and mediate nucleotide binding[232]. Based on a structural model, a similar mechanism is assumed for the human ABCD1 transporter[236]. Additionally, a salt bridge between the sole CH and the EH was shown to stabilize the transmission interface in the human type V ABC transporter ABCG2[237,238].

This study aimed to identify additional interactions of the CHs in the bacterial ABC transporter BmrA. We hypothesized that the first segment of the large cytosolic linker, which envelops the NBD and connects the TMD and NBD, might be crucial for establishing such interactions. This hypothesis was based on the observation that linker residues are in close proximity to both CHs in the 3D structures of both the IF and OF BmrA conformations[79,80]. A previous study highlighted a critical interaction between Gln333 of the linker and Tyr408 of the NBD and discussed the linker's putative role in securing proper CH-NBD interactions[239]. Therefore, we focused on residues Glu323-Thr328 in the linker, directly adjacent to the CHs, and conducted an Ala scanning mutagenesis analysis.

The functional characterization of the respective Ala variants in membranes revealed that Glu326 plays a particularly crucial role in conformational switching and substrate translocation (Figure 22). In the absence of ATP, vanadate failed to trap the E326A variant in the OF conformation, suggesting an impaired NBD dimerization, ATP binding, and hydrolysis. *In vitro* analysis of E326A's ATPase activity confirmed this assumption, as no activity was detected (Figure 23B). This compromised activity was not due to the partial unfolding or misfolding of the purified E326A protein because the variant remained active when the E326A NBDs were artificially dimerized.

Recently, our group and another demonstrated that the NBDs of BmrA can be cross-linked by introducing a Cys residue into the C-terminal helix, thereby restraining NBD separation[79,199]. Contrary to Di Cesare *et al*.'s findings, where the cross-linked BmrA variant A582C exhibited wt-like ATPase and Hoechst 33342 transport activities, cross-linking the adjacent residue Asn581 increased the BmrA ATPase activity fourfold compared to wt levels (Figure 24B). However, when

we restrained the NBDs of E326A using this approach, the ATPase activity returned to wt levels and became fully sensitive to cleavage of the S-S bond. Thus, the E326A substitution did not render the NBDs nonfunctional *per se* but rather caused a global perturbation of the transporter's conformational spectrum.

To further support the importance of Glu326 in establishing an active BmrA structure, we conducted cryo-EM analysis on purified BmrA E326A. Rigid-body docking suggested a potential, non-physiological, tetrameric assembly (dimer of dimers) of E326A (Figure 28C). In this arrangement, the NBDs of both E326A dimers are detached from the TMDs. In our model, NBDs from two different BmrA dimers interact, forming an NBD-NBD contact. Notably, this new contact does not stimulate ATP hydrolysis, as evidenced by our ATPase measurements, suggesting an uncommon interface. However, it is essential to consider that the assembly observed in the cryo-EM analysis is not physiologically relevant, as the tetrameric organization would not form when two interacting BmrA molecules are embedded within the same membrane (and not detergent-solubilized). More likely, in a membrane-embedded state, the TMDs retain their positions while the NBDs are not tightly attached to the CHs, allowing for more degrees of freedom. Transferring the observed E326A dimer to the wt, it is reasonable to assume that Glu326 establishes a salt bridge that correctly positions the NBD relative to the TMD. The loss of this prearrangement results in NBD separation, preventing functional NBD-NBD dimerization. Taken together, Glu326 appears to be a promising candidate for establishing crucial interactions with CH residues.

In the published BmrA structures of the IF (PDB: [8QOE][79]) and OF (PDB: [7OW8][80]**)** conformations, Glu326 protrudes into the NBD-TMD interface. Within a spatial proximity of less than 10 Å, four positively charged residues that could engage in electrostatic interactions with Glu326 were identified (Figure 25)[79,80]. Specifically, these residues include two Lys (Lys109 in ICL1 and Lys217 in CH2 of ICL2) and two Arg residues, both of which are located within the NBD. Functional characterization of the corresponding Ala variants revealed that all residues except for Lys109, which is the most distant from Glu326, are essential for the BmrA activity (Figure 26 and Figure 27). A recent study suggested that NBD residues Arg389 and Arg414 comprise a communication hinge between the TMD and NBD via the CH2 region[234]. Notably, purified R389A and R414A BmrA proteins were unstable during purification, resulting in rapid turbidity increase of the protein solutions and altered CD spectra (Figure S6). Therefore, results obtained with these variants should be interpreted with caution, as their instability may indicate the residues' broader importance for BmrA's overall structure and stability, extending beyond their potential contribution to the proposed salt bridge.

Due to the similar results for E326A and K217A, as well as their close proximity (3.7 Å in the IF and 5.9 Å in the OF conformation)[234], we propose the formation of a salt bridge between Lys217 and Glu326. Furthermore, the salt bridge between a Lys residue in CH2 and a Glu residue in the linker appears to be a conserved feature among various bacterial ABC exporters and some

members of the human ABCC family, such as ABCC2 and ABCC4 (Figure 29 and Figure S8)[235]. However, it is challenging to generalize our hypothesis, as the putative amino acids are not suitably positioned to form a proper salt bridge in all ABCC family members. Nevertheless, our study clearly emphasizes the importance of stabilizing interactions between the CH2 (harboring Lys217 in BmrA) and the transporter's surrounding structural elements, underscoring CH2's critical role in NBD-TMD communication[88,141].

5 Literature

1. Rothfield, L. I. editor. *Structure and Function of Biological Membranes*. (Academic Press Inc., 1971).
2. Watson, H. Biological membranes Structure and organization of membranes. *Essays Biochem* **59**, 43–70 (2015).
3. Escribá, P. V. *et al.* Membranes: a meeting point for lipids, proteins and therapies. *J. Cell. Mol. Med.* **12**, 829–875 (2008).
4. Stillwelll, W. *An Introduction to Biological Membranes: Composition, Structure and Function*. (Academic Press Inc., 2016).
5. Singer, S. J. & Nicolson, G. L. The Fluid Mosaic Model of the Structure of Cell Membranes. *Science* **175**, 720–731 (1972).
6. van Meer, G., Voelker, D. R. & Feigenson, G. W. Membrane lipids: where they are and how they behave. *Nat. Rev. Mol. Cell Biol.* **9**, 112–124 (2008).
7. Janmey, P. A. & Kinnunen, P. K. J. Biophysical properties of lipids and dynamic membranes. *Trends Cell Biol.* **16**, 538–546 (2006).
8. Jouhet, J. Importance of the hexagonal lipid phase in biological membrane organization. *Front. Plant Sci.* **4**, 494 (2013).
9. Hill, W. G. & Zeidel, M. L. Reconstituting the Barrier Properties of a Water-tight Epithelial Membrane by Design of Leaflet-specific Liposomes. *J. Biol. Chem.* **275**, 30176–30185 (2000).
10. Lee, A. G. How lipids affect the activities of integral membrane proteins. *Biochim. Biophys. Acta - Biomembr.* **1666**, 62–87 (2004).
11. Lundbæk, J. A., Collingwood, S. A., Ingólfsson, H. I., Kapoor, R. & Andersen, O. S. Lipid bilayer regulation of membrane protein function: gramicidin channels as molecular force probes. *J. R. Soc. Interface* **7**, 373–395 (2010).
12. Sohlenkamp, C. & Geiger, O. Bacterial membrane lipids: diversity in structures and pathways. *FEMS Microbiol. Rev.* **40**, 133–159 (2016).
13. Guidotti, G. The Composition of Biological Membranes. *Arch. Intern. Med.* **129**, 194 (1972).
14. Wallin, E. & Von Heijne, G. Genome-wide analysis of integral membrane proteins from eubacterial, archaean, and eukaryotic organisms. *Protein Sci.* **7**, 1029–1038 (1998).
15. Overington, J. P., Al-Lazikani, B. & Hopkins, A. L. How many drug targets are there? *Nat. Rev. Drug Discov.* **5**, 993–996 (2006).
16. Li, F. *et al.* Highlighting membrane protein structure and function: A celebration of the Protein Data Bank. *J. Biol. Chem.* **296**, 100557 (2021).

17. Hedin, L. E., Illergård, K. & Elofsson, A. An introduction to membrane proteins. *J. Proteome Res.* **10**, 3324–3331 (2011).
18. Madeira, A., Moura, T. F. & Soveral, G. Detecting aquaporin function and regulation. *Front. Chem.* **4**, 182454 (2016).
19. Wood, I. S. & Trayhurn, P. Glucose transporters (GLUT and SGLT): expanded families of sugar transport proteins. *Br. J. Nutr.* **89**, 3–9 (2003).
20. Holland, I. B. Rise and rise of the ABC transporter families. *Res. Microbiol.* **170**, 304–320 (2019).
21. Sadée, W., Drübbisch, V. & Amidon, G. L. Biology of Membrane Transport Proteins. *Pharm. Res. An Off. J. Am. Assoc. Pharm. Sci.* **12**, 1823–1837 (1995).
22. Wright, E. M., Hirsch, J. R., Loo, D. D. F. & Zampighi, G. A. Regulation of Na+/Glucose Cotransporters. *J. Exp. Biol.* **200**, 287–293 (1997).
23. Pivovarov, A. S., Calahorro, F. & Walker, R. J. Na+/K+-pump and neurotransmitter membrane receptors. *Invertebr. Neurosci. 2018 191* **19**, 1–16 (2018).
24. Pardee, A. B. Membrane Transport Proteins. *Science* **162**, 632–637 (1968).
25. Wilkens, S. Structure and mechanism of ABC transporters. *F1000Prime Rep.* **7**, 14 (2015).
26. Hwang, J.-U. *et al.* Plant ABC Transporters Enable Many Unique Aspects of a Terrestrial Plant's Lifestyle. *Mol. Plant* **9**, 338–355 (2016).
27. Holland, I. B., Cole, S. P. C., Kuchler, K., and Higgins, C. F. *ABC Proteins: From Bacteria to Man*. (Academic Press, 2002).
28. Rees, D. C., Johnson, E. & Lewinson, O. ABC transporters: the power to change. *Nat. Rev. Mol. Cell Biol.* **10**, 218–227 (2009).
29. Higgins, C. F. *et al.* A family of related ATP-binding subunits coupled to many distinct biological processes in bacteria. *Nature* **323**, 448–450 (1986).
30. Tomii, K. & Kanehisa, M. A Comparative Analysis of ABC Transporters in Complete Microbial Genomes. *Genome Res.* **8**, 1048–1059 (1998).
31. Davidson, A. L., Dassa, E., Orelle, C. & Chen, J. Structure, Function, and Evolution of Bacterial ATP-Binding Cassette Systems. *Microbiol. Mol. Biol. Rev.* **72**, 317–364 (2008).
32. Alam, A. & Locher, K. P. Structure and Mechanism of Human ABC Transporters. *Annu. Rev. Biophys.* **52**, 275–300 (2023).
33. Kang, J. *et al.* Plant ABC Transporters. *Arabidopsis Book* **9**, e0153 (2011).
34. Catalano, A. *et al.* Multidrug Resistance (MDR): A Widespread Phenomenon in Pharmacological Therapies. *Molecules* **27**, (2022).
35. Sheppard, D. N. & Welsh, M. J. Structure and function of the CFTR chloride channel. *Physiol. Rev.* **79**, (1999).
36. Neumann, J., Rose-Sperling, D. & Hellmich, U. A. Diverse relations between ABC transporters and lipids: An overview. *Biochim. Biophys. Acta - Biomembr.* **1859**, 605–618

(2017).

37. Molday, R. S., Zhong, M. & Quazi, F. The role of the photoreceptor ABC transporter ABCA4 in lipid transport and Stargardt macular degeneration. *Biochim. Biophys. Acta - Mol. Cell Biol. Lipids* **1791**, 573–583 (2009).
38. Rust, S. *et al.* Tangier disease is caused by mutations in the gene encoding ATP-binding cassette transporter 1. *Nat. Genet. 1999 224* **22**, 352–355 (1999).
39. Behl, T. *et al.* The Interplay of ABC Transporters in Aβ Translocation and Cholesterol Metabolism: Implicating Their Roles in Alzheimer's Disease. *Mol. Neurobiol. 2020 584* **58**, 1564–1582 (2020).
40. Lacabanne, D. *et al.* Gradient reconstitution of membrane proteins for solid-state NMR studies. *J. Biomol. NMR* **69**, 81–91 (2017).
41. Dean, M., Hamon, Y. & Chimini, G. The human ATP-binding cassette (ABC) transporter superfamily. *J. Lipid Res.* **42**, 1007–1017 (2001).
42. Tusnády, G. E., Sarkadi, B., Simon, I. & Váradi, A. Membrane topology of human ABC proteins. *FEBS Lett.* **580**, 1017–1022 (2006).
43. Thomas, C. *et al.* Structural and functional diversity calls for a new classification of ABC transporters. *FEBS Lett.* **594**, 3767–3775 (2020).
44. Scheepers, G. H., Lycklama a Nijeholt, J. A. & Poolman, B. An updated structural classification of substrate-binding proteins. *FEBS Lett.* **590**, 4393–4401 (2016).
45. Oldham, M. L., Khare, D., Quiocho, F. A., Davidson, A. L. & Chen, J. Crystal structure of a catalytic intermediate of the maltose transporter. *Nature* **450**, 515–521 (2007).
46. Korkhov, V. M., Mireku, S. A. & Locher, K. P. Structure of AMP-PNP-bound vitamin B12 transporter BtuCD–F. *Nature* **490**, 367–372 (2012).
47. Xu, K. *et al.* Crystal structure of a folate energy-coupling factor transporter from Lactobacillus brevis. *Nature* **497**, 268–271 (2013).
48. Dawson, R. J. P. & Locher, K. P. Structure of a bacterial multidrug ABC transporter. *Nature* **443**, 180–185 (2006).
49. Nöll, A. *et al.* Crystal structure and mechanistic basis of a functional homolog of the antigen transporter TAP. *Proc. Natl. Acad. Sci. U. S. A.* **114**, E438–E447 (2017).
50. Bi, Y., Mann, E., Whitfield, C. & Zimmer, J. Architecture of a channel-forming O-antigen polysaccharide ABC transporter. *Nature* **553**, 361–365 (2018).
51. Luo, Q. *et al.* Structural basis for lipopolysaccharide extraction by ABC transporter LptB2FG. *Nat. Struct. Mol. Biol.* **24**, 469–474 (2017).
52. Crow, A., Greene, N. P., Kaplan, E. & Koronakis, V. Structure and mechanotransmission mechanism of the MacB ABC transporter superfamily. *Proc. Natl. Acad. Sci. U. S. A.* **114**, 12572–12577 (2017).
53. Higgins, C. F. ABC Transporters: From microorganisms to man. *Annu. Rev. Cell Biol.* **8**, 67–

113 (1992).

54. Kerr, I. D. Structure and association of ATP-binding cassette transporter nucleotide-binding domains. *Biochim. Biophys. Acta - Biomembr.* **1561**, 47–64 (2002).
55. Walker, J. E., Saraste, M., Runswick, M. J. & Gay, N. J. Distantly related sequences in the alpha- and beta-subunits of ATP synthase, myosin, kinases and other ATP-requiring enzymes and a common nucleotide binding fold. *EMBO J.* **1**, 945–951 (1982).
56. Matte, A. & Delbaere, L. T. ATP-binding Motifs. in *Encyclopedia of Life Sciences* (Wiley, 2010).
57. Schneider, E. & Hunke, S. ATP-binding-cassette (ABC) transport systems: Functional and structural aspects of the ATP-hydrolyzing subunits/domains. *FEMS Microbiol. Rev.* **22**, 1–20 (1998).
58. Orelle, C. *et al.* Conformational Change Induced by ATP Binding in the Multidrug ATP-Binding Cassette Transporter BmrA†. *Biochemistry* **47**, 2404–2412 (2008).
59. Kerr, I. D., Jones, P. M. & George, A. M. Multidrug efflux pumps: The structures of prokaryotic ATP-binding cassette transporter efflux pumps and implications for our understanding of eukaryotic P-glycoproteins and homologues. *FEBS J.* **277**, 550–563 (2010).
60. Orelle, C., Dalmas, O., Gros, P., Di Pietro, A. & Jault, J. M. The Conserved Glutamate Residue Adjacent to the Walker-B Motif is the Catalytic Base for ATP Hydrolysis in the ATP-binding Cassette Transporter BmrA. *J. Biol. Chem.* **278**, 47002–47008 (2003).
61. Locher, K. P., Lee, A. T. & Rees, D. C. The E. coli BtuCD structure: A framework for ABC transporter architecture and mechanism. *Science* **296**, 1091–1098 (2002).
62. Loo, T. W., Claire Bartlett, M. & Clarke, D. M. The 'LSGGQ' motif in each nucleotide-binding domain of human P-glycoprotein is adjacent to the opposing Walker A sequence. *J. Biol. Chem.* **277**, 41303–41306 (2002).
63. Schmitt, L. & Tampé, R. Structure and mechanism of ABC transporters. *Curr. Opin. Struct. Biol.* **12**, 754–760 (2002).
64. Ford, R. C. & Hellmich, U. A. What monomeric nucleotide binding domains can teach us about dimeric ABC proteins. *FEBS Lett.* **594**, 3857–3875 (2020).
65. Jones, P. M. & George, A. M. Subunit interactions in ABC transporters: towards a functional architecture. *FEMS Microbiol. Lett.* **179**, 187–202 (1999).
66. Yang, R. *et al.* Glutamine residues in Q-loops of multidrug resistance protein MRP1 contribute to ATP binding via interaction with metal cofactor. *Biochim. Biophys. Acta - Biomembr.* **1808**, 1790–1796 (2011).
67. Schmitt, L., Benabdelhak, H., Blight, M. A., Holland, I. B. & Stubbs, M. T. Crystal Structure of the Nucleotide-binding Domain of the ABC-transporter Haemolysin B: Identification of a Variable Region Within ABC Helical Domains. *J. Mol. Biol.* **330**, 333–342 (2003).
68. Jones, P. M. & George, A. M. Mechanism of ABC transporters: A molecular dynamics

simulation of a well characterized nucleotide-binding subunit. *Proc. Natl. Acad. Sci.* **99**, 12639–12644 (2002).

69. Dalmas, O. *et al.* The Q-loop Disengages from the First Intracellular Loop during the Catalytic Cycle of the Multidrug ABC Transporter BmrA. *J. Biol. Chem.* **280**, 36857–36864 (2005).
70. Hung, L. W. *et al.* Crystal structure of the ATP-binding subunit of an ABC transporter. *Nature* **396**, 703–707 (1998).
71. Jones, P. M. & George, A. M. Role of the D-loops in allosteric control of ATP hydrolysis in an ABC transporter. *J. Phys. Chem. A* **116**, 3004–3013 (2012).
72. Grossmann, N. *et al.* Mechanistic determinants of the directionality and energetics of active export by a heterodimeric ABC transporter. *Nat. Commun.* **5**, 5419 (2014).
73. Vakkasoglu, A. S., Srikant, S. & Gaudet, R. D-helix influences dimerization of the ATP-binding cassette (ABC) transporter associated with antigen processing 1 (TAP1) nucleotide-binding domain. *PLoS One* **12**, e0178238 (2017).
74. Zaitseva, J., Jenewein, S., Jumpertz, T., Holland, I. B. & Schmitt, L. H662 is the linchpin of ATP hydrolysis in the nucleotide-binding domain of the ABC transporter HlyB. *EMBO J.* **24**, 1901–1910 (2005).
75. Prieß, M., Göddeke, H., Groenhof, G. & Schäfer, L. V. Molecular Mechanism of ATP Hydrolysis in an ABC Transporter. *ACS Cent. Sci.* **4**, 1334–1343 (2018).
76. Smith, P. C. *et al.* ATP Binding to the Motor Domain from an ABC Transporter Drives Formation of a Nucleotide Sandwich Dimer. *Mol. Cell* **10**, 139–149 (2002).
77. Ambudkar, S. V., Kim, I. W., Xia, D. & Sauna, Z. E. The A-loop, a novel conserved aromatic acid subdomain upstream of the Walker A motif in ABC transporters, is critical for ATP binding. *FEBS Lett.* **580**, 1049–1055 (2006).
78. ter Beek, J., Guskov, A. & Slotboom, D. J. Structural diversity of ABC transporters. *J. Gen. Physiol.* **143**, 419–435 (2014).
79. Di Cesare, M. *et al.* The transport activity of the multidrug ABC transporter BmrA does not require a wide separation of the nucleotide-binding domains. *J. Biol. Chem.* **300**, 105546 (2024).
80. Chaptal, V. *et al.* Substrate-bound and substrate-free outward-facing structures of a multidrug ABC exporter. *Sci. Adv.* **8**, 9215 (2022).
81. Licht, A. & Schneider, E. ATP binding cassette systems: Structures, mechanisms, and functions. *Cent. Eur. J. Biol.* **6**, 785–801 (2011).
82. Loo, T. W. & Clarke, D. M. Mutational analysis of ABC proteins. *Arch. Biochem. Biophys.* **476**, 51–64 (2008).
83. Chufan, E. E., Sim, H. M. & Ambudkar, S. V. Molecular Basis of the Polyspecificity of P-Glycoprotein (ABCB1): Recent Biochemical and Structural Studies. *Adv. Cancer Res.* **125**,

71–96 (2015).

84. Naoe, Y. *et al.* Crystal structure of bacterial haem importer complex in the inward-facing conformation. *Nat. Commun.* **7**, 13411 (2016).
85. Chen, S., Oldham, M. L., Davidson, A. L. & Chen, J. Carbon catabolite repression of the maltose transporter revealed by X-ray crystallography. *Nature* **499**, 364–368 (2013).
86. Velamakanni, S., Yao, Y., Gutmann, D. A. P. & Van Veen, H. W. Multidrug transport by the ABC transporter Sav1866 from Staphylococcus aureus. *Biochemistry* **47**, 9300–9308 (2008).
87. Mourez, M., Hofnung, M. & Dassa, E. Subunit interactions in ABC transporters: a conserved sequence in hydrophobic membrane proteins of periplasmic permeases defines an important site of interaction with the ATPase subunits. *EMBO J.* **16**, 3066–3077 (1997).
88. Furuta, T., Yamaguchi, T., Kato, H. & Sakurai, M. Analysis of the Structural and Functional Roles of Coupling Helices in the ATP-Binding Cassette Transporter MsbA through Enzyme Assays and Molecular Dynamics Simulations. *Biochemistry* **53**, 4261–4272 (2014).
89. Tóth, Á., Janaszkiewicz, A., Crespi, V. & Di Meo, F. On the interplay between lipids and asymmetric dynamics of an NBS degenerate ABC transporter. *Commun. Biol.* **6**, 149 (2023).
90. Smriti, Zou, P. & Mchaourab, H. S. Mapping Daunorubicin-binding Sites in the ATP-binding Cassette Transporter MsbA Using Site-specific Quenching by Spin Labels. *J. Biol. Chem.* **284**, 13904–13913 (2009).
91. Szöllősi, D., Rose-Sperling, D., Hellmich, U. A. & Stockner, T. Comparison of mechanistic transport cycle models of ABC exporters. *Biochim. Biophys. Acta - Biomembr.* **1860**, 818–832 (2018).
92. Hollenstein, K., Frei, D. C. & Locher, K. P. Structure of an ABC transporter in complex with its binding protein. *Nature* **446**, 213–216 (2007).
93. Roberts, A. G. The Structure and Mechanism of Drug Transporters. *Methods Mol. Biol.* **2342**, 193–234 (2021).
94. Reyes, C. L. & Chang, G. Structure of the ABC transporter MsbA in complex with ADP·vanadate and lipopolysaccharide. *Science* **308**, 1028–1031 (2005).
95. Jones, P. M. & George, A. M. The Switch and Reciprocating Models for the Function of ABC Multidrug Exporters: Perspectives on Recent Research. *Int. J. Mol. Sci.* **24**, 2624 (2023).
96. Gutmann, D. A. P., Ward, A., Urbatsch, I. L., Chang, G. & van Veen, H. W. Understanding polyspecificity of multidrug ABC transporters: closing in on the gaps in ABCB1. *Trends Biochem. Sci.* **35**, 36–42 (2010).
97. Higgins, C. F. & Linton, K. J. The ATP switch model for ABC transporters. *Nat. Struct. Mol. Biol.* **11**, 918–926 (2004).
98. Janas, E. *et al.* The ATP Hydrolysis Cycle of the Nucleotide-binding Domain of the Mitochondrial ATP-binding Cassette Transporter Mdl1p. *J. Biol. Chem.* **278**, 26862–26869

(2003).

99. van der Does, C. & Tampé, R. How do ABC transporters drive transport? *Biol. Chem.* **385**, 927–933 (2004).

100. Chen, J., Lu, G., Lin, J., Davidson, A. L. & Quiocho, F. A. A Tweezers-like Motion of the ATP-Binding Cassette Dimer in an ABC Transport Cycle. *Mol. Cell* **12**, 651–661 (2003).

101. Senior, A. E., Al-Shawi, M. K. & Urbatsch, I. L. The catalytic cycle of P-glycoprotein. *FEBS Lett.* **377**, 285–289 (1995).

102. Jones, P. M. & George, A. M. Opening of the ADP-bound active site in the ABC transporter ATPase dimer: Evidence for a constant contact, alternating sites model for the catalytic cycle. *Proteins Struct. Funct. Bioinforma.* **75**, 387–396 (2009).

103. Sauna, Z. E. & Ambudkar, S. V. About a switch: how P-glycoprotein (ABCB1) harnesses the energy of ATP binding and hydrolysis to do mechanical work. *Mol. Cancer Ther.* **6**, 13–23 (2007).

104. Sauna, Z. E. *et al.* Catalytic cycle of ATP hydrolysis by P-glycoprotein: Evidence for formation of the E·S reaction intermediate with ATP-γ-S, a nonhydrolyzable analogue of ATP. *Biochemistry* **46**, 13787–13799 (2007).

105. Siarheyeva, A., Liu, R. & Sharom, F. J. Characterization of an Asymmetric Occluded State of P-glycoprotein with Two Bound Nucleotides. *J. Biol. Chem.* **285**, 7575–7586 (2010).

106. Petronilli, V. & Ames, G. F. L. Binding protein-independent histidine permease mutants. Uncoupling of ATP hydrolysis from transmembrane signaling. *J. Biol. Chem.* **266**, 16293–16296 (1991).

107. Hrycyna, C. A. *et al.* Both ATP sites of human P-glycoprotein are essential but not symmetric. *Biochemistry* **38**, 13887–13899 (1999).

108. Hou, Y. xian, Riordan, J. R. & Chang, X. bao. ATP binding, not hydrolysis, at the first nucleotide-binding domain of multidrug resistance-associated protein MRP1 enhances ADP·Vi trapping at the second domain. *J. Biol. Chem.* **278**, 3599–3605 (2003).

109. Hopfner, K. P. & Tainer, J. A. Rad50/SMC proteins and ABC transporters: unifying concepts from high-resolution structures. *Curr. Opin. Struct. Biol.* **13**, 249–255 (2003).

110. Hopfner, K. P. *et al.* Structural biology of Rad50 ATPase: ATP-driven conformational control in DNA double-strand break repair and the ABC-ATPase superfamily. *Cell* **101**, 789–800 (2000).

111. Borst, P. & Elferink, R. O. Mammalian ABC Transporters in Health and Disease. *Annu. Rev. Biochem.* **71**, 537–592 (2002).

112. Morita, M. & Imanaka, T. Peroxisomal ABC transporters: Structure, function and role in disease. *Biochim. Biophys. Acta - Mol. Basis Dis.* **1822**, 1387–1396 (2012).

113. Deme, J. C. *et al.* Purification and interaction analyses of two human lysosomal vitamin B 12 transporters: LMBD1 and ABCD4. *Mol. Membr. Biol.* **31**, 250–261 (2014).

114. Navarro-Quiles, C., Mateo-Bonmatí, E. & Micol, J. L. ABCE proteins: From molecules to development. *Front. Plant Sci.* **9**, 380112 (2018).
115. Murina, V. *et al.* ABCF ATPases Involved in Protein Synthesis, Ribosome Assembly and Antibiotic Resistance: Structural and Functional Diversification across the Tree of Life. *J. Mol. Biol.* **431**, 3568–3590 (2019).
116. Gottesman, M. M. & Pastan, I. Biochemistry of multidrug resistance mediated by the multidrug transporter. *Annu. Rev. Biochem.* **62**, 385–427 (1993).
117. Hartz, A. M. S. & Bauer, B. ABC Transporters in the CNS – An Inventory. *Curr. Pharm. Biotechnol.* **12**, 656–673 (2011).
118. Fromm, M. F. Importance of P-glycoprotein at blood-tissue barriers. *Trends Pharmacol. Sci.* **25**, 423–429 (2004).
119. Ueda, K. *et al.* The mdrl gene, responsible for multidrug-resistance, codes for P-glycoprotein. *Biochem. Biophys. Res. Commun.* **141**, 956–962 (1986).
120. Riordan, J. R. *et al.* Identification of the Cystic Fibrosis Gene: Cloning and Characterization of Complementary DNA. *Science* **245**, 1066–1073 (1989).
121. Dean, M., Moitra, K. & Allikmets, R. The human ATP-binding cassette (ABC) transporter superfamily. *Hum. Mutat.* **43**, 1162–1182 (2022).
122. Marson, F. A. L., Bertuzzo, C. S. & Ribeiro, J. D. Classification of CFTR mutation classes. *Lancet Respir. Med.* **4**, e37–e38 (2016).
123. Steinfels, E. *et al.* Highly efficient over-production in E. coli of YvcC, a multidrug-like ATP-binding cassette transporter from Bacillus subtilis. *Biochim. Biophys. Acta - Biomembr.* **1565**, 1–5 (2002).
124. Steinfels, E. *et al.* Characterization of YvcC (BmrA), a Multidrug ABC Transporter Constitutively Expressed in Bacillus subtilis. *Biochemistry* **43**, 7491–7502 (2004).
125. van Veen, H. W. *et al.* A bacterial antibiotic-resistance gene that complements the human multidrug-resistance P-glycoprotein gene. *Nature* **391**, 291–295 (1998).
126. Krügel, H. *et al.* Cervimycin C resistance in Bacillus subtilis is due to a promoter up-mutation and increased mRNA stability of the constitutive ABC-transporter gene bmrA. *FEMS Microbiol. Lett.* **313**, 155–163 (2010).
127. Gobet, A. *et al.* Rhodamine6G and Hœchst33342 narrow BmrA conformational spectrum for a more efficient use of ATP. *Nat. Commun. 2025 161* **16**, 1–14 (2025).
128. Lacabanne, D. *et al.* Flexible-to-rigid transition is central for substrate transport in the ABC transporter BmrA from Bacillus subtilis. *Commun. Biol.* **2**, (2019).
129. Mehmood, S., Domene, C., Forest, E. & Jault, J.-M. Dynamics of a bacterial multidrug ABC transporter in the inward- and outward-facing conformations. *Proc. Natl. Acad. Sci.* **109**, 10832–10836 (2012).
130. Javed, W. *et al.* Structural Insights into the Catalytic Cycle of a Bacterial Multidrug ABC

Efflux Pump. *J. Mol. Biol.* **434**, 167541 (2022).

131. Lacabanne, D. *et al.* Solid-State NMR Reveals Asymmetric ATP Hydrolysis in the Multidrug ABC Transporter BmrA. *J. Am. Chem. Soc.* **144**, 12431–12442 (2022).
132. Johnson, Z. L. & Chen, J. ATP Binding Enables Substrate Release from Multidrug Resistance Protein 1. *Cell* **172**, 81-89.e10 (2018).
133. Hutter, C. A. J. *et al.* The extracellular gate shapes the energy profile of an ABC exporter. *Nat. Commun.* **10**, 2260 (2019).
134. Manuse, S. *et al.* Bacterial persisters are a stochastically formed subpopulation of low-energy cells. *PLOS Biol.* **19**, e3001194 (2021).
135. Fribourg, P. F. *et al.* 3D Cryo-Electron Reconstruction of BmrA, a Bacterial Multidrug ABC Transporter in an Inward-Facing Conformation and in a Lipidic Environment. *J. Mol. Biol.* **426**, 2059–2069 (2014).
136. Orelle, C., Schmitt, L. & Jault, J. M. Waste or die: The price to pay to stay alive. *Trends Microbiol.* **31**, 233–241 (2023).
137. Kunert, B. *et al.* Efficient and stable reconstitution of the ABC transporter BmrA for solid-state NMR studies. *Front. Mol. Biosci.* **1**, (2014).
138. Ravaud, S. *et al.* The ABC transporter BmrA from Bacillus subtilis is a functional dimer when in a detergent-solubilized state. *Biochem. J.* **395**, 345–353 (2006).
139. Srinivasan, V., Pierik, A. J. & Lill, R. Crystal Structures of Nucleotide-Free and Glutathione-Bound Mitochondrial ABC Transporter Atm1. *Science* **343**, 1137–1140 (2014).
140. Zaitseva, J. *et al.* Functional characterization and ATP-induced dimerization of the isolated ABC-domain of the haemolysin B transporter. *Biochemistry* **44**, 9680–9690 (2005).
141. Oancea, G. *et al.* Structural arrangement of the transmission interface in the antigen ABC transport complex TAP. *Proc. Natl. Acad. Sci. U. S. A.* **106**, 5551–5556 (2009).
142. Loo, T. W., Bartlett, M. C. & Clarke, D. M. Human P-glycoprotein Contains a Greasy Ball-and-Socket Joint at the Second Transmission Interface. *J. Biol. Chem.* **288**, 20326–20333 (2013).
143. Guggino, W. B. & Stanton, B. A. New insights into cystic fibrosis: molecular switches that regulate CFTR. *Nat. Rev. Mol. Cell Biol.* **7**, 426–436 (2006).
144. Jin, M. S., Oldham, M. L., Zhang, Q. & Chen, J. Crystal structure of the multidrug transporter P-glycoprotein from Caenorhabditis elegans. *Nature* **490**, 566–569 (2012).
145. Gibson, D. G. *et al.* Enzymatic assembly of DNA molecules up to several hundred kilobases. *Nat. Methods* **6**, 343–345 (2009).
146. Chung, C. T., Niemela, S. L. & Miller, R. H. One-step preparation of competent Escherichia coli: transformation and storage of bacterial cells in the same solution. *Proc. Natl. Acad. Sci.* **86**, 2172–2175 (1989).
147. Mathieu, K. *et al.* Functionality of membrane proteins overexpressed and purified from E. coli is highly dependent upon the strain. *Sci. Rep.* **9**, 2654 (2019).

148. Gasteiger, E. ExPASy: the proteomics server for in-depth protein knowledge and analysis. *Nucleic Acids Res.* **31**, 3784–3788 (2003).
149. Laemmli, U. K. Cleavage of structural proteins during the assembly of the head of bacteriophage T4. *Nature* **227**, 680–685 (1970).
150. Keppler, A. *et al.* A general method for the covalent labeling of fusion proteins with small molecules in vivo. *Nat. Biotechnol.* **21**, 86–89 (2003).
151. Schneider, C. A., Rasband, W. S. & Eliceiri, K. W. NIH Image to ImageJ: 25 years of image analysis. *Nat. Methods* **9**, 671–675 (2012).
152. Anbazhagan, V., Munz, C., Tome, L. & Schneider, D. Fluidizing the Membrane by a Local Anesthetic: Phenylethanol Affects Membrane Protein Oligomerization. *J. Mol. Biol.* **404**, 773–777 (2010).
153. Parasassi, T. & Gratton, E. Membrane lipid domains and dynamics as detected by Laurdan fluorescence. *J. Fluoresc.* **5**, 59–69 (1995).
154. Khurana, R. *et al.* Mechanism of thioflavin T binding to amyloid fibrils. *J. Struct. Biol.* **151**, 229–238 (2005).
155. Consortium, T. U. *et al.* UniProt: the Universal Protein Knowledgebase in 2025. *Nucleic Acids Res.* **53**, D609–D617 (2025).
156. Madeira, F. *et al.* The EMBL-EBI Job Dispatcher sequence analysis tools framework in 2024. *Nucleic Acids Res.* **52**, W521–W525 (2024).
157. Robert, X. & Gouet, P. Deciphering key features in protein structures with the new ENDscript server. *Nucleic Acids Res.* **42**, W320–W324 (2014).
158. Osten, V. & Schneider, D. Membrane properties control the ATPase activity of the ABC transporter BmrA. *Biochim. Biophys. Acta - Biomembr.* **1867**, 184430 (2025).
159. Willdigg, J. R. & Helmann, J. D. Mini Review: Bacterial Membrane Composition and Its Modulation in Response to Stress. *Front. Mol. Biosci.* **8**, 634438 (2021).
160. Poolman, B., Spitzer, J. J. & Wood, J. M. Bacterial osmosensing: roles of membrane structure and electrostatics in lipid–protein and protein–protein interactions. *Biochim. Biophys. Acta - Biomembr.* **1666**, 88–104 (2004).
161. Sachs, J. N. & Engelman, D. M. Introduction to the Membrane Protein Reviews: The Interplay of Structure, Dynamics, and Environment in Membrane Protein Function. **27**, 51 (2025).
162. Hoffmann, L. *et al.* The ABC transporter MsbA in a dozen environments. *Structure* **33**, 916-923.e4 (2025).
163. Lee, A. G. Lipid–protein interactions in biological membranes: a structural perspective. *Biochim. Biophys. Acta - Biomembr.* **1612**, 1–40 (2003).
164. E. Cybulski, L. & de Mendoza, D. Bilayer Hydrophobic Thickness and Integral Membrane Protein Function. *Curr. Protein Pept. Sci.* **12**, 760–766 (2011).
165. Pannwitt, S., Stangl, M. & Schneider, D. Lipid Binding Controls Dimerization of the Coat

Protein p24 Transmembrane Helix. *Biophys. J.* **117**, 1554–1562 (2019).

166. Contreras, F.-X. *et al.* Molecular recognition of a single sphingolipid species by a protein's transmembrane domain. *Nature* **481**, 525–529 (2012).
167. Anbazhagan, V. & Schneider, D. The membrane environment modulates self-association of the human GpA TM domain—Implications for membrane protein folding and transmembrane signaling. *Biochim. Biophys. Acta - Biomembr.* **1798**, 1899–1907 (2010).
168. Petrache, H. I., Grossfield, A., MacKenzie, K. R., Engelman, D. M. & Woolf, T. B. Modulation of glycophorin A transmembrane helix interactions by lipid bilayers: molecular dynamics calculations. *J. Mol. Biol.* **302**, 727–746 (2000).
169. Bondar, A.-N., del Val, C. & White, S. H. Rhomboid Protease Dynamics and Lipid Interactions. *Structure* **17**, 395–405 (2009).
170. Dassa, E. & Bouige, P. The ABC of ABCs: a phylogenetic and functional classification of ABC systems in living organisms. *Res. Microbiol.* **152**, 211–229 (2001).
171. Higgins, C. F., Hiles, I. D., Whalley, K. & Jamieson, D. J. Nucleotide binding by membrane components of bacterial periplasmic binding protein-dependent transport systems. *EMBO J.* **4**, 1033–1039 (1985).
172. Hanekop, N., Zaitseva, J., Jenewein, S., Holland, I. B. & Schmitt, L. Molecular insights into the mechanism of ATP-hydrolysis by the NBD of the ABC-transporter HlyB. *FEBS Lett.* **580**, 1036–1041 (2006).
173. Oldham, M. L., Davidson, A. L. & Chen, J. Structural insights into ABC transporter mechanism. *Curr. Opin. Struct. Biol.* **18**, 726–733 (2008).
174. Bao, H., Dalal, K., Wang, V., Rouiller, I. & Duong, F. The maltose ABC transporter: Action of membrane lipids on the transporter stability, coupling and ATPase activity. *Biochim. Biophys. Acta - Biomembr.* **1828**, 1723–1730 (2013).
175. Schölz, C. *et al.* Specific Lipids Modulate the Transporter Associated with Antigen Processing (TAP). *J. Biol. Chem.* **286**, 13346–13356 (2011).
176. Sharom, F. J. Complex Interplay between the P-Glycoprotein Multidrug Efflux Pump and the Membrane: Its Role in Modulating Protein Function. *Front. Oncol.* **4**, 75085 (2014).
177. Ambudkar, S. V., Lelong, I. H., Zhang, J. & Cardarelli, C. Purification and reconstitution of human P-glycoprotein. *Methods Enzymol.* **292**, 492–504 (1998).
178. Hirayama, H., Kimura, Y., Kioka, N., Matsuo, M. & Ueda, K. ATPase activity of human ABCG1 is stimulated by cholesterol and sphingomyelin. *J. Lipid Res.* **54**, 496–502 (2013).
179. Ambudkar, S. V. *et al.* Partial purification and reconstitution of the human multidrug-resistance pump: characterization of the drug-stimulatable ATP hydrolysis. *Proc. Natl. Acad. Sci.* **89**, 8472–8476 (1992).
180. Liu, R. & Sharom, F. J. Site-Directed Fluorescence Labeling of P-Glycoprotein on Cysteine Residues in the Nucleotide Binding Domains. *Biochemistry* **35**, 11865–11873 (1996).

181. Jensen, M. & Mouritsen, O. G. Lipids do influence protein function—the hydrophobic matching hypothesis revisited. *Biochim. Biophys. Acta - Biomembr.* **1666**, 205–226 (2004).
182. van den Brink-van der Laan, E., Antoinette Killian, J. & de Kruijff, B. Nonbilayer lipids affect peripheral and integral membrane proteins via changes in the lateral pressure profile. *Biochim. Biophys. Acta - Biomembr.* **1666**, 275–288 (2004).
183. Levental, I. & Lyman, E. Regulation of membrane protein structure and function by their lipid nano-environment. *Nat. Rev. Mol. Cell Biol.* **24**, 107–122 (2023).
184. Palsdottir, H. & Hunte, C. Lipids in membrane protein structures. *Biochim. Biophys. Acta - Biomembr.* **1666**, 2–18 (2004).
185. Stangl, M. & Schneider, D. Functional competition within a membrane: Lipid recognition vs. transmembrane helix oligomerization. *Biochim. Biophys. Acta - Biomembr.* **1848**, 1886–1896 (2015).
186. Nouel Barreto, A., Cuello, L. G. & Zoghbi, M. E. ABC transporter activity is affected by the size of lipid nanodiscs. *FEBS Lett.* **599**, 502–511 (2025).
187. Lomize, M. A., Pogozheva, I. D., Joo, H., Mosberg, H. I. & Lomize, A. L. OPM database and PPM web server: resources for positioning of proteins in membranes. *Nucleic Acids Res.* **40**, (2012).
188. Kučerka, N., Tristram-Nagle, S. & Nagle, J. F. Structure of Fully Hydrated Fluid Phase Lipid Bilayers with Monounsaturated Chains. *J. Membr. Biol.* **208**, 193–202 (2006).
189. Klein, N., Hellmann, N. & Schneider, D. Anionic Lipids Modulate the Activity of the Aquaglyceroporin GlpF. *Biophys. J.* **109**, 722–731 (2015).
190. Harris, N. J. & Booth, P. J. Folding and stability of membrane transport proteins in vitro. *Biochim. Biophys. Acta - Biomembr.* **1818**, 1055–1066 (2012).
191. Raetz, C. R. H. & Dowhan, W. Biosynthesis and function of phospholipids in Escherichia coli. *J. Biol. Chem.* **265**, 1235–1238 (1990).
192. Mitra, K., Ubarretxena-Belandia, I., Taguchi, T., Warren, G. & Engelman, D. M. Modulation of the bilayer thickness of exocytic pathway membranes by membrane proteins rather than cholesterol. *Proc. Natl. Acad. Sci.* **101**, 4083–4088 (2004).
193. den Kamp, J. A. F. O., Redai, I. & van Deenen, L. L. M. Phospholipid Composition of Bacillus subtilis. *J. Bacteriol.* **99**, 298–303 (1969).
194. Nickels, J. D. *et al.* Bacillus subtilis Lipid Extract, A Branched-Chain Fatty Acid Model Membrane. *J. Phys. Chem. Lett.* **8**, 4214–4217 (2017).
195. van de Vossenberg, J. L. C. ., Driessen, A. J. M., da Costa, M. S. & Konings, W. N. Homeostasis of the membrane proton permeability in Bacillus subtilis grown at different temperatures. *Biochim. Biophys. Acta - Biomembr.* **1419**, 97–104 (1999).
196. Kučerka, N. *et al.* Areas of Monounsaturated Diacylphosphatidylcholines. *Biophys. J.* **97**, 1926–1932 (2009).

197. Nishibori, A., Kusaka, J., Hara, H., Umeda, M. & Matsumoto, K. Phosphatidylethanolamine domains and localization of phospholipid synthases in Bacillus subtilis membranes. *J. Bacteriol.* **187**, 2163–2174 (2005).
198. Kawai, F. *et al.* Cardiolipin Domains in Bacillus subtilis Marburg Membranes. *J. Bacteriol.* **186**, 1475–1483 (2004).
199. Osten, V., Oepen, K. & Schneider, D. The C-terminal α-helix is crucial for the activity of the bacterial ABC transporter BmrA. *J. Biol. Chem.* **301**, 108098 (2025).
200. Tiefenauer, L. & Demarche, S. Challenges in the Development of Functional Assays of Membrane Proteins. *Materials (Basel).* **5**, 2205–2242 (2012).
201. Lewinson, O. & Livnat-Levanon, N. Mechanism of Action of ABC Importers: Conservation, Divergence, and Physiological Adaptations. *J. Mol. Biol.* **429**, 606–619 (2017).
202. Locher, K. P. Mechanistic diversity in ATP-binding cassette (ABC) transporters. *Nat. Struct. Mol. Biol.* **23**, 487–493 (2016).
203. Licht, A. & Schneider, E. ATP binding cassette systems: Structures, mechanisms, and functions. *Cent. Eur. J. Biol.* **6**, 785–801 (2011).
204. Hyde, S. C. *et al.* Structural Model of ATP-binding Proteins associated with Cystic Fibrosis, Multidrug Resistance and Bacterial Transport. *Nature* **346**, 362–365 (1990).
205. Bolhuis, H. *et al.* Multidrug resistance in Lactococcus lactis: evidence for ATP-dependent drug extrusion from the inner leaflet of the cytoplasmic membrane. *EMBO J.* **15**, 4239–4245 (1996).
206. Putman, M., van Veen, H. W. & Konings, W. N. Molecular Properties of Bacterial Multidrug Transporters. *Microbiol. Mol. Biol. Rev.* **64**, 672–693 (2000).
207. Alam, A., Kowal, J., Broude, E., Roninson, I. & Locher, K. P. Structural insight into substrate and inhibitor discrimination by human P-glycoprotein. *Science* **363**, 753–756 (2019).
208. Jones, P. M. & George, A. M. The ABC transporter structure and mechanism: Perspectives on recent research. *Cell. Mol. Life Sci.* **61**, 682–699 (2004).
209. Schmitt, L. & Tampé, R. Structure and mechanism of ABC transporters. *Curr. Opin. Struct. Biol.* **12**, 754–760 (2002).
210. Davidson, A. L. & Chen, J. ATP-binding cassette transporters in bacteria. *Annu. Rev. Biochem.* **73**, 241–268 (2004).
211. Orelle, C. *et al.* Conformational change induced by ATP binding in the multidrug ATP-binding cassette transporter BmrA. *Biochemistry* **47**, 2404–2412 (2008).
212. Buchaklian, A. H. & Klug, C. S. Characterization of the LSGGQ and H motifs from the Escherichia coli lipid A transporter MsbA. *Biochemistry* **45**, 12539–12546 (2006).
213. Ambudkar, S. V., Kim, I.-W., Xia, D. & Sauna, Z. E. The A-loop, a novel conserved aromatic acid subdomain upstream of the Walker A motif in ABC transporters, is critical for ATP binding. *FEBS Lett.* **580**, 1049–1055 (2006).

214. Ward, A. B., Reyes, C. L., Yu, J., Roth, C. B. & Chang, G. Flexibility in the ABC transporter MsbA: Alternating access with a twist. *Proc. Natl. Acad. Sci. U. S. A.* **104**, 19005–19010 (2007).
215. Damas, J. M., Oliveira, A. S. F., Baptista, A. M. & Soares, C. M. Structural consequences of ATP hydrolysis on the ABC transporter NBD dimer: Molecular dynamics studies of HlyB. *Protein Sci.* **20**, 1220–1230 (2011).
216. Stefan, E., Hofmann, S. & Tampé, R. A single power stroke by ATP binding drives substrate translocation in a heterodimeric ABC transporter. *Elife* **9**, 1–17 (2020).
217. Lu, G., Westbrooks, J. M., Davidson, A. L. & Chen, J. ATP hydrolysis is required to reset the ATP-binding cassette dimer into the resting-state conformation. *Proc. Natl. Acad. Sci.* **102**, 17969–17974 (2005).
218. Diederichs, K. *et al.* Crystal structure of Malk, the ATPase subunit of the trehalose/maltose ABC transporter of the archaeon Thermococcus litoralis. *EMBO J.* **19**, 5951–5961 (2000).
219. Schaedler, T. A. *et al.* Structures and functions of mitochondrial ABC transporters. *Biochem. Soc. Trans.* **43**, 943–51 (2015).
220. Steinfels, E. *et al.* Highly efficient over-production in E. coli of YvcC, a multidrug-like ATP-binding cassette transporter from Bacillus subtilis. *Biochim. Biophys. Acta - Biomembr.* **1565**, 1–5 (2002).
221. Dalmas, O. *et al.* Time-resolved fluorescence resonance energy transfer shows that the bacterial multidrug ABC half-transporter BmrA functions as a homodimer. *Biochemistry* **44**, 4312–4321 (2005).
222. Pérez Carrillo, V. H., Rose-Sperling, D., Tran, M. A., Wiedemann, C. & Hellmich, U. A. Backbone NMR assignment of the nucleotide binding domain of the Bacillus subtilis ABC multidrug transporter BmrA in the post-hydrolysis state. *Biomol. NMR Assign.* **16**, 81–86 (2022).
223. Hanekop, N., Zaitseva, J., Jenewein, S., Holland, I. B. & Schmitt, L. Molecular insights into the mechanism of ATP-hydrolysis by the NBD of the ABC-transporter HlyB. *FEBS Lett.* **580**, 1036–1041 (2006).
224. Timachi, M. H. *et al.* Exploring conformational equilibria of a heterodimeric ABC transporter. *Elife* **6**, 1–28 (2017).
225. Oepen, K., Mater, V. & Schneider, D. Unfolding Individual Domains of BmrA, a Bacterial ABC Transporter Involved in Multidrug Resistance. *Int. J. Mol. Sci.* **24**, 5239 (2023).
226. Newell, N. E. Mapping side chain interactions at protein helix termini. *BMC Bioinformatics* **16**, 1–21 (2015).
227. Davidson, A. L. & Sharma, S. Mutation of a single MalK subunit severely impairs maltose transport activity in Escherichia coli. *J. Bacteriol.* **179**, 5458–5464 (1997).
228. Nikaido, K. & Ames, G. F.-L. One Intact ATP-binding Subunit Is Sufficient to Support ATP Hydrolysis and Translocation in an ABC Transporter, the Histidine Permease. *J. Biol. Chem.*

274, 26727–26735 (1999).

229. Jardetzky, O. Simple Allosteric Model for Membrane Pumps. *Nature* **211**, 969–970 (1966).
230. Ambudkar, S. V., Kim, I. W. & Sauna, Z. E. The power of the pump: Mechanisms of action of P-glycoprotein (ABCB1). *Eur. J. Pharm. Sci.* **27**, 392–400 (2006).
231. Locher, K. P., Lee, A. T. & Rees, D. C. The E. coli BtuCD Structure: A Framework for ABC Transporter Architecture and Mechanism. *Science* **296**, 1091–1098 (2002).
232. Novischi, S. Y. P. *et al.* Probing the allosteric NBD-TMD crosstalk in the ABC transporter MsbA by solid-state NMR. *Commun. Biol. 2024 71* **7**, 1–11 (2024).
233. Kluth, M. *et al.* A Mutation within the Extended X Loop Abolished Substrate-induced ATPase Activity of the Human Liver ATP-binding Cassette (ABC) Transporter MDR3. *J. Biol. Chem.* **290**, 4896–4907 (2015).
234. Pérez Carrillo, V. H. *et al.* Bidirectional communication between nucleotide and substrate binding sites in a type IV multidrug ABC transporter. *bioRxiv* 2025.01.15.633140 (2025) [Preprint].
235. Mao, Y. X. *et al.* Transport mechanism of human bilirubin transporter ABCC2 tuned by the inter-module regulatory domain. *Nat. Commun. 2024 151* **15**, 1–12 (2024).
236. Andreoletti, P. *et al.* Predictive Structure and Topology of Peroxisomal ATP-Binding Cassette (ABC) Transporters. *Int. J. Mol. Sci.* **18**, 1593 (2017).
237. Khunweeraphong, N., Stockner, T. & Kuchler, K. The structure of the human ABC transporter ABCG2 reveals a novel mechanism for drug extrusion. *Sci. Rep.* **7**, 13767 (2017).
238. Khunweeraphong, N. & Kuchler, K. The first intracellular loop is essential for the catalytic cycle of the human ABCG2 multidrug resistance transporter. *FEBS Lett.* **594**, 4059–4075 (2020).
239. Cao, M. A. Do *et al.* Probing the conformation of the resting state of a bacterial multidrug ABC transporter, BmrA, by a site-directed spin labeling approach. *Protein Sci.* **18**, 1507–1520 (2009).
240. Januliene, D. & Moeller, A. Cryo-EM of ABC transporters: an ice-cold solution to everything? *FEBS Lett.* **594**, 3776–3789 (2020).
241. Punjani, A., Rubinstein, J. L., Fleet, D. J. & Brubaker, M. A. cryoSPARC: algorithms for rapid unsupervised cryo-EM structure determination. *Nat. Methods* **14**, 290–296 (2017).
242. Bepler, T. *et al.* Positive-unlabeled convolutional neural networks for particle picking in cryo-electron micrographs. *Nat. Methods* **16**, 1153–1160 (2019).
243. Pettersen, E. F. *et al.* UCSF ChimeraX: Structure visualization for researchers, educators, and developers. *Protein Sci.* **30**, 70–82 (2021).

6 Appendix

6.1 Plasmid maps

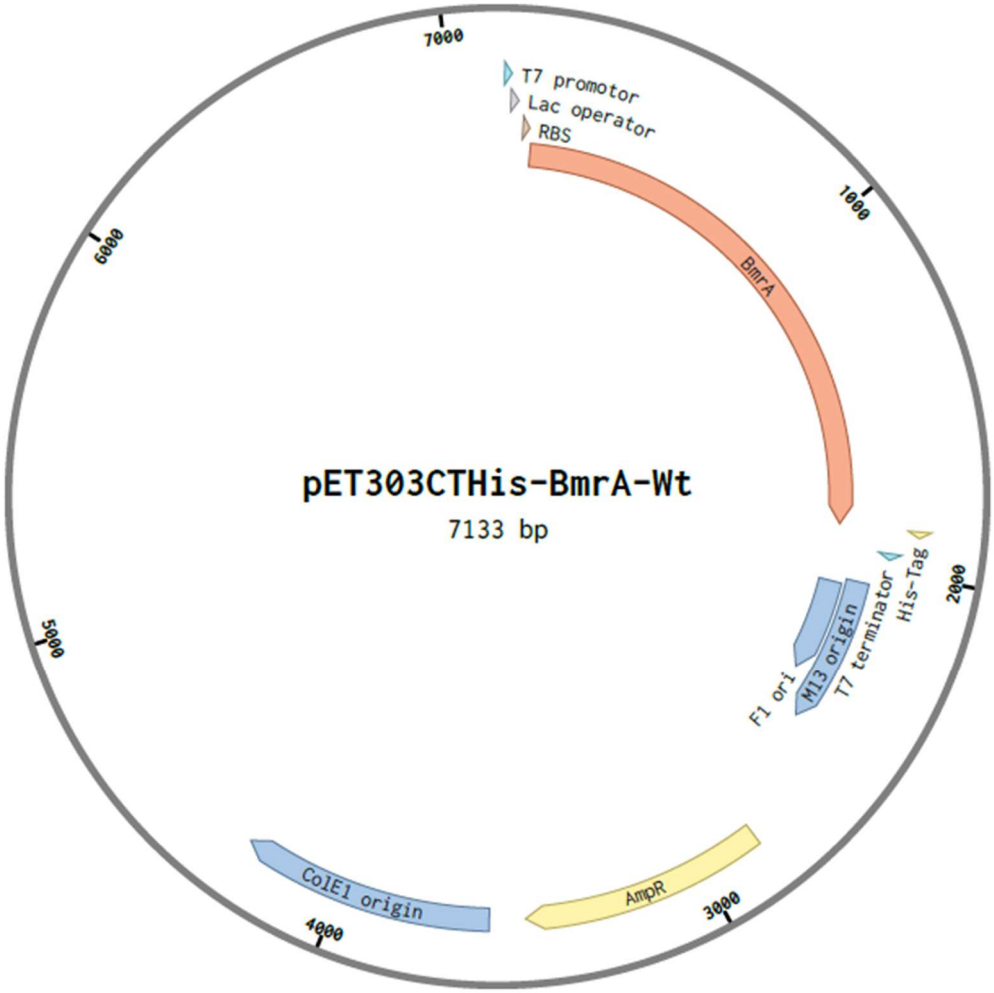

Figure A1: pET303CT-His-BmrA-wt plasmid.

Plasmid map of pET303CT-His-BmrA-wt. Shown are the positions of common features of the pET303 vector and the BmrA wt sequence. RBS = ribosome binding site, origin = origin of replication, AmpR = ampicillin resistance cassette. The map was created with Benchling.

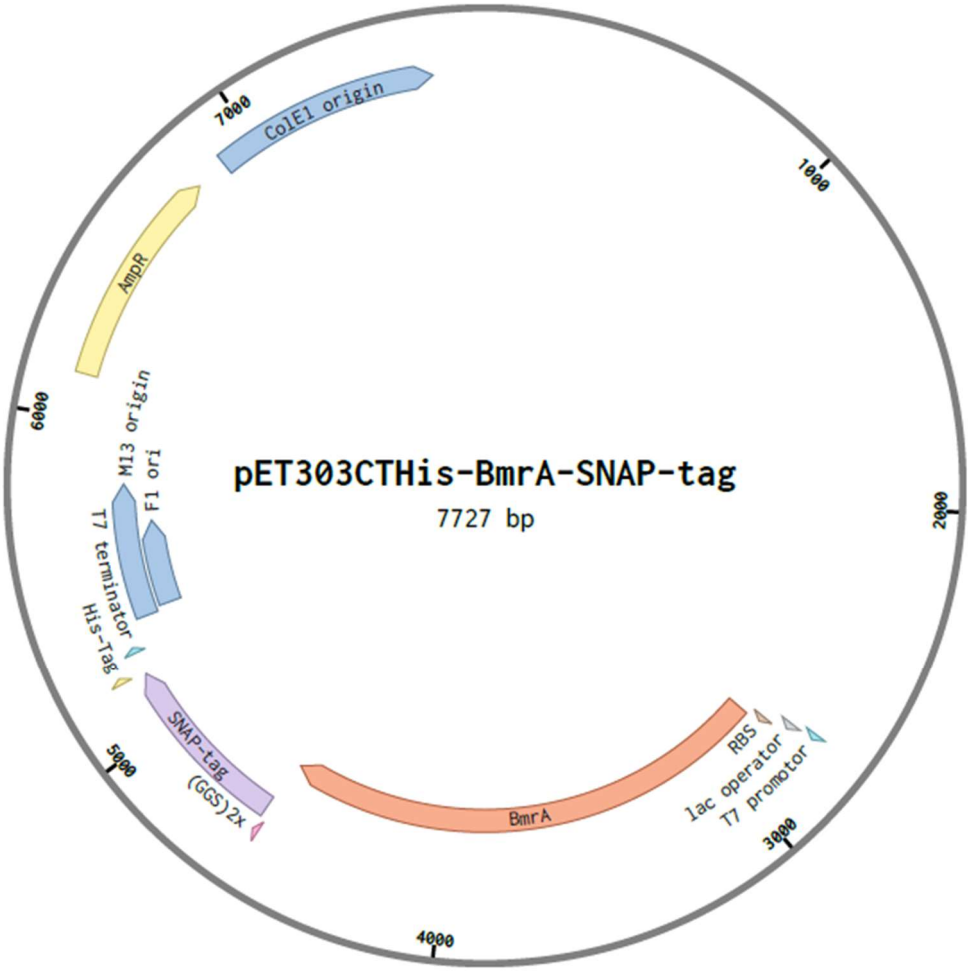

Figure A2: pET303CT-His-BmrA-SNAP-tag plasmid.

Plasmid map of pET303CT-His-BmrA-SNAP-tag. Shown are the positions of common features of the pET303 vector and the BmrA wt sequence. RBS = ribosome binding site, (GGS)2x = $(GGS)_2$-linker, origin = origin of replication, AmpR = ampicillin resistance cassette. The map was created with Benchling.

6.2 Sequences

```
        10         20         30         40         50         60
MPTKKQKSKS KLKPFFALVR RTNPSYGKLA FALALSVVTT LVSLLIPLLT KQLVDGFSMS

        70         80         90        100        110        120
NLSGTQIGLI ALVFFVQAGL SAYATYALNY NGQKIISGLR ELLWKKLIKL PVSYFDTNAS

       130        140        150        160        170        180
GETVSRVTND TMVVKELITT HISGFITGII SVIGSLTILF IMNWKLTLLV LVVVPLAALI

       190        200        210        220        230        240
LVPIGRKMFS ISRETQDETA RFTGLLNQIL PEIRLVKASN AEDVEYGRGK MGISSLFKLG

       250        260        270        280        290        300
VREAKVQSLV GPLISLVLMA ALVAVIGYGG MQVSSGELTA GALVAFILYL FQIIMPMGQI

       310        320        330        340        350        360
TTFFTQLQKS IGATERMIEI LAEEEEDTVT GKQIENAHLP IQLDRVSFGY KPDQLILKEV

       370        380        390        400        410        420
SAVIEAGKVT AIVGPSGGGK TTLFKLLERF YSPTAGTIRL GDEPVDTYSL ESWREHIGYV

       430        440        450        460        470        480
SQESPLMSGT IRENICYGLE RDVTDAEIEK AAEMAYALNF IKELPNQFDT EVGERGIMLS

       490        500        510        520        530        540
GGQRQRIAIA RALLRNPSIL MLDEATSSLD SQSEKSVQQA LEVLMEGRTT IVIAHRLSTV

       550        560        570        580        590
VDADQLLFVE KGEITGRGTH HELMASHGLY RDFAEQQLKM NADLENKAGL EHHHHHH
```

Figure A3: Amino acid sequence of BmrA wt.

Amino acid sequence of BmrA wt with annotations. The TMD sequence is highlighted in cyan, the NBD sequence in magenta, and the 6xHis-tag sequence in yellow. Amino acids that were replaced with alanine or cysteine in this study are shown in bold.

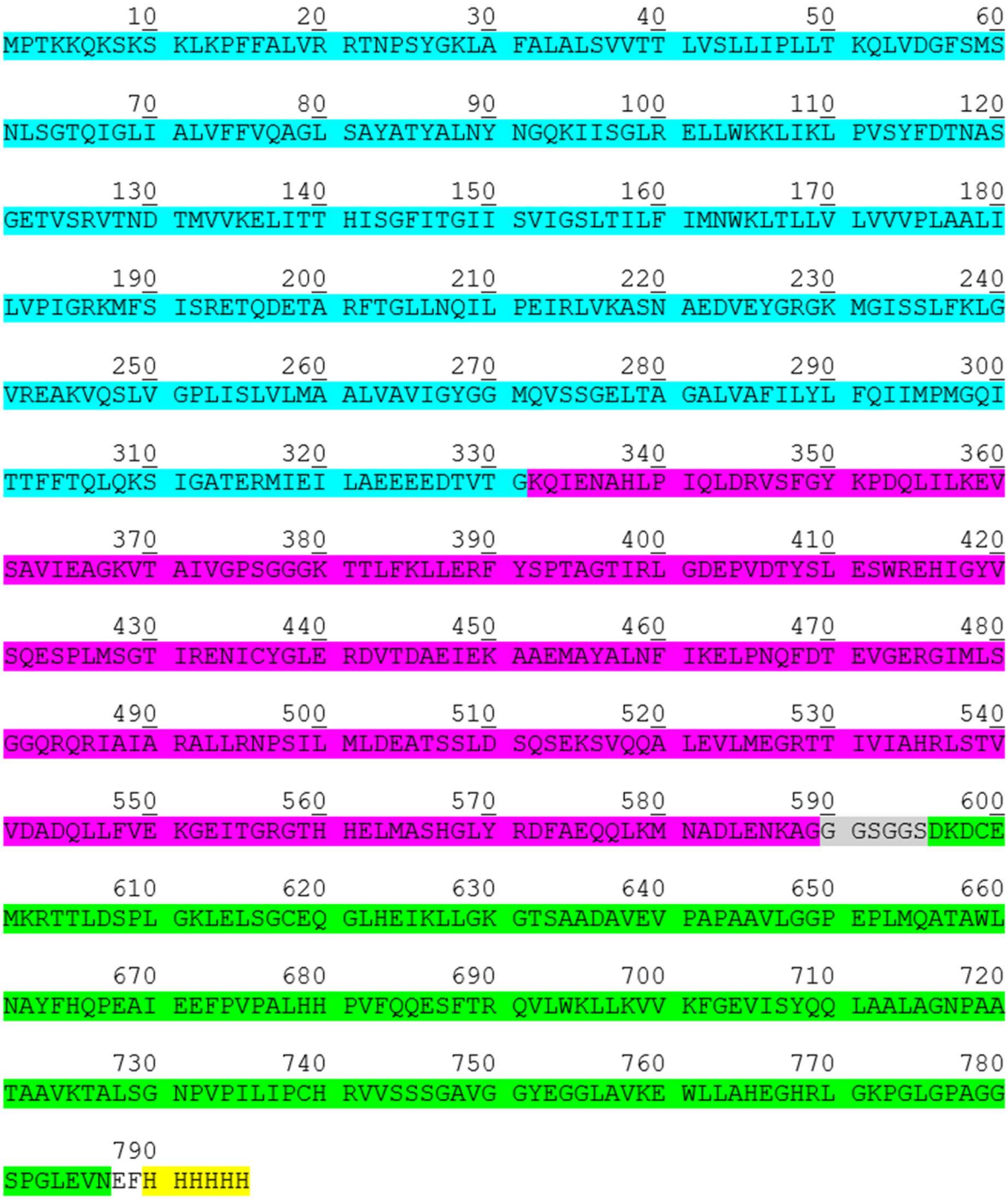

Figure A4: Amino acid sequence of BmrA-SNAP-tag.

Amino acid sequence of BmrA-SNAP-tag with annotations. The TMD sequence is highlighted in cyan, the NBD sequence in magenta, the $(GGS)_2$-linker sequence in gray, the SNAP-tag sequence in green, and the 6xHis-tag sequence in yellow.

6.3 Supplement

Table S1: Liposome destabilization with Triton-X 100.

Amounts of Triton-X 100 [mM] used for destabilizing liposomes of different lipids. The quantity required for liposomes with mixed lipids was calculated as a percentage from the quantities given.

Lipid composition	Triton-X 100 [mM]
EPL	2.4
14:1PC	1.3
16:1PC	2
DOPC (100%)	2.6
20:1PC	3.3
22:1PC	3.9
DOPE (70%) + DOPC (30%)	3.8
DOPG (100%)	1.3
DOPS (100%)	1.6
CL (70%) + DOPC (30%)	4.8
DOPE (70%) + DOPG (30%)	3.8
POPC	2.2

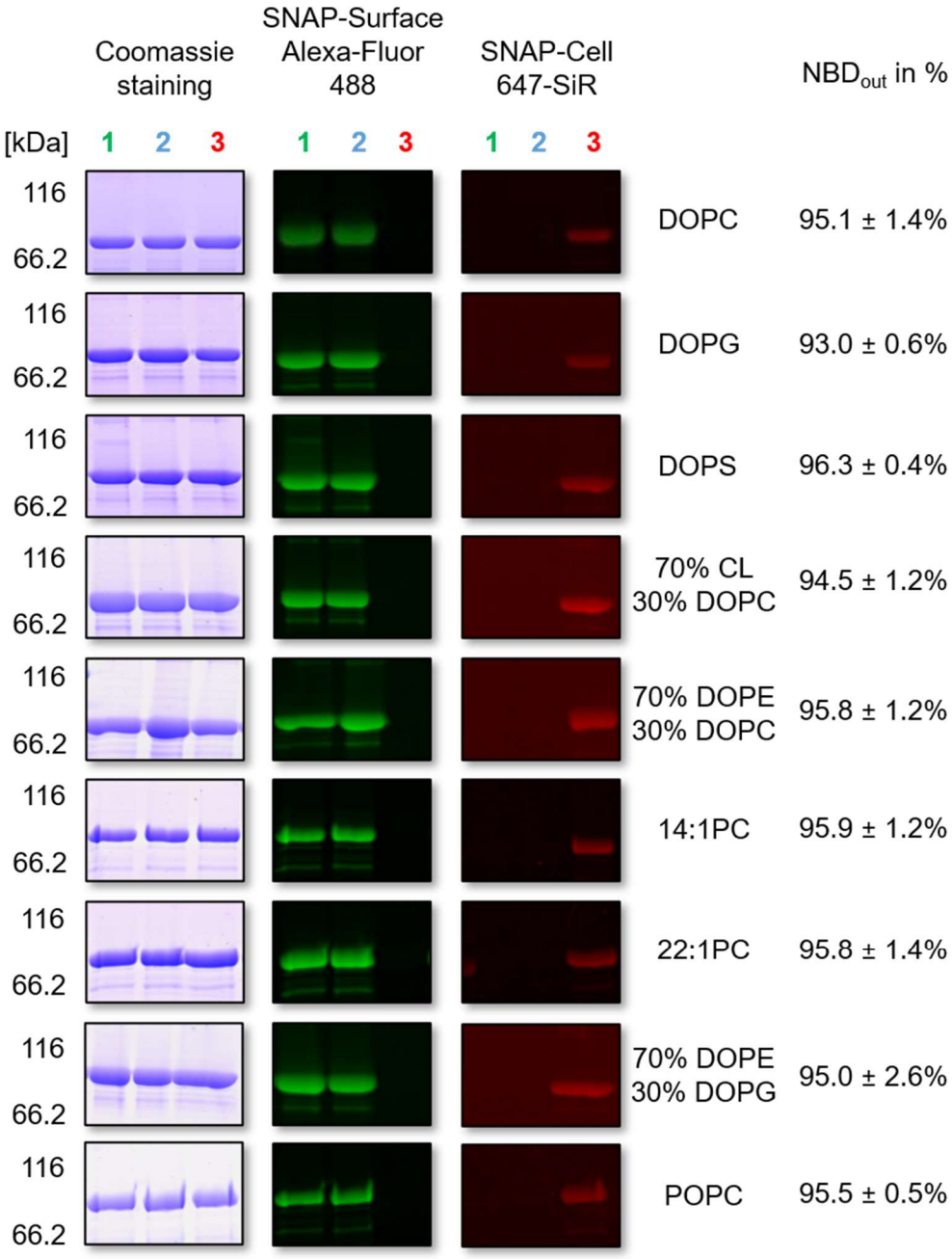

Figure S1: Orientation of BmrA-SNAP-tag reconstituted into liposomes with varying lipid compositions.

Unlabeled BmrA-SNAP-tag was reconstituted into liposomes (lipid mixture always indicated) and afterwards labeled either (1) with the membrane-impermeable SNAP-tag dye (SNAP-Surface® Alexa Fluor® 488), (2) subsequently also with a membrane-permeable SNAP-tag dye (SNAP-Cell® 647-SIR) or (3) only with the membrane-permeable dye. Afterwards, labeled proteins were separated on a 10% SDS-PAGE gel, and the in-gel fluorescence was determined, followed by Coomassie staining. The NBD_{out} orientation in %, calculated based on two independent proteoliposome preparations, is given.

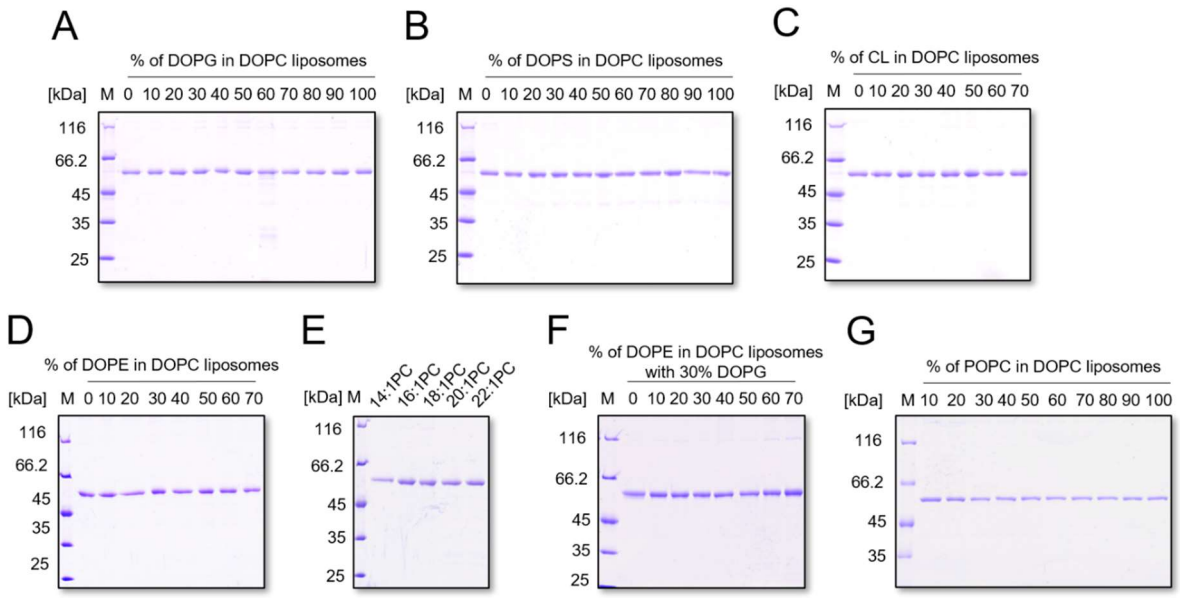

Figure S2: BmrA reconstituted into liposomes containing varying lipids.

SDS-PAGE analyses of BmrA reconstituted into liposomes containing different ratios of **(A)** DOPG/DOPC, **(B)** DOPS/DOPC, **(C)** CL/DOPC, **(D)** DOPE/DOPC, **(E)** containing (100% each) 14:1PC – 22:1PC, **(F)** DOPE/DOPC/DOPG, or **(G)** POPC/DOPC. In total, 2.5 µg of protein were separated on a 10% SDS-PAGE gel to verify successful reconstitution.

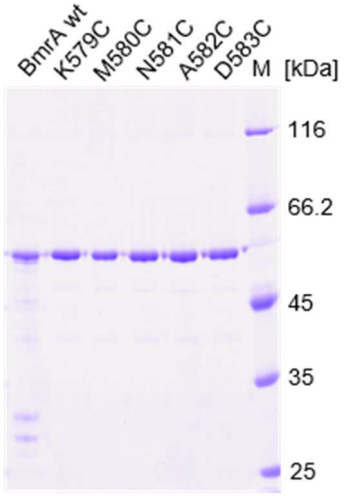

Figure S3: Purified BmrA wt and Cys variants analyzed.

SDS-PAGE analysis of purified BmrA Cys variants. The calculated mass for each variant is around 65.6 kDa. M = marker.

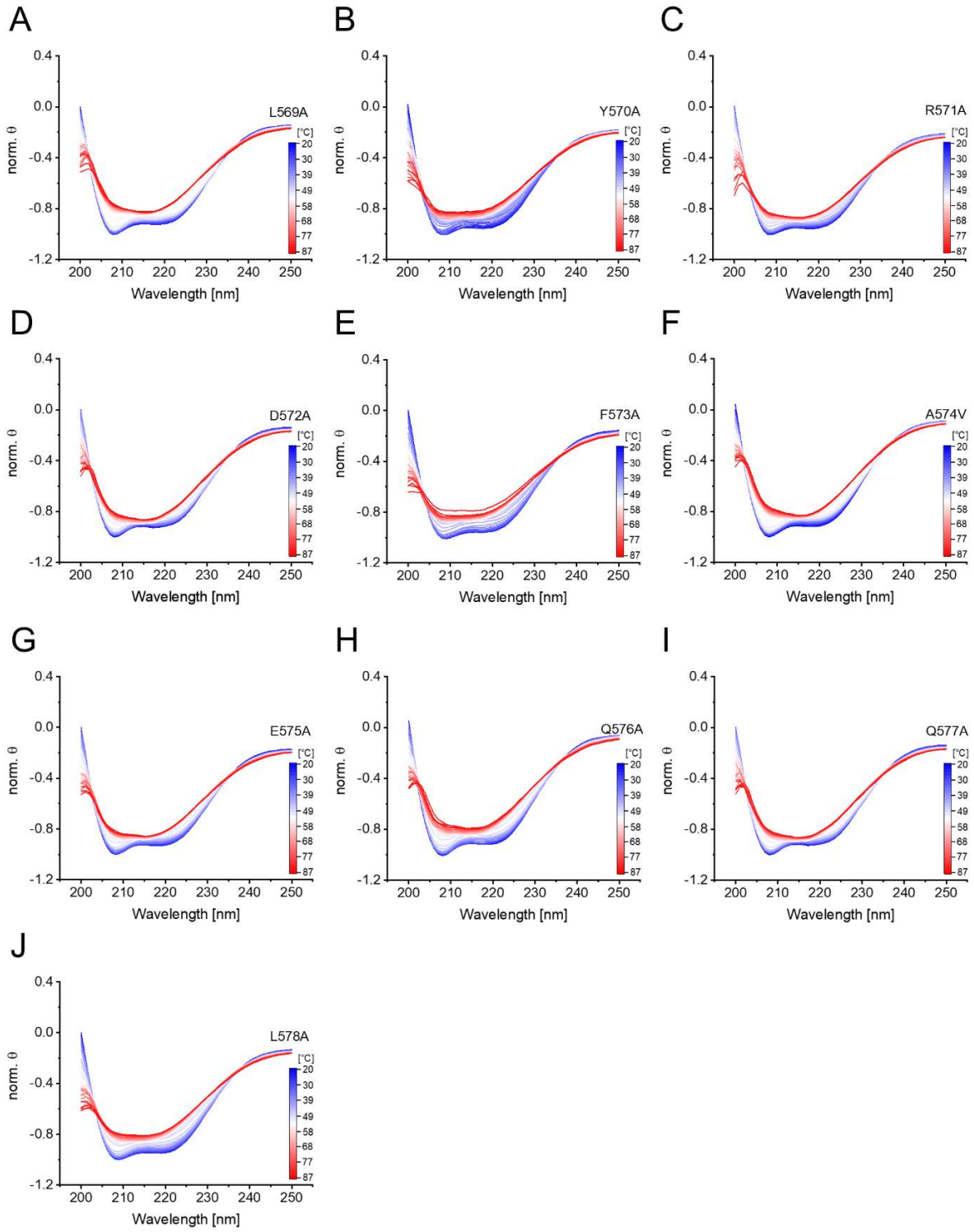

Figure S4: Thermal denaturation of the NBD variants L569A-L578A.

CD spectra of the NBD variants **(A)** L569A, **(B)** Y570A, **(C)** R571A, **(D)** D572A, **(E)** F573A, **(F)** E575A, **(H)** Q576A, **(I)** Q577A, and **(J)** L578A recorded at increasing temperatures (20 °C, blue – 88 °C, red). For each temperature the mean value determined using three independent purifications was normalized (θ of 250 nm was set to 0; minimum θ was set to -1).

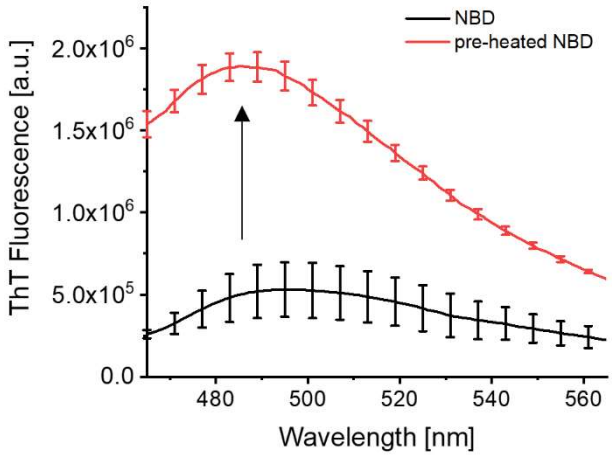

Figure S5: ThT binding to (pre-heated) NBD suggests the formation of amyloid-like structures.

Emission spectra of ThT after incubation with untreated (black) or pre-heated NBD (red). The fluorescence emission between 465-565 nm (slit width 5 nm) was recorded upon excitation at 450 nm (slit width 5 nm). Shown are the mean spectra of measurements of three independent purifications with SD, and the increase of ThT fluorescence at 482 nm is indicated.

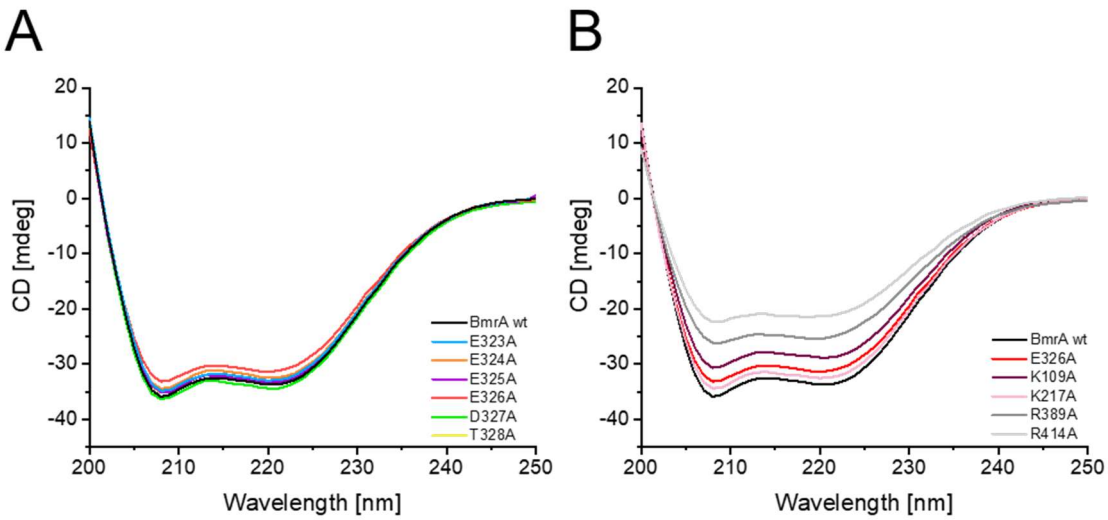

Figure S6: Secondary structure of BmrA wt and Ala variants.

Mean CD spectra of **(A)** purified BmrA wt (black), E323A (blue), E324A (orange), E325A (violet), E326A (red), D327A (green), and T328A (yellow) and **(B)** purified BmrA wt (black), E326A (red), K109A (dark red), K217A (rose), R389A (dark gray), and R414A (light gray) in the presence of 5 mM DDM in phosphate buffer (50 mM NaH_2PO_4/Na_2HPO_4, 150 mM NaCl, 10% glycerol, pH = 8.0). Spectra were measured at 25 °C with a protein concentration of 0.25 mg/mL in triplicate using three independent protein purifications.

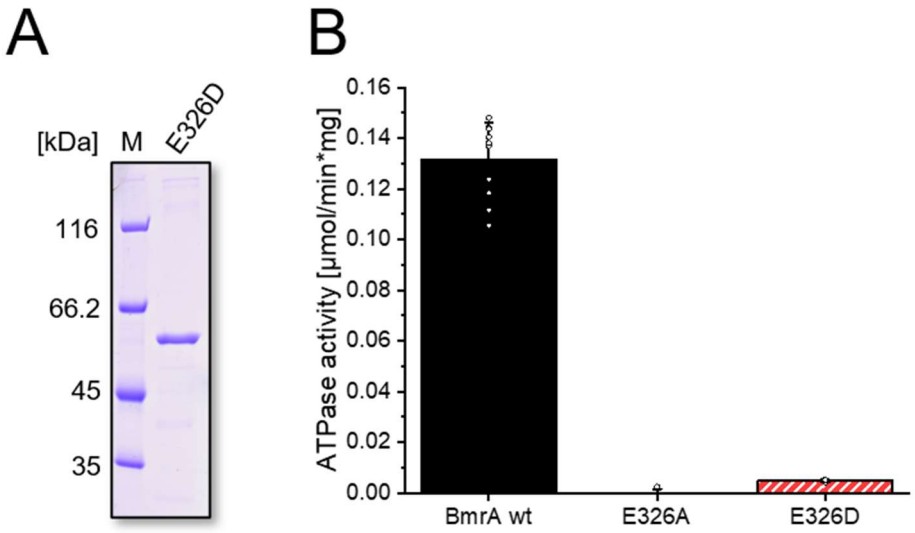

Figure S7: ATPase activity of purified BmrA wt and the variants E326A and E326D.

(A) SDS-PAGE analysis of 1.5 µg BmrA E326D purified via Ni-NTA chromatography. The calculated mass for E326D is about 65 kDa. M = Marker. **(B)** Mean ATPase activities of 1 µM BmrA wt (black, n = 11 ± SD, single-colored), E326A (red, single-colored), and E326D (red, cross-hatched) (n = 3 ± SD). Single data points of independent protein purifications are shown.

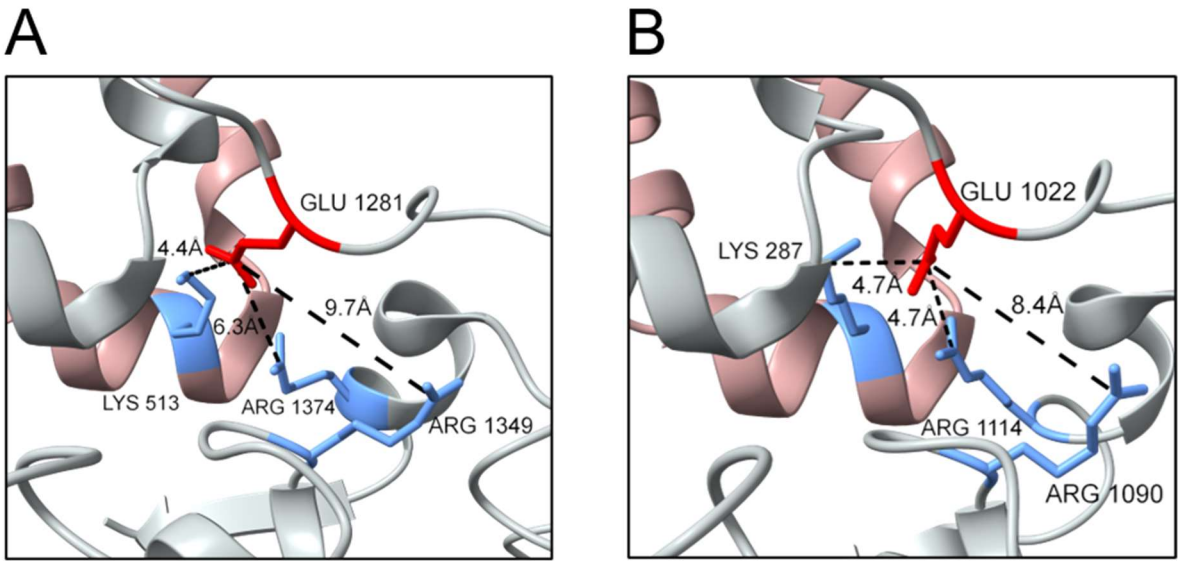

Figure S8: Positively charged amino acids in close proximity to the conserved Glu in the linker region.

View of **(A)** Glu1281 of ABCC2 (PDB: [8JX7][235]) and **(B)** Glu1022 of ABC-C4 (PDB: [8I4B]), each in the IF conformation (red in stick representation). In close proximity (< 10 Å) to Glu1281/1022 are three positively charged amino acids (blue in stick representation). On the C-terminal half-transporter (gray), Arg1374/1114 and Arg1349/1090 are located within the NBD. Lys513/287 is located on the CH2 of the N-terminal half-transporter (rose). Shown are the distances between the Glu and each positively charged amino acid. For the sake of simplicity, the C-terminal amino acids starting at Pro1381/1121 are not shown.

6.4 Methods performed by Collaborators

The following methods were performed in cooperation with [redacted]

Results obtained through this cooperation can be found in chapter 4.3.

6.4.1 Cryo-EM Sample Preparation and Data Collection

Cryo-EM grids were prepared following established protocols adapted from Januliene and Moeller, 2021[240]. Briefly, 3 µL sample were applied onto glow-discharged (PELCO easiGlow, 15 mA for 45 s) C-flat holy-carbon grids (Protochips; CF-1.2/1.3-3Cu-50). The grids were immediately plunge-frozen in liquid ethane using a Vitrobot Mark IV (Thermo Fisher) at 4 °C and at a relative humidity of 100%. Blotting was performed for 10 to 15 seconds using a blot-force of 8.

Data acquisition was conducted on a 200kV Glacios transmission electron microscope (Thermo Fisher Scientific) at a magnification of 165000, corresponding to a pixel size of 0.68 Å. The microscope was equipped with a Selectris energy filter (Thermo Fisher) with a slit width of 10 eV and coupled with a Falcon 4i direct electron detector (Thermo Fisher Scientific). Automated image acquisition was carried out using the EPU software (v.2.9, Thermo Fisher) in aberration-free image shift mode. Movies were collected with an electron dose of approximately 50 $e^-/Å^2$ across a defocus range of -0.8 to -2.0 µm and stored in electron-event representation format.

6.4.2 Cryo-EM Data Processing

All cryo-EM datasets were analyzed using CryoSPARC software (v.4.2-4)[241]. Movies underwent initial preprocessing steps involving patch-based motion correction and CTF estimation, followed by filtering based on a CTF fit threshold of 6 Å in CryoSPARC Live. Particle coordinates identified independently by blob picker, template picker, and Topaz picker[242] were merged, duplicates removed, and particle images extracted at a box size of 384 pixels with an initial binning factor of 4 to 96 pixels. Subsequent particle sorting included 2 to 3 iterative rounds of 2D classification. Only classes with clear structural features were retained. Selected particle subsets were then subjected to *ab initio* reconstructions into 2 to 3 distinct classes. Individual BmrA classes were refined separately using heterogeneous refinement (HR) followed by non-uniform refinement (NUR). Final particle subsets were re-extracted without binning and underwent additional rounds of HR, NUR, and local refinement.

6.4.3 Model Building

The potential assembly of BmrA E326A was visualized via manual, rigid body docking of an initial model (8QOE) into the density in ChimeraX (Pettersen *et al.*, 2021)[243].

Abbreviations

14:1PC	1,2-dimyristoleoyl-sn-glycero-3-phosphocholine
16:1PC	1,2-dipalmitoleoyl-sn-glycero-3-phosphocholine
20:1PC	1,2-dieicosenoyl-sn-glycero-3-phosphocholine
22:1PC	1,2-dierucoyl-sn-glycero-3-phosphocholine
8xM	K4A-K5A-K7A-K9A-K11A-K13A-R20A-R21A
ABC	ATP-binding cassette
ADP	Adenosine diphosphate
APS	Ammonium persulfate
ATP	Adenosine triphosphate
ATPase	Adenosine triphosphatase
B. subtilis	*Bacillus subtilis*
BCA	Bicinchoninic acid
BisTris	Bis-(2-hydroxyethyl)-amino-tris-(hydroxymethyl)-methane
BmrA	*Bacillus* multidrug resistance ATP
BN-PAGE	Blue native-polyacrylamide gel electrophoresis
CD	Circular dichroism
CHs	Coupling helices
CLs	Cardiolipins
CL	1',3'-bis[1,2-dioleoyl-sn-glycero-3-phospho]-glycerol
cryo-EM	Cryo-electron microscopy
DDM	Dodecyl-β-D-maltoside
DMSO	Dimethyl sulfoxide
DNA	Deoxyribonucleic acid
dNTPs	Deoxynucleoside triphosphates
DOPC	1,2-dioleoyl-sn-glycero-3-phosphocholine
DOPE	1,2-dioleoyl-sn-glycero-3-phosphoethanolamine
DOPG	1,2-dioleoyl-sn-glycero-3-phospho-(1'-rac-glycerol)
DOPS	1,2-dioleoyl-sn-glycero-3-phospho-L-serine

DTT	Dithiothreitol
E. coli	*Escherichia coli*
EDTA	Ethylenediamine tetraacetate
EH	Elbow helix
EPL	*E. coli* polar lipid
EPR	Electron paramagnetic resonance
GLUTs	Insulin-independent glucose transporters
GP	Generalized Polarization
HDL	High density lipoprotein
HDX-MS	H/D exchange coupled with mass spectrometry
Hepes	4-(2-hydroxyethyl)-1-piperazineethanesulfonic acid
HI	Hexagonal I
HII	Hexagonal II
HF	Heterogeneous refinement
Hoechst 33342	2'-[4-ethoxyphenyl]-5-[4-methyl-1-piperazinyl]-2,5'-bis-1H-benzimidazole
HSP	High-speed pellet
HSS	High-speed supernatant
ICLs	Intracellular loops
IF	Inward-facing
IMVs	Inverted membrane vesicles
IPTG	Isopropyl-β-D-thiogalacto-pyranoside
L. lactis subsp. cremoris	*Lactococcus lactis subsp. cremoris*
LB	Lysogeny broth
LmrA	*Lactococcus* multidrug resistance ATP
LSP	Low-speed pellet
LSS	Low-speed supernatant
MD	Molecular dynamic
MDR	Multidrug resistance
MGDG	Monogalactosyldilinolenoylglycerol
MLVs	Multilamellar vesicles

MRPs	MDR-associated proteins
MWCO	Molecular weight cut-off
NAD^+	Oxidized nicotinamide adenine dinucleotide
NADH	Reduced nicotinamide adenine dinucleotide
NBDs	Nucleotide-binding domains
NBSs	Nucleotide-binding sites
Ni-NTA	Ni^{2+}-nitrilotriacetic acid
NMR	Nuclear magnetic resonance
NUR	Non-uniform refinement
OF	Outward-facing
PA	Phosphatic acid
PC	Phosphatidylcholine
PCR	Polymerase chain reaction
PE	Phosphatidylethanolamines
PEG	Polyethylene glycol
PEP	Phosphoenolpyruvate
PG	Phosphatidylglycerols
P-gp	Permeability glycoprotein
PhEtOH	2-Phenylethanol
PI	Phosphatidylinositols
PK/LDH	Pyruvate kinase/lactic dehydrogenase
PMSF	Phenylmethylsulfonyl fluoride
POPC	1-palmitoyl-2-oleoyl-glycero-3-phosphocholine
PS	Phosphatidylserines
RT	Room temperature
S. aureus	*Staphylococcus aureus*
SANS	Small-angle neutron scattering
SBPs	Substrate-binding proteins
SD	Standard deviation
SDS	Sodium dodecyl sulfate
SDS-PAGE	Sodium dodecyl sulfate polyacrylamide gel electrophoresis

SEC	Size-exclusion chromatography
SGLT	Na^+/glucose cotransporter
TAP	Transporter associated with antigen processing
TEMED	*N*,*N*,*N*′,*N*′-Tetramethylethane-1,2-diamine
ThT	Thioflavin T
TM	Transmembrane helices
TMDs	Transmembrane domains
TmrAB	*Thermus thermophilus* multidrug resistance proteins A and B
Tris-HCl	Tris-(hydroxymethyl)-aminomethane-hydrochloride
TSB	Tryptic Soy Broth
wt	Wild-type

List of Figures

Figure 1: Typical membrane lipids. 8
Figure 2: Polymorphism of phospholipids 9
Figure 3: Classification of the ABC transporter superfamily into type I-VII based on their TMD fold. 13
Figure 4: Conserved motifs of ABC transporter NBDs exemplified by the *Sav*1866 NBDs. 14
Figure 5: TM helices arrangement of BmrA in the IF and OF conformation. 16
Figure 6: The two main ABC transport cycle models. 18
Figure 7: Substrate transport by BmrA. 22
Figure 8: Protein and DNA standards. 37
Figure 9: Preparation, ATPase activity, and topology of BmrA in EPL proteoliposomes. 61
Figure 10: ATPase activity of BmrA proteoliposomes in thinner/thicker membranes. 62
Figure 11: ATPase activity of BmrA in proteoliposomes containing negatively charged lipids. 64
Figure 12: Positively charged amino acids in the elbow helix of BmrA do not cooperate crucially with the negative charged membrane surface. 65
Figure 13: ATPase activity of BmrA proteoliposomes in membranes with varying fluidity. 66
Figure 14: The ABC transporter BmrA in the IF and OF conformation. 76
Figure 15: ATPase, Hoechst 33342 transport activities, and limited proteolysis of C-terminally truncated BmrA variants. 77
Figure 16: Antiparallel C-terminal helix dimer of BmrA. 79
Figure 17: ATPase, Hoechst 33342 transport activities, and dimerization propensities of BmrA wt and variants L569A-L578A. 80
Figure 18: Secondary structure of NBD wt and the variants with Ala (Val) mutations in the C-terminal helix part L569A-L578A. 81
Figure 19: Transition temperatures of NBD wt and the variants with Ala (Val) mutations in the C-terminal helix part L569A-L578A determined via CD measurements. 83
Figure 20: Structure of BmrA with putative interaction partners of crucial residues at the C-terminal end. 85
Figure 21: Structure of BmrA in the IF- and OF conformation and the position of the ICLs. 91
Figure 22: Hoechst 33342 transport activity and limited proteolysis by Trypsin of BmrA wt and variants (E323A-T328A) overexpressed in IMVs. 94
Figure 23: ATPase activity of purified BmrA wt and variants (E323A-T328A). 95
Figure 24: ATP hydrolysis of E326A is restored via artificial dimerization of the NBDs. 96
Figure 25: Positively charged amino acids in close proximity to Glu326. 97
Figure 26: Hoechst 33342 transport activity and limited Trypsin proteolysis of IMV-incorporated BmrA wt and variants (E326A, K109A, K217A, R389A, and R414A). 98
Figure 27: ATPase activities of purified BmrA wt and variants (E326A, K109A, K217A, R389A, and R414A). 99

Figure 28: Single particle cryo-EM analysis of purified BmrA wt and E326A. 100
Figure 29: Sequence alignment of the linker region of different bacterial ABC exporters and the human ABCC family. 101

Figure A1: pET303CT-His-BmrA-wt plasmid. 123
Figure A2: pET303CT-His-BmrA-SNAP-tag plasmid. 124
Figure A3: Amino acid sequence of BmrA wt. 125
Figure A4: Amino acid sequence of BmrA-SNAP-tag. 126

Figure S1: Orientation of BmrA-SNAP-tag reconstituted into liposomes with varying lipid compositions. 128
Figure S2: BmrA reconstituted into liposomes containing varying lipids. 129
Figure S3: Purified BmrA wt and Cys variants analyzed. 129
Figure S4: Thermal denaturation of the NBD variants L569A-L578A. 130
Figure S5: ThT binding to (pre-heated) NBD suggests the formation of amyloid-like structures. 131
Figure S6: Secondary structure of BmrA wt and Ala variants. 131
Figure S7: ATPase activity of purified BmrA wt and the variants E326A and E326D. 132
Figure S8: Positively charged amino acids in close proximity to the conserved Glu in the linker region. 132

List of Tables

Table 3.1: IUPAC nomenclature and abbreviation of phospholipids used in this study. 29
Table 3.2: Composition of the buffers, solutions, and media used in this study. 29
Table 3.3: Bacterial strains used in this study and their genotype and manufacturers. 33
Table 3.4: Plasmids used in this study. 34
Table 3.5: Oligonucleotides used in this study. Fw=forward, re=reverse. 35
Table 3.6 Protein and DNA standards used in this study. 36
Table 3.7: Enzymes and kits used in this study and their application. 37
Table 3.8: Consumables used in this study 38
Table 3.9: Instruments used in this study. 38
Table 3.10: Softwares used in this study. 39
Table 3.11: Composition of a standard PCR used for site-directed mutagenesis or molecular cloning by Gibson assembly. 41
Table 3.12: PCR temperature program. 41
Table 3.13: Calculated extinction coefficients and molecular masses of BmrA wt and variants. 46
Table 3.14: Composition of SDS-PAGE separation and stacking gels. 48
Table 3.15: Composition of the studied lipids mixtures. 49
Table 4.1: Author contribution of the article titled as "Membrane properties control the ATPase activity of the ABC transporter BmrA". 57
Table 4.2: Author contribution of the article titled as "The C-terminal α-helix is crucial for the activity of the bacterial ABC transporter BmrA". 73
Table 4.3: Author contribution of the manuscript titled as "A salt bridge pre-arranges the BmrA structure for proper NBD dimerization". 89

Use of AI-tools

The following AI-tools were used in this thesis:

- DeepL Translate, DeepL Write and Quillbot throughout the work, for spelling and grammar correction.
- ChatGPT for structuring and rephrasing parts of introductory chapters.

Acknowledgments/ Danksagung

[redacted]

Curriculum vitae